Increasing Optical Disc Data Density by Using Nano-scale Metallic Wire Polarisers

Allan Tzu-Kang Chin

A thesis submitted in partial fulfilment of the requirements
for the Degree of Master of Engineering
in
Electrical and Computer Engineering
at the
University of Canterbury,
Christchurch, New Zealand

30th January 2006

ABSTRACT

CD and DVD became the major portable and backup data storage devices because their reliability and economical cost when mass produced. As the computer technology grew, higher data storage density on CD/DVD disc was demanded. Using a shorter wavelength light source was the common technique to achieve this goal from both research and industry. However, the limit of wavelength had almost reached for applying it to optical storage. The nano-scale metallic wire polariser that was designed in this thesis provided a possible solution.

This thesis introduces the method of using the nano-scale metallic wires to form a grating polariser as the data pit on CD/DVD disc. The polariser is a type of scattering polariser and could transmit one linear polarisation of the light and reject its orthogonal counter part. The designed pattern was tested by using XFDTD, an electromagnetic simulation program based on the finite difference time domain method. As the wave source was a red laser with a wavelength of 650nm, the simulation cell size was set to be 10nm. The dispersive materials were simulated by the Debye model. The electric field results were measured on X, Y, and Z components. The results were analysed by a pre-written Matlab program to find the transmission and crosstalk coefficients.

The single polariser simulations showed that there are great potentials in this design. However, inter-cell crosstalk became the major problem in the polariser array simulations. The groove pattern and titanium material were used to optimise the polarisation effect. The simulation showed that a standard-sized disc with a titanium polariser array could have 5.5GB storage capacity and a 15 to 20dB inter-cell extinction ratio for an optical pickup with a red laser (650nm) and a numerical aperture (NA) of 0.6. Although the improvement is only marginal over existing optical data storage technology, there are many further researches possible to carry on such as the fabrication of the polariser arrays.

ACKNOWLEDGEMENTS

The author of this thesis would like to express his grateful appreciation to his supervisor, Associate Professor Richard Blaikie. His professional knowledge on such fields guided the author always on the right track. His positive attitude gave the author massive motivation. The author would also like to thank his co-supervisor Dr. Maan Alkaisi, Dr. Stuart Lansley, and Sharee MacNab for their great support on this research.

All the postgraduate fellows of the Nanostructure Engineering, Science and Technology (NEST) group deserve thanks from the author of this thesis. Especially Patrick Kuo, David Melville, Alan Wright, Han-Hao Cheng, Wei-Lun Chiu, Steve Drake, Mark Konijn, William Lee, Chito Kendrick, James Muys, and Leo Shuler.

Finally, the author would like to thank all his friends, families, parents, and be loved Lydia who cared and encouraged him for all this effort on this research.

TABLE OF CONTENTS

LIST OF FIGURES

LIST OF TABLES

1.0 INTRODUCTION

The Compact Disc (CD) and Digital Versatile Disc (DVD) are two important data storage technologies for the computer industry. CD/DVD technology uses optical data reading principles that have many advantages over magnetic storage. The CD/DVD ROM disc has a compact size, large storage capacity, high portability, and a low cost when mass produced. With these advantages, CD/DVD storage has replaced floppy disc (floppies) storage in the current computer market.

As computer functionalities increase and computer users request higher performance, more storage capacity is required. This requirement does not only apply to stationary data storage but also to portable data storage devices.

1.1 Motivation

Long before the computer was invented, data storage was developed for every day functions, for example, vinyl long-playing discs and cassette tapes, which both store music information. After the computer was created, digital data storage devices were demanded in different forms and capacities, for example, hard drives, floppies, CD-ROMs, and even on-chip computer memories. All of them are in different forms and some are based on different principles but they all serve the same aim, storing data. The other common factor that they share is that their capacity keeps growing and access speed gets faster as time progresses.

There are different types of computer data storage. There are not only system and program files but also multimedia files in a personal computer. The multimedia data, which includes music, video and computer games, usually occupies a large amount of data capacity. Fortunately, these types of data are not a compulsory element of the computer and therefore can be stored in an external data storage device, such as CD-ROMs.

The CD-ROM and DVD-ROM drives are based on optical technology. Data is encoded and fabricated as patterns onto the CD-ROM disc, which is a transparent plastic plate. By focusing a laser at these patterns, data can be retrieved from the reflected laser signal and decoded by the drive. Hence, the CD-ROM data capacity is related to the laser source wavelength. In order to increase the data capacity of the CD-ROM, the shorter wavelength, or higher frequency, laser source can be applied.

However there is a limit for the laser wavelength/frequency and it has almost been reached. For a shorter wavelength laser source, the light may not penetrate the patterned substrate and has an insufficient amount of reflection.

Conquering the wavelength limit would increase CD-ROM data storage capacity. Polarization and nanotechnology provide a possible solution. Within one laser spot size area, multiple nano-scale metallic polarisers can be laid onto the CD-ROM substrate as the patterns. By using the polarised laser as the light source, the pattern information may be read. Therefore, the CD-ROM data capacity is increased beyond the wavelength limit. The aim of this project is to investigate the technical feasibility of such an enhanced optical data storage system.

1.2 Types of Data Storage

Data is a collection of information, which can be recorded, reviewed, rewritten, and removed. For computer related technologies, the type of data storage can roughly be divided into three categories: magnetic, optical, and flash memories. Each category of data storage is based on different principles and is applied for different purposes.

1.2.1 Magnetic Data Storage

Magnetic storage is one of the traditional storage devices for recording a large amount of data. From the functionality point of view, the magnetic data storage can be divided into three classes [1, 2]. First is the system storage component, which is known as the hard disc drives. These are capable of storing all kinds of data including the system and application files. Hard drive discs provide a large amount of data capacity and high speed data accessibility [3]. The second class is the floppy-like disc. It offers less data capacity but higher portability. The third class is the backup type data storage device, such as magnetic tape which is used for backing up the system [2, 4]. It trades off data access speed with a massive amount of storage capacity [5].

There are five major components inside a hard disc drive. They are the base, the media discs, the motors, the read write heads and the controlling PCB. The hard drive is also known as a “Winchester Disc Drive”, which was first created by IBM in 1973, named 3340 [3]. There are one or more media discs in the hard drive base and they are driven by the motors. The media disc is made from aluminium alloy or glass. On both sides of the media discs, the surface is evenly coated with magnetic powder.

When the heads read or write data into the discs, this magnetic powder acts like tiny magnets, which are re-orientated by the applied magnetic field. There is one read/write head for each side of each media disc and these heads process the data simultaneously. The 3340 Winchester disc drive had a single media disc with 30MB on each side. In today's market, hard drives with more than 100GB data capacities are commonly used in personal computers. These hard drives contain multiple media discs, which have about 80GB data capacity on each single disc.

The floppy and magnetic tape also have a similar structure to the hard drive disc. However, the media are packed separately from the motors and the heads. These mechanical components are built inside the floppy drive or the tape drive. Therefore, the floppy disc and magnetic tape are portable and can be stored individually.

The first floppy disc was created in 1971 with a dimension of 8 inch in diameter. In 1978, the 5¼ inch floppy disc became the standard data storage device for carrying files around. The 5¼ inch floppy was able to store 360KB in a double sided disc. IBM created the next standard of the floppy disc in 1984 which are 3.5 inch in diameter and stored 1.44MB data in one disc. The 3.5 inch floppy is still commonly used today. File size increases as technology improves; the 1.44MB is no longer enough for carrying data around. The new generation floppies, for example LS-120, were developed for larger storage capacity. However, these new floppies were not popular in the market as the CD-ROM had already taken that place with its higher storage capacity.

The first commercially used magnetic tape was created by Imation, which was a branch of a company called 3M, in 1952. In the same year, the first commercial computer was released on to the market. The tape was designed for IBM's tape drive, model 726, and became the first device for storing digital data in a computer. It had storage of about 1MB with a 100 bpi (bits per inch) data density. The tape from Imation today has a maximum 400GB data capacity for backing up the medium or large network systems. Imation predicts the capacity for the magnetic tape could reach 1 TB in the next decade.

1.2.2 Optical Data Storage

CD and DVD, which require a light source for data reading, are known as forms of optical data storage. Similar to the floppy, CD/DVD ROMs are plastic discs and

require the CD/DVD drive to read or write the digital data onto the discs. Because of a CD's excellent sound quality, it replaced the cassette tape and became the major music storage medium. However, a CD can store not only music data but also be used for all kinds of digital data storage. Therefore, it is widely used for the modern computer data backup and as an application storage device.

The formal name of DVD is Digital Versatile Disc as it is capable of storing massive amounts of data compared to a CD and can therefore be used for many applications. A DVD uses the same technology as a CD but with a shorter wavelength light source so the data density is greatly improved. Due to its large data capacity, a DVD is specially designed for storing high quality video and audio information. DVDs are now utilised by the film industry for the purpose of replacing the original standard VHS video tapes.

The CD-ROM disc data capacity is about 700MB and it can store up to 80 minutes of music. A DVD-ROM disc has about 4.7GB in data capacity and it is capable of storing two hours of film with both audio and video. The physical dimensions of both CD and DVD discs are 1.2mm thick and 120mm in diameter. This provides excellent portability with large data capacity. The advantage of optical storage devices over magnetic ones is that CD/DVDs can maintain the data for a long time without being influenced by thermal or external magnetic effects.

1.2.3 Flash Memory

Flash Memory is a Non-Volatile Random Access Memory (NVRAM). Unlike Dynamic Random Access Memory (DRAM) or cache memory, flash memory can maintain data even while the power is off. Although flash memory does not have fast access speed like DRAM and cache memory, the large data capacity has resulted in flash memory becoming a very popular new data storage medium.

Data in flash memories can be modified by applying a current. However, to write data requires modifying the memory in a block rather than a byte. One block is usually 256KB or more. A flash memory device can be modified approximately one million times and it is able to maintain the data for 10 years. Therefore, thousands of applications now use flash memory.

Flash memory was first introduced by Intel in 1980 in order to replace the Electrically Erasable Programmable Read-Only Memory (EEPROM or E^2PROM) [6, 7].

EEPROM is also a NVRAM but has a slower data modifying speed and smaller data capacity. Flash memory costs less to manufacture and has a smaller memory cell, which gives higher memory density. It also has other advantages such as being small in size, lightweight, and has low power consumption. These are the reasons why flash memory is replacing the floppy and other media and is becoming a major data storage device.

As a storage device, flash memory has many applications, for example digital cameras, cell phones, and handheld computers. These devices either have built-in flash memories or support flash memory card extensions. There are many different types of flash memory cards: Compact Flash (CF) type I and II; Secured Digital and Multi Media Card (SD/MMC); Memory Stick (MS); Smart Media (SM); and others. Although these memory cards are not interchangeable and may have different specifications, they all types of flash memories. The maximum data storage of the flash memory card is 2GB at the moment, but this will inevitably increase over time.

1.3 CD/DVD Technology

A CD-ROM is a 1.2mm thick and 120mm diameter disc. There are three layers in the disc structure as shown in Figure 1. The substrate is a transparent layer, which supports the whole disc and is the base for fabricating other layers. On top of the substrate is the reflective layer. It is made of metal, like aluminium, and has a lacquer protective coating. This layer is where the data pattern is fabricated. The last layer is the protective layer, which is on top of the reflective layer and protects it from scratches. The CD cover tag is printed on the protective layer.

In order to store data on to a CD-ROM disc, this data has to be digitized into a series of “1” and “0” signals. To represent these digital signals, the CD-ROM disc substrate layer is stamped to form grooves. When the reflective layer is applied to the substrate, the metal materials fill the grooves and form the data pits. These pits are the physical representation of the digital signals on the CD-ROM. The orientations of the pits are according to the signal series. On the CD-ROM disc, the pits are aligned as circular tracks around the disc centre. The CD-ROM drive can then read or write the data by moving the laser head along the disc radius while the disc is spinning. To access the data pit, it requires a phenomenon called destructive interference. As the light propagates as a wave, the reflected wave will interfere with the incident wave. This

interference effect reaches its maximum when the phase difference between two waves is a half wavelength and these two waves cancel out each other. Therefore, the pit and the groove thickness have to be a quarter of the light source wavelength.

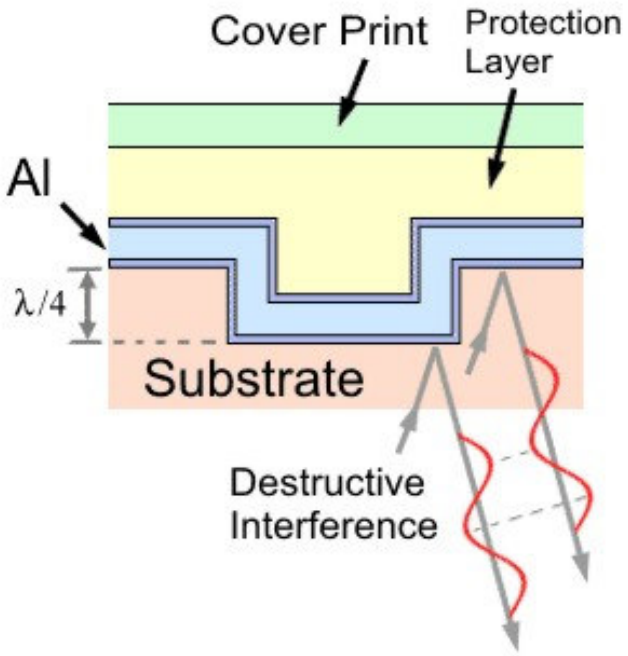

Figure 1: Cross-sectional view of a compact disc structure [3].

The technologies behind the CD and DVD are very similar. CDs and DVDs both use lasers as the light source with 780nm and 650nm wavelengths respectively. A DVD disc has a much higher data storage density than a CD disc. This is because a DVD uses a shorter wavelength laser source and lens with a higher Numerical Aperture (NA). NA is a unit-less measurement of the lenses ability to focus the light,

$$NA = n \sin \theta, \tag{1-3-1}$$

where n is the refractive index of the lens and θ is the angle of the light as it curves to the focus point [8], as shown in Figure 2. A higher NA value represents a better focus power of the lens and results in a smaller spot size. The lens has a NA of 0.45 in the CD-ROM drive and 0.6 in the DVD-ROM drive.

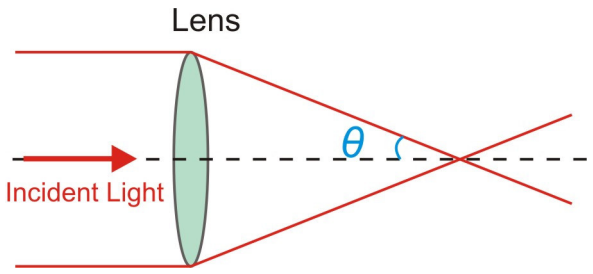

Figure 2: A lens with a specific NA and refractive index *n* results the incident light to have an angle of *θ*.

The CD and DVD technologies, which are discussed above, are not writable or re-writable. In order to back up the information, CD-R/DVD-R and CD-RW/DVD-RW have been developed [9]. The basic structure of CD-R is very similar to CD-ROM but CD-R has an extra layer called the dye layer. This dye layer covers the reflective layer, which was flat in a CD-R. While writing data into the disc, a laser is focused onto the dye layer, which absorbs the optical energy and converts it into heat [10]. The temperature of this point may be raised to above 250°C, which melts the dye layer to form the pit.

CD-R is a write-once data storage device. After the data is written into the disc, the information can not be modified. In order to achieve re-write functionality, the CD-RW, which is formerly called CD-Erasable [11], has been developed and it has a much more complicated structure than CD-R. There are three layers, which are related to recording, in a CD-RW. These three layers are the upper dielectric layer, the recording layer and the lower dielectric layer [12]. This structure is used for the CD-RW recording principle called phase change [13].

Phase change recording is based on the reflectivity difference between the crystallisation phase and the amorphous phase of the recording layer [13]. At various laser power ratings, different temperatures can be applied onto the recording layer to change the phase. The recording layer has a crystallisation temperature of 200°C and a melting temperature of 600°C.

1.4 How to Increase Data Capacity in CD/DVD

In order to increase the data capacity of a CD or DVD disc, the general method is to apply a shorter wavelength laser as the source to give a smaller laser spot size on the disc. Therefore, the data pits on the disc can be made smaller.

The key factors for increasing optical data storage density can be found by comparing CD and DVD technologies, and key parameters are listed in Table 1-1. In the current technology, a CD uses a 780nm wavelength light source and a 0.45 NA lens. A CD-ROM disc has 0.83μm in minimum pit diameter and 1.6μm for minimum track pitch. A DVD uses a 650nm wavelength red laser and its lens has a NA of 0.6. A DVD-ROM disc has a 0.4μm minimum pit diameter and a 0.74μm minimum track pitch.

	CD	DVD
Numeric Aperture (NA)	0.45	0.6
Laser Wavelength	780nm	650nm
Laser Spot Size	1733nm	1083nm
Pit Diameter	830nm	400nm
Track Pitch	1600nm	740nm
Capacity	700MB	4.7GB

Table 1-1: Comparison of CD/DVD details.

The comparison of CD and DVD technology shows that increasing NA and decreasing laser wavelength both increase the data storage density on the disc. These results are applied to the new optical storage technology, called blue-laser DVD.

The idea of blue-laser DVD is simple. It uses a blue laser as a light source instead of the red laser in the original DVD drive. The blue laser has a wavelength of 405nm [14], but the technology itself is quite complicated. Currently there are two standards of the blue laser DVD, Blue-ray Disc (BD) and High Definition DVD (HD-DVD), which are compared in Table 1-2.

	Blue-Ray Disc	HD-DVD
Numeric Aperture (NA)	0.85	0.65
Laser Wavelength	405nm	405nm
Laser Spot Size	476nm	623nm
Pit Length	149nm	220nm
Track Pitch	320nm	400nm
Capacity/side/layer	25GB	15GB

Table 1-2: Technical details on blue-ray disc and HD-DVD.

The Blue-ray disc standard was developed by Sony [15] and is supported by the 9 Companies (9C) of the Blue-ray Disc Association, which includes Sony, Matsushita, Hitachi, Pioneer, Sharp, Philips, Thomson, Samsung, and LG. This standard applies an 0.85 NA lens [16] and 405nm wavelength blue laser into the optical system to shrink the laser spot size, and shrink the track pitch to 320nm [17]. The thickness of the BD is 1.2mm, the same as the CD and DVD discs. It has a 1.1mm base plus 0.1mm cover and protective layer. Therefore, the optical reading on a BD is very sensitive to disc pollution, for example finger prints and dust. Due to the short

wavelength and high NA value, the data density is so high that the disc defect is quite significant to the data reading accuracy. However, the BD provides huge data storage capacity; 25GB for a one-sided single-layer disc or 50GB for a double-layer disc [18].

The HD-DVD standard was introduced by Toshiba and NEC [19, 20]. It is also called the Advanced Optical Disc (AOD) [21]. HD-DVD technology also uses a 405nm wavelength blue laser but its lens has a NA of 0.65 [22]. The track pitch is about 400nm and the disc can store 15GB for a one-sided single-layer disc. The capacity is smaller than the BD but the HD-DVD's structure is more similar to the original DVD. It has a 0.6mm protective layer within the 1.2mm disc thickness, therefore it is more scratch tolerant than the BD.

The blue laser DVD technology was developed based on using a shorter wavelength light source to obtain a smaller laser spot. However, industries may have reached a bottleneck in finding the short wavelength light source. They are now focusing on other methods for solving the problem of increasing the optical storage density.

One possible solution is the super-resolution near field structure (Super-RENS) technology. The near field is where the distance is within one wavelength or less from a source or scattering object [23, 24]. Therefore, Super-RENS is a sub-wavelength optical technology. On the disc structure, there are two extra layers with a thickness in the nano scale [25]. Hence, a Super-RENS disc has dimensions the same as the original discs. Because the optical effect happens at less than one wavelength, the laser spot size could focus into an extremely small dimension and therefore, the track pitch could be less than 100nm. The result is more than 100GB data capacity on a single disc. This technology is still in the research phase [26].

Pioneer is a member of the blue-ray disc association and they also have another idea for the next generation optical storage. They have introduced a new technology, which uses an electron beam as the source for reading the disc information [27]. The electron beam is usually used for the electron microscopy as the wavelength of the electron beam can be controlled by varying the acceleration voltage and is typically much shorter than the wavelength of normal light or a laser [28]. Pioneer applies this technology for reading the 70nm track pitch from a disc, which stores 510GB in a single layer.

1.5 Metallic Wire Grating Polariser Data Pit Structure

This thesis investigates the nano-scale wire grating polariser for improving optical storage density. A two by two metallic wire grating polariser array, as shown in Figure 3, within the size of one focused laser spot (around 1μm diameter in DVD) could store four times the information of an ordinary CD/DVD. This pattern can be made by using nano-fabrication on the DVD disc.

The two by two polariser array pattern represents one optical data pit on the disc. There are two vertically oriented and two horizontally oriented polarisers in each data pit as shown in Figure 3. It potentially stores four bits of data in this structure. In order to fetch the data from this pattern, both theta (horizontal) polarised light and phi (vertical) polarised light are illuminated on the data pit. Theoretically, the theta polarised light could transmit through the vertical oriented polarisers Q_0 and Q_1 but will be blocked by the horizontal orientated polarisers Q_2 and Q_3. The phi polarised light case is vice versa.

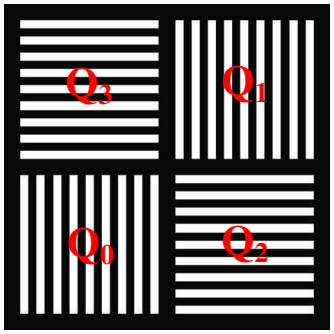

Figure 3: Illustration of a single polariser array data pit on optical disc.

The polarised transmissions are detected individually by the sensors and the digital information is fed into a digital signal process (DSP) unit. The theta transmission gives the first two bits of data Q_0 and Q_1 and the phi transmission gives the last two bits Q_2 and Q_3. The data series order is ($Q_3Q_2Q_1Q_0$). The successful transmission represents a low signal '0'. Hence, the case in Figure 3 indicates the data series (0000). A high signal '1' occurs when the transmission is blocked from the certain pixel. As shown in Figure 4, the data bit Q2 is blocked and the data series is (0100).

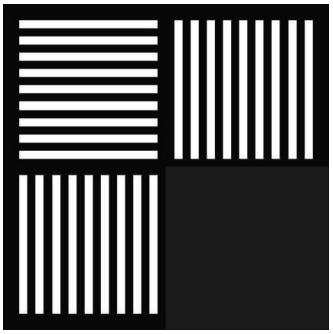

Figure 4: Illustration of a (0100) data pit structure.

For far field detection individual sub-cell sensors will not be possible, however, by using separate far field detectors for each polarisation improved data storage density will still be possible. Each detector recognises the data signal by detecting the transmission level for one polarisation. The levels are high (above 70%), medium (30% to 70%) and low (below 30%) which represents the data (11); (10) or (01); and (00) respectively. For theta polarised transmission, the high level, (11), corresponds to both sub-cell polarisers Q_0 and Q_1 being unblocked. The low level, (00), corresponds to both sub-cell polarisers Q_2 and Q_3 being blocked. The medium level transmission is an unsure state where the data set could be either (10) or (01). The true data orientation requires additional information, which can be derived from the previous data set as the laser spot is moved along a track.

A data track with four data pits is shown in Figure 5. Each data pit is a two by two polariser array and has four bits of data. Every single polariser sub-cell has orthogonal orientation to its adjacent and forms the chessboard format. The first pit, the most right hand site, is the data pack header. All four pixels of the pack header are arbitrarily unblocked and it contains no information in the data series. The pack header is used to address the data series and for deriving the unsure states.

The unsure state could be derived from the confirmed previous state with an additional illumination in the middle of two data pits. For example as shown in Figure 5, the first theta data set (DS1) is an unsure state. Because of the pack head contains data set as (0000) and the second illumination, the middle circle, gives also a medium level transmission, the unsure state for (Q_1Q_0) is derived to be (10) rather than (01).

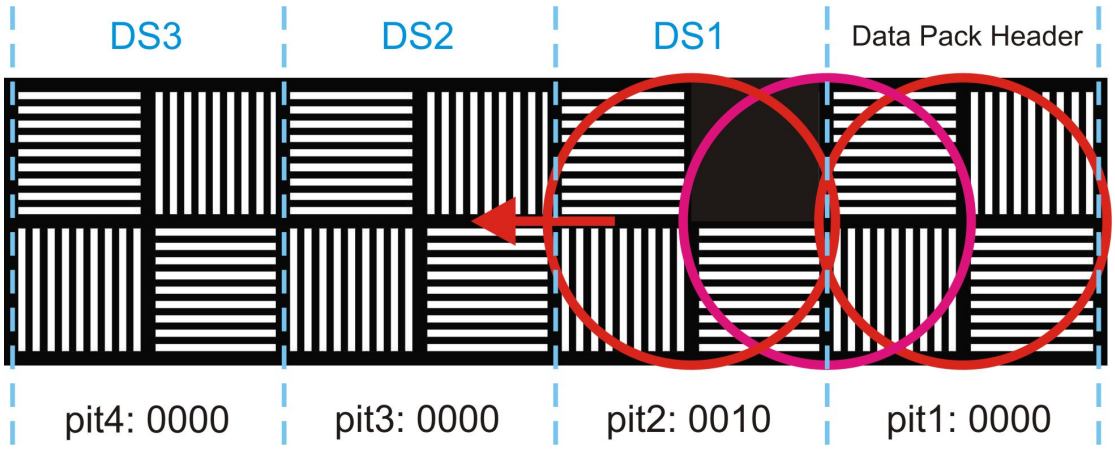

Figure 5: Grating polariser data track orientation for a four-pit section of track.

The DVD drive uses a laser source with a wavelength of 650nm and produces a laser spot size of 1,083nm. This thesis investigated the grating polariser pattern which contains four bits of data within this spot dimension. The quadruple increasing on data storage density results 5.5GB data storage on a one side single layer optical disc.

In summary, the designed data pattern pit contains two vertical and two horizontal oriented polarisers to represent four bits of data. The coded information on such pattern could be fetched by illuminating by theta and phi polarised light and detecting the far-field transmission level. The data pack header and the middle illumination between two data pits were introduced to solve the unsure state and reduce the data error rate.

1.6 Thesis Arrangement

This thesis reports the simulations and analysis of this new method for increasing the CD/DVD data storage capacities by using polarised light through nano-scale polarisers. The simulation focuses on the polarisation effect as different characteristics of the metal polarisers and light sources are varied. The crosstalk effect and its solution are also discussed. The thesis structure as follows.

Chapter Two outlines the background principles and theories. First, Maxwell's equations are introduced. These are the bases of the electric and magnetic world. Under well-defined conditions, Maxwell's equations can describe electromagnetic wave behaviour. The second topic in Chapter Two is polarisation and polarised light in optics. As one of the fundamental properties of light, polarisation is important to this project. There are a number of methods to polarise light. There are also a few

tools which measure the degree of polarisation. Then the Finite Difference Time Domain (FDTD) method for modelling electromagnetic wave time-dependent propagation is discussed. FDTD is a method which, based on Maxwell's equations, models electromagnetic behaviour. The last topic in Chapter Two introduces the simulation program, XFDTD. Based on the FDTD method, XFDTD is a commercial software package for simulating the electromagnetic wave and its behaviour when it interacts with different materials.

Chapter Three contains a description of a simulation of polarised light propagating through single nano-scale metal polarisers. The simulation focuses on three major factors of the polariser and the laser source: the grating period of the metal polariser; the polariser materials; and the laser spot size, which focuses on the polariser.

Chapters Four and Five continue discussing the polarised light simulations, this time concentrating on multi-polariser array patterns. Not only is the transmission performance monitored, but also the crosstalk between the polarisers.

Chapter Six further studies the polarisation effect on the two-dimensional polariser pattern illuminated with a Gaussian beam source. Hybrid-material polarisers are discussed and compared to the uniform material case. A three by three polariser pattern simulation is also introduced to discuss the crosstalk effect to the neighbouring pixels with respect to the spot size.

In the Conclusion, the final result of the capability of this CD/DVD data storage capacity increasing technique is finalised. Suggestions for the potential development and application of this research are also discussed here.

2.0 BACKGROUND

2.1 Maxwell's Equations

The principle of CD and DVD data storage is based on optical effects. Digital information, which is coded on to the disc, can be read by focusing a laser beam on to the data pit. Maxwell's equations describe the relation of an electric field and a magnetic field [29]. As light is an electromagnetic wave, Maxwell's equations also help to explain the optical phenomena of CD/DVD data storage principles.

In 1863, James Clerk Maxwell wrote the Maxwell equations as follows: [30, 31]

$$\nabla \cdot \mathbf{D} = \rho . \tag{2-1-1a}$$

$$\nabla \cdot \mathbf{B} = 0 \tag{2-1-1b}$$

$$\nabla \times \mathbf{E} = -\frac{\partial \mathbf{B}}{\partial t} \tag{2-1-1c}$$

$$\nabla \times \mathbf{H} = \mathbf{J} + \frac{\partial \mathbf{D}}{\partial t}, \tag{2-1-1d}$$

where **D** is the electric flux density (C/m^2), **B** is the magnetic flux density (T), **E** is the electric field (V/m), **H** is the magnetic field (A/m), **J** is the current density (A/m^2), and ρ is the charge density (C/m^3) [32]. These four mathematical equations fully describe classic electromagnetism. However, in order to model electromagnetic wave propagation, some definitions and conditions are required.

For plane wave propagating through a simple medium, it is assumed that there are no free charges or currents. Maxwell's equations are then:

$$\nabla \cdot \mathbf{D} = 0 \tag{2-1-2a}$$

$$\nabla \cdot \mathbf{B} = 0 \tag{2-1-2b}$$

$$\nabla \times \mathbf{E} = -\frac{\partial \mathbf{B}}{\partial t} = -\mu \frac{\partial \mathbf{H}}{\partial t} \tag{2-1-2c}$$

$$\nabla \times \mathbf{H} = \frac{\partial \mathbf{D}}{\partial t} = \varepsilon \frac{\partial \mathbf{E}}{\partial t}, \tag{2-1-2d}$$

where μ is the magnetic permeability (H/m) and ε is the electric permittivity (F/m).

Assuming the uniform plane wave propagates along the z direction only, then the partial differentiations with respect to x and y are zero. Therefore, the two curl equations lead to the following:

$$\nabla \times \mathbf{E} = -\mu \frac{\partial \mathbf{H}}{\partial t} \quad \Rightarrow \quad \begin{cases} -\dfrac{\partial E_y}{\partial z} = -\mu \dfrac{\partial H_x}{\partial t} & \text{(2-1-3a)} \\ \dfrac{\partial E_x}{\partial z} = -\mu \dfrac{\partial H_y}{\partial t} & \text{(2-1-3b)} \\ 0 = -\mu \dfrac{\partial H_z}{\partial t} & \text{(2-1-3c)} \end{cases}$$

$$\nabla \times \mathbf{H} = \varepsilon \frac{\partial \mathbf{E}}{\partial t} \quad \Rightarrow \quad \begin{cases} -\dfrac{\partial H_y}{\partial z} = \varepsilon \dfrac{\partial E_x}{\partial t} & \text{(2-1-4a)} \\ \dfrac{\partial H_x}{\partial z} = \varepsilon \dfrac{\partial E_y}{\partial t} & \text{(2-1-4b)} \\ 0 = \varepsilon \dfrac{\partial E_z}{\partial t} & \text{(2-1-4c)} \end{cases}$$

As the plane wave propagates along the z direction, the time derivations of the z components of the electric and magnetic fields are zero. The remaining four equations form two independent sets. The first set is equation (2-1-3a) and (2-1-4b), which contains E_y and H_x. Equation (2-1-3b) and (2-1-4a) forms the second set, which is related to E_x and H_y. Both sets can describe wave propagation and the fact that there are two independent sets gives rise to the concept of polarisation that we are trying to exploit for increased CD/DVD data storage density. In the set with E_x and H_y, when equation (2-1-3b) and equation (2-1-4a) are partially differentiated with respect to z and t respectively, the result is:

$$\frac{\partial^2 E_x}{\partial z^2} = -\mu \frac{\partial^2 H_y}{\partial z \partial t}, \qquad -\frac{\partial^2 H_y}{\partial z \partial t} = \varepsilon \frac{\partial^2 E_x}{\partial t^2} \tag{2-1-5}$$

These two equations may be combined:

$$\frac{\partial^2 E_x}{\partial z^2} = \mu\varepsilon \frac{\partial^2 E_x}{\partial t^2} \tag{2-1-6}$$

This differential equation is called the one-dimensional wave equation. It has a general solution, which describes the wave propagation along the z direction, as follows:

$$E_x(z,t) = f_1\left(t - \frac{z}{v}\right) + f_2\left(t + \frac{z}{v}\right), \tag{2-1-7}$$

The wave has a velocity v, which is defined as follows:

$$v = \frac{1}{\sqrt{\mu\varepsilon}} \tag{2-1-8}$$

For the steady-state sinusoid wave, the one-dimensional wave equation can be rewritten as its phasor equivalent by replacing the time derivative $\frac{\partial}{\partial t}$ with the complex phasor component $j\omega$, so that the equation becomes:

$$\frac{d^2 E_x}{dz^2} = -\omega^2 \mu\varepsilon E_x \tag{2-1-9}$$

This phasor equivalent is called the one-dimensional Helmholtz equation. Its general solution contains exponentials of the form:

$$E_x = c_1 e^{-jkz} + c_2 e^{jkz} \tag{2-1-10}$$

where $k = \omega\sqrt{\mu\varepsilon}$ or $k = \frac{\omega}{v}$

The one-dimensional wave equation and one-dimensional Helmholtz equation describe the wave propagation behaviour along the z direction in one dimension. To be more practical, the equation is required to model the wave characteristic in a three-dimensional space. By taking the curl of the last two Maxwell equations, equation (2-1-2c) and (2-1-2d), the following are derived:

$$\begin{aligned} \nabla\times\nabla\times\mathbf{E} &= -\nabla^2\mathbf{E} + \nabla(\nabla\cdot\mathbf{E}) \\ &= -\mu\frac{\partial}{\partial t}(\nabla\times\mathbf{H}) = -\mu\frac{\partial}{\partial t}\left(\varepsilon\frac{\partial\mathbf{E}}{\partial t}\right) = -\mu\varepsilon\frac{\partial^2\mathbf{E}}{\partial t^2} \end{aligned} \tag{2-1-11}$$

If there is no free charge or extra source influence, $\nabla\cdot\mathbf{E} = 0$. Therefore:

$$\nabla^2\mathbf{E} = \mu\varepsilon\frac{\partial^2\mathbf{E}}{\partial t^2} \tag{2-1-12}$$

This is the *three-dimensional wave equation*.

The complex phasor equivalent, which is called the three-dimensional Helmholtz equation, is derived by replacing the time derivative $\frac{\partial}{\partial t}$ with the complex phasor component $j\omega$.

$$\nabla^2\mathbf{E} = -k^2\mathbf{E} \tag{2-1-13}$$

$$k^2 = \omega^2\mu\varepsilon$$

2.2 Polarisation

Light is an electromagnetic wave [33]. It has interference [34]and diffraction effects [35]. A light wave has transverse vibration [8], as shown space in equation (2-1-5) for example. Unlike the longitudinal wave which is symmetrical to the propagation direction, the transverse wave could be dissymmetrical such as polarised light [36]. Like intensity, wavelength, and coherence, the polarisation of light is one of its fundamental properties [37].

In 1808, French army engineer Etienne-Louis Malus discovered the polarisation when he observed the reflection of the sun through a calcite crystal from a window. He saw two images, which were formed by double refraction[1], which disappeared alternately when he rotated the calcite crystal. In 1812, Sir David Brewster discovered that polarisation occurs when the image is viewed at a particular angle; therefore this is called the Brewster angle or polarising angle. His investigation showed that there was a relation between the Brewster angle and the refractive index of the medium, the window glass [38].

2.2.1 Classical Description of Polarisation

Polarisation is one of the most basic properties of light [39]. There are three types of polarisation, namely linear polarisation, circular polarisation and elliptical polarisation [40]. Figure 6 illustrates four examples of polarisation states which are (a) horizontally polarised, (b) vertically polarised, (c) right circularly polarised and (d) left circularly polarised. The horizontal and vertical polarisations are linear polarisation as the vibration direction is linear. These two are also the polarisations that have been used in this project simulation. Elliptical polarisation includes the first two types and is a special case of the other two polarisations [41].

[1] Refraction occurs when light passes through a media to another with an angle. Some materials, like calcite crystal, cause the light bend into two directions and therefore form the double refraction.

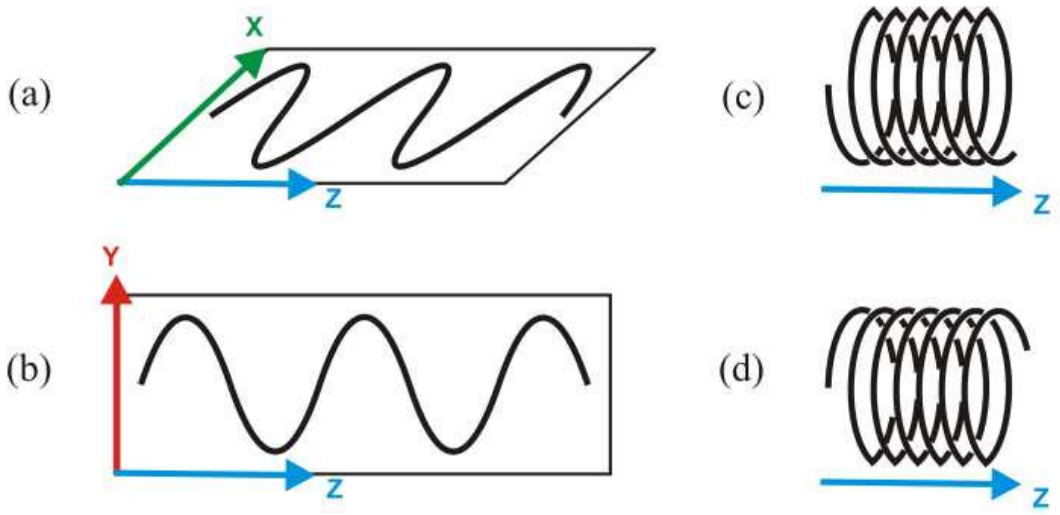

Figure 6: Pictorial description of the polarised light: (a) horizontal polarised, (b) vertically polarised, (c) right circularly polarised, (d) left circularly polarised.

The cross-sectional pattern, as shown in Figure 7, is a notation for representing the polarisations. This technique is simple, clear and also functional. The polarisations are represented by its geometrical symbol. The notation of the linear polarisation is a straight line with an angle between it and the horizontal axis. The circular polarisation notation is a circle with an arrow to indicate the polarisation direction. The elliptic polarisation notation is an ellipse that contains both the arrow and the angle. It has both linear and circular characteristics. The arrow indicates the polarisation direction and the angle between its major semi-axis and the horizontal axis indicates the inclination.

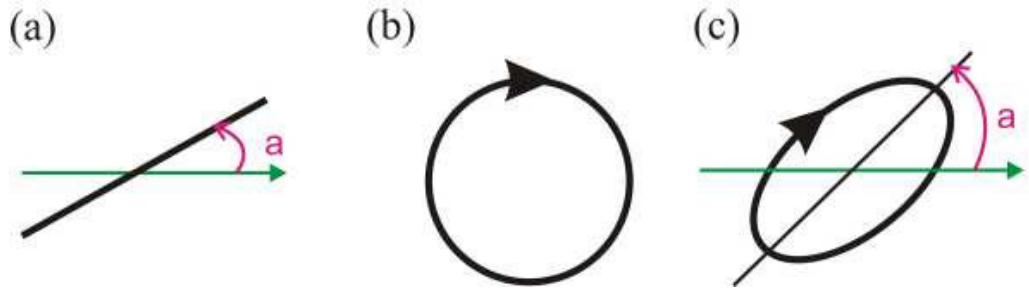

Figure 7: Polarisation sectional pattern: (a) linear polarisation, (b) circular polarisation, (c) elliptic polarisation.

2.2.2 Polarisation Ellipse

The elliptic polarisation includes both linear and circular polarisation characteristics [42]. Therefore, if there is an expression of the elliptic polarisation, it could describe all polarisations. The wave equations mentioned in Section 2.1 describe the optical field in the Cartesian coordinates. For a three dimensional optical field, the wave equations are as follows:

$$\nabla^2 u_x(\mathbf{r},t) = \frac{1}{v^2}\frac{\partial^2 u_x(\mathbf{r},t)}{\partial t^2} \tag{2-2-1a}$$

$$\nabla^2 u_y(\mathbf{r},t) = \frac{1}{v^2}\frac{\partial^2 u_y(\mathbf{r},t)}{\partial t^2} \tag{2-2-1b}$$

$$\nabla^2 u_z(\mathbf{r},t) = \frac{1}{v^2}\frac{\partial^2 u_z(\mathbf{r},t)}{\partial t^2} \tag{2-2-1c}$$

where v is the propagation velocity.

In the Cartesian system, $u_x(\mathbf{r},t)$ and $u_y(\mathbf{r},t)$ are the transverse components and $u_z(\mathbf{r},t)$ is the longitudinal component. If the wave propagates along the z direction only, only transverse components exist. Therefore, the optical field in free space is described by the following:

$$u_x(\mathbf{z},t) = u_{0x}\cos(\omega t - \mathbf{k}z + \delta_x) \tag{2-2-2a}$$

$$u_y(\mathbf{z},t) = u_{0y}\cos(\omega t - \mathbf{k}z + \delta_y) \tag{2-2-2b}$$

where u_{0x} and u_{0y} are the maximum amplitudes and δ_x and δ_y are the phases of the oscillation. By introducing the propagator, $\tau = \omega t - kz$, the transverse components are rewritten as follows:

$$E_x(\mathbf{z},t) = E_{0x}\cos(\tau + \delta_x) \tag{2-2-3a}$$

$$E_y(\mathbf{z},t) = E_{0y}\cos(\tau + \delta_y) \tag{2-2-3b}$$

$E_x(z,t)$ and $E_y(z,t)$ are the vectors of the oscillation on the x and y directions of the optical field. The resultant vector from $E_x(z,t)$ and $E_y(z,t)$ forms a locus, which will be described and rewritten as follows:

$$\frac{E_x}{E_{0x}} = \cos\tau\cos\delta_x - \sin\tau\sin\delta_x \tag{2-2-4a}$$

$$\frac{E_y}{E_{0y}} = \cos\tau\cos\delta_y - \sin\tau\sin\delta_y \tag{2-2-4b}$$

$$\frac{E_x}{E_{0x}}\sin\delta_y - \frac{E_y}{E_{0y}}\sin\delta_x = \cos\tau\sin\left(\delta_y - \delta_x\right) \tag{2-2-5a}$$

$$\frac{E_x}{E_{0x}}\cos\delta_y - \frac{E_y}{E_{0y}}\cos\delta_x = \sin\tau\sin\left(\delta_y - \delta_x\right) \tag{2-2-5b}$$

$$\frac{E_x^2}{E_{0x}^2} + \frac{E_y^2}{E_{0y}^2} - 2\frac{E_x}{E_{0x}}\frac{E_y}{E_{0y}}\cos\delta = \sin^2\delta \tag{2-2-6}$$

$$\delta = \delta_y - \delta_x$$

This is an equation of an ellipse which is called the polarisation ellipse. This ellipse equation describes the polarisation of a light as E_{0x}, E_{0y} and δ defines the polarisation characteristic. There are four special forms of polarisation which can be described by the polarisation ellipse equation. The conditions are as follows:

1. $E_{0y} = 0$

$$E_x(z,t) = E_{0x}\cos\left(\tau + \delta_x\right) \tag{2-2-7a}$$

$$E_y(z,t) = 0 \tag{2-2-7b}$$

The two transverse component equations show that there is oscillation only in the x direction. This is called linear horizontally polarised light. Similarly, if $E_{0x} = 0$, $E_y \neq 0$, then oscillation only occurs in the y direction and is called linear vertically polarised light.

2. $\delta = 0$ *or* π

$$\frac{E_x^2}{E_{0x}^2} + \frac{E_y^2}{E_{0y}^2} \pm 2\frac{E_x}{E_{0x}}\frac{E_y}{E_{0y}} = 0 \tag{2-2-8a}$$

$$\left(\frac{E_x}{E_{0x}} \pm \frac{E_y}{E_{0y}}\right)^2 = 0 \tag{2-2-8b}$$

$$E_y = \pm\left(\frac{E_{0y}}{E_{0x}}\right)E_x \tag{2-2-8c}$$

Equation (2-2-8) represents a straight line with a slope $\pm\left(\frac{E_{0y}}{E_{0x}}\right)$ on the polarisation ellipse. It indicates the linearly polarised light with slope $\pm\left(\frac{E_{0y}}{E_{0x}}\right)$. The $\delta = 0$ gives a negative slope and $\delta = \pi$ gives a positive slope. When $E_{0x} = E_{0y}$, the slope is +1 or -1,

which represents *linear +45° polarised light* and *linear -45° polarised light* respectively.

3. $\delta = \frac{\pi}{2}$ *or* $\frac{3\pi}{2}$

$$\frac{E_x^2}{E_{0x}^2} + \frac{E_y^2}{E_{0y}^2} = 1 \qquad (2\text{-}2\text{-}9)$$

This gives the standard ellipse on the polarisation ellipse.

4. $E_{0x} = E_{0y} = E_0$ *and* $\delta = \frac{\pi}{2}$ *or* $\frac{3\pi}{2}$

$$\frac{E_x^2}{E_0^2} + \frac{E_y^2}{E_0^2} = 1 \qquad (2\text{-}2\text{-}10)$$

This is an equation of a circle. When $\delta = \frac{\pi}{2}$, the light is *right circularly polarised*, and $\delta = \frac{3\pi}{2}$ shows that the light is *left circularly polarised*.

2.2.3 Stokes Polarisation Parameters

Equation (2-2-6) represents the equation of the polarisation ellipse. For a monochromatic light, the equation as a function of time is written as follows:

$$\frac{E_x^2(t)}{E_{0x}^2} + \frac{E_y^2(t)}{E_{0y}^2} - 2\frac{E_x(t)}{E_{0x}}\frac{E_y(t)}{E_{0y}}\cos\delta = \sin^2\delta \qquad (2\text{-}2\text{-}11)$$

It should be noted that both amplitudes and phases are time invariant for monochromatic light, therefore they are constants in equation (2-2-11). In order to describe the wave more simply, time average is taken over the transverse components from equation (2-2-11).

$$\frac{\langle E_x^2(t)\rangle}{E_{0x}^2} + \frac{\langle E_y^2(t)\rangle}{E_{0y}^2} - 2\frac{\langle E_x(t)E_y(t)\rangle}{E_{0x}E_{0y}}\cos\delta = \sin^2\delta \qquad (2\text{-}2\text{-}12)$$

The parentheses < > represents the average function of the content function or functions. By executing the average and reorientation, (2-2-12) can be re-written as a perfect square equation:

$$\left(E_{0x}^2 + E_{0y}^2\right)^2 = \left(E_{0x}^2 - E_{0y}^2\right)^2 + \left(2E_{0x}E_{0y}\cos\delta\right)^2 + \left(2E_{0x}E_{0y}\sin\delta\right)^2 \qquad (2\text{-}2\text{-}13)$$

Equation (2-2-13) is in the form of:

$$S_0^2 = S_1^2 + S_2^2 + S_3^2 \tag{2-2-14}$$

S_0, S_1, S_2, and S_3 are called Stokes parameters [43], where:

$$S_0 = E_{0x}^2 + E_{0y}^2 \tag{2-2-15a}$$

$$S_1 = E_{0x}^2 - E_{0y}^2 \tag{2-2-15b}$$

$$S_2 = 2E_{0x}E_{0y}\cos\delta \tag{2-2-15c}$$

$$S_3 = 2E_{0x}E_{0y}\sin\delta \tag{2-2-15d}$$

These parameters can be gathered to form a vector as in the following:

$$\mathbf{S} = \begin{pmatrix} E_{0x}^2 + E_{0y}^2 \\ E_{0x}^2 - E_{0y}^2 \\ 2E_{0x}E_{0y}\cos\delta \\ 2E_{0x}E_{0y}\sin\delta \end{pmatrix} \tag{2-2-16}$$

This is called the Stokes vector for a plane wave.

2.2.4 Mueller Matrix

The Stokes parameters and the Stokes vector represent the state of a polarisation. The Mueller matrix is another mathematical expression tool, which extends from the Stokes vector. It is a transfer function matrix that represents a state change for a wave propagating through a polarising element.

If it is assumed that there is a polarised wave propagating through a polarising medium, the incident wave will have Stokes parameters of S_0, S_1, S_2, and S_3. The emerging wave after the polarising medium will have Stoke parameters S'_0, S'_1, S'_2, and S'_3. The transformation can therefore be written in to the following matrix equation:

$$\begin{pmatrix} S'_0 \\ S'_1 \\ S'_2 \\ S'_3 \end{pmatrix} = \begin{pmatrix} m_{00} & m_{01} & m_{02} & m_{03} \\ m_{10} & m_{11} & m_{12} & m_{13} \\ m_{20} & m_{21} & m_{22} & m_{23} \\ m_{30} & m_{31} & m_{32} & m_{33} \end{pmatrix} \begin{pmatrix} S_0 \\ S_1 \\ S_2 \\ S_3 \end{pmatrix} \tag{2-2-17a}$$

$$\mathbf{S}' = \mathbf{M} \cdot \mathbf{S} \tag{2-2-17b}$$

The 4 by 4 matrix **M** is the Mueller matrix.

2.2.5 Jones Vector/Matrix

The Jones vector and Jones Matrix are the tools of describing the polarisation states. The difference between the Jones and the Mueller is that Jones Matrix involves the complex terms while Mueller matrix only deals with real numbers.

The transverse components of a plane wave with complex terms in the optical field can be written as the fowling:

$$E_x(z,t) = E_{0x} e^{i(kz-\omega t+\delta_x)} \tag{2-2-18a}$$

$$E_y(z,t) = E_{0y} e^{i(kz-\omega t+\delta_y)} \tag{2-2-18b}$$

The Jones vector is formed by combining these two equations with the propagator term $kz - \omega t$ being removed.

$$\mathbf{E} = \begin{pmatrix} E_x \\ E_y \end{pmatrix} = \begin{pmatrix} E_{0x} e^{i\delta_x} \\ E_{0y} e^{i\delta_y} \end{pmatrix} \tag{2-2-19}$$

Note that E_x and E_y are complex quantities because the exponential terms. The total intensity **I** of the superposed wave in the filed can be found from the Jones vector:

$$\mathbf{I} = \begin{pmatrix} E_x^* & E_y^* \end{pmatrix} \cdot \begin{pmatrix} E_x \\ E_y \end{pmatrix} \tag{2-2-20}$$

For a wave propagating through a medium, assume the emerged components are linearly related to the incident ones, and then the relation can be described by the following matrix equation:

$$\begin{pmatrix} E_x' \\ E_y' \end{pmatrix} = \begin{pmatrix} j_{xx} & j_{xy} \\ j_{yx} & j_{yy} \end{pmatrix} \begin{pmatrix} E_x \\ E_y \end{pmatrix} \tag{2-2-21a}$$

$$\mathbf{E}' = \mathbf{J} \cdot \mathbf{E} \tag{2-2-21b}$$

The 2 * 2 matrix **J** is the Jones matrix.

2.2.6 Polariser

There are many ways to produce a polarised light. One practical method is using a polariser with the unpolarised light source. The principle of polarisation using a polariser is to transmit one component of the unpolarised light and rejects its orthogonal. There are different classes of polarisers and some of these will be introduced here.

Based on the type of polarisation required, there are linear, circular and elliptical polarisers. If a polariser contains a single uniform layer, it is called a homogeneous polariser. If a polariser contains more than one layer, it is called inhomogeneous or multilayer polariser [41]. Polarisers can be categorised into four types: dichroic polarisers, birefringence polarisers, reflection polarisers and scattering polarisers.

Dichroic is the most important and major type of polariser. It is based on the dichroism optical mechanism. When an unpolarised light propagates through the dichroic polariser, the orthogonal of the transmitted component will be absorbed by the polariser and hence the light is polarised. The dichroic polariser is an important component in the liquid crystal display (LCD) [44].

The birefringence polariser polarises the light by splitting the incident wave into two components. These two components are polarised orthogonal to each other. One component is transmitted through the polariser while the other one is reflected or absorbed internally.

If a monochromatic beam propagates to a glass or dielectric surface with an angle, the beam will be split into reflected and the refracted beam. Both cases are partially linearly polarised. Hence, the reflection polariser could be made with several glass or dielectric material surfaces, or a single interface at the Brewster angle. .

An incident light that passes through scattering particles, such as dust in the air and gas molecules, may be polarised. This applies to the scattering polariser. Another example is the metallic wire gratings. If the spacing between the gratings is significantly smaller than the light wavelength, the grating could be a good polariser to this light. In this thesis project, the metallic wire grating polariser is applied as the fabricated data pattern on optical disc. This polariser is chosen because the simplicity of the polariser structure and the convenience of the nano-fabrication.

2.3 Finite-Difference Time-Domain Method

There are several ways of solving the electromagnetic field problems such as experimental and numerical methods. Experimental methods are expensive on resources and time. The numerical methods find approximated solutions but they are efficient. The finite difference time domain (FDTD) technique is one numerical method for computational calculation of the electromagnetic problems [45]. It is

capable of calculating the complex electric and magnetic fields in a reasonable time period with the massive computer power today.

The finite difference method is a technique that uses approximations to solve the partial differential equations (PDE) [46, 47]. This method finds the solution by following three steps: divide the field into a grid of cells, finds the finite difference equivalent of the differential equation which describes the field, solve the difference equations base on the boundary and initial conditions[48].

2.3.1 Cell size

Before forming a grid, the cell size must be defined. The Nyquist sampling theory states that at least two samplings are required per wavelength to obtain a significant result. Disobeying the theory may result in aliasing errors. There are researches about the technique to reduce this error [49]. The standard cell size that is required in FDTD is 1/10 of the shortest wavelength of interest. The smaller the cell size is the more sampling nodes are calculated and the better accuracy the result is. For example the radar scattering field calculation may require 1/20 wavelength cell size for an accurate estimation. However, the higher sampling rate consumes more computer power and resources, hence non-uniform cell size may be used for some situations [50]. A smaller cell size is used in higher density fields and larger cell size is used in blank or low density fields. There are researches about how to determine the cell size for particular situations such as modelling ferrites and lossy materials [51]. In this thesis, the experiment uses 10nm cell size for all simulations where the source has a wavelength of 650nm.

2.3.2 Time Step

The time step size is a factor that relates to the simulation stability. The maximum time step size can be determined by the Courant condition after the cell size is confirmed [52]. For a three dimensional field and cubical cells, the Courant stability condition is:

$$\Delta t = \frac{\Delta x}{\sqrt{3c}}, \qquad (2\text{-}3\text{-}1)$$

where c is the light speed and Δx is the cell side dimension [50].

An oversized time step may cause the wave component of interest to exist in more than one simulation cell. This will result the simulation becoming unstable. In this thesis, the time step size is calculated and set by the simulation program automatically. Each time step is 17.33as (1as = 10^{-18}s).

2.3.3 Boundary Conditions

In the real world, electromagnetic phenomena usually exist in an open space, however, the FDTD method calculates the effect in a closed domain. Hence, there is the need to apply boundary conditions in the FDTD method. In such bounded space, the simulated component will be absorbed or reflected from the boundary. Also, the simulation cells at the boundary of the grid require the neighbouring cells for estimating the calculation result. The boundary condition therefore is important to the FDTD simulation.

There are many types of boundary condition. The absorbing boundary condition (ABC) is a common types and there are many researches about the stability of it [53]. Other boundary type such as the perfectly matched layer (PML) boundary condition can be used to simulate the 2D and 3D electromagnetic fields [54].

2.3.4 Dispersive Materials

The FDTD method is commonly used in a wide range of science and engineering fields. One important use of FDTD is to simulate the wave propagation and its reaction to dispersive materials [55]. They are materials with dielectric properties that depend on the incident frequency [56]. Three dispersion models, Debye, Drude and Lorentz, will be introduced here.

Debye Dispersion

The first order Debye model contains one first order pole. The Debye medium as a susceptibility function is shown in equation (2-3-2) [57].

$$\chi(\omega) = \frac{\varepsilon_s - \varepsilon_\infty}{1 + j\omega t_0}, \qquad (2\text{-}3\text{-}2)$$

where ε_s is the static permittivity, ε_∞ is the inifinite frequency permittivity and t_0 is the pole relaxation time. It could also be described by the complex relative permittivity as shown in equation (2-3-3) [50].

$$\hat{\varepsilon}(\omega) = \varepsilon' - j\varepsilon'' = \varepsilon_\infty + \frac{\varepsilon_s - \varepsilon_\infty}{1 + j\omega t_0} = \varepsilon_\infty + \chi(\omega), \tag{2-3-3}$$

where $\hat{\varepsilon}$ is the complex relative permittivity, ε' and ε'' are the real and imaginary components respectively. The relative permittivity can be calculated by the refractive index n and constant k [30, 58]:

$$\begin{aligned} \varepsilon' &= n^2 - k^2 \\ \varepsilon'' &= 2nk \end{aligned} \tag{2-3-4}$$

Drude Dispersion

The Drude dispersion model of the susceptibility function is shown in equation (2-3-5) [50]:

$$\hat{\varepsilon}(\omega) = 1 + \frac{\omega_p^2}{\omega(jv_c - \omega)} = \varepsilon_\infty + \chi(\omega), \tag{2-3-5}$$

where ω_p is the radian plasma frequency and v_c is the collision frequency. This function has two poles, $\omega = 0$ and $\omega = jv_c$.

Lorentz Dispersion

The previous two models are the first order dispersion examples. The Lorentz models the second order dispersive materials and is introduced here in equation (2-3-6):

$$\hat{\varepsilon}(\omega) = \varepsilon_\infty + (\varepsilon_s - \varepsilon_\infty)\frac{\omega_p^2}{\omega_p^2 + 2j\omega\delta_p - \omega^2}, \tag{2-3-6}$$

where ω_p is the undamped resonant frequency of the pole pairs and δ_p is the damping coefficient. This equation has one pair of second order Lorentz poles.

2.4 XFDTD

XFDTD is a three-dimensional full-wave electromagnetic analysis software package that was used in this work. Its algorithm is based on the finite different time domain (FDTD) method. The software is applicable for a wide range of areas such as communication devices, optics and biomedical devices.

The core of the XFDTD software is based on the FDTD method. There are four steps to conduct a XFDTD simulation. They are defining the geometry, setup of the

simulation parameters, requesting the results and analysing the results. The details of each step will be expressed in the following sub-section.

2.4.1 Geometry

To start a XFDTD simulation, the first step is creating the geometry. To a simulation, the geometry is a combination of the grid and the simulation object. The grid is defined by setting up the dimension of the simulation space in the number of cells. There are three fundamental settings required for defining a grid. They are grid type, cell size and grid size. Additional settings for specific requirements are also available. The details will be expressed in the following and referred to Figure 8. The simulation object can be created only after the grid is constructed.

Three options can be chosen for the grid type. The first and the default one is auto. By choosing this option, the program will detect if there is magnetic material and define the grid type automatically. The second option is electric grid type. This is the general grid type for simulating non-magnetic materials. In this grid type, only an electric mesh will be created by the program. The last option is dual grid, which is a situation when magnetic materials are present. This creates one magnetic material mesh and one electric material mesh for placing the simulation objects. In this project, the electric grid is used as there is no magnetic material applied.

On top of the grid type is the grid units as shown in Figure 8. This box defines the unit of the cell dimension. Nanometers is chosen in this project because the desired pattern dimension and the source wavelength are best defined in these units.

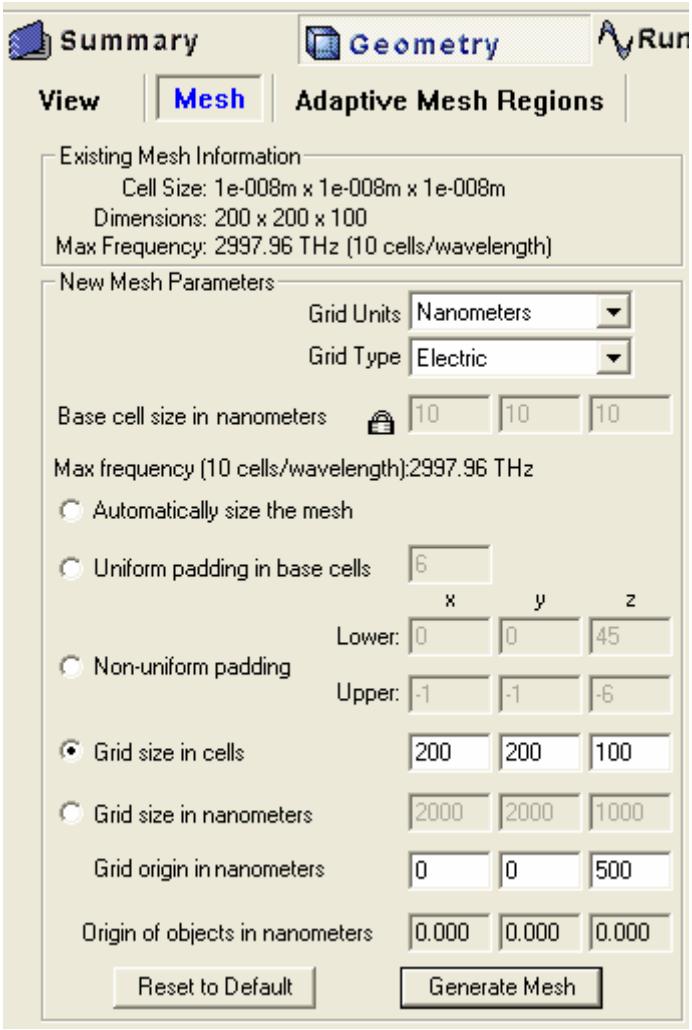

Figure 8: Geometry setting field in XFDTD.

The cell is the basic space unit in the simulation grid. The cell size is the dimension of the unit box. To the program, the cell size determines the simulation time steps and the maximum allowed frequency. Hence, there is a limitation of defining the cell size. For the simulation to be significant there must be ten or more cells per source wavelength. In other words, the cell size must not exceed one tenth of the wavelength. In this project, the cell size is 10nm in each dimension. This allows the maximum frequency to be around 3000THz. The simulation source in this project is 650nm in wavelength and 461.538THz in frequency, so the cells are always less than one tenth of the wavelength.

The dimension of the simulation space is defined by the grid size. The rectangular space is created by defining the value of the three dimensions. There are two ways to specify the grid size, the grid size in cells or the grid size in the grid unit. The first

method allows user to define the space with the number of cells in each axis. The second method allows entering the actual length of each axis.

The mesh can be generated after the grid settings are defined. The simulation objects can then be constructed upon this mesh. The principle of the object design is similar to other CAD design programs.

There are three requirements for defining an object: the shape, the dimension and the material. XFDTD provides a library which contains various shapes for the user to choose from, which include block, cylinder, pyramid and sphere as the basic 3D shapes. Others like helix and spiral antenna are the shape for specific simulation use. There is also plate and quad plate for 2D object simulations. The polariser strips in this simulation are modelled by rectangular blocks. It requires three coordinates and the thickness to define the block dimension and its position in the simulation grid as shown in Figure 9. In the block creating menu, the material can also be chosen. The material is required to be customised if the choice is other than free space or perfect electric conducting (PEC).

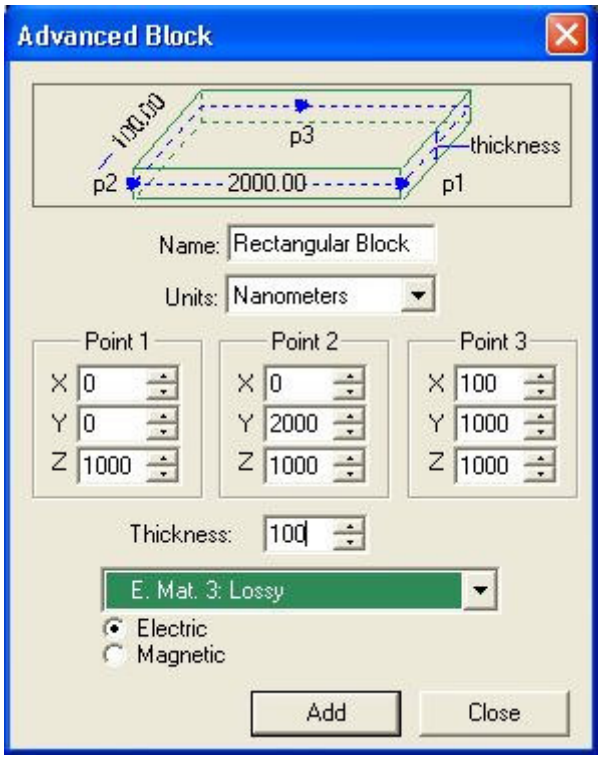

Figure 9: Block setup menu for creating the block shape simulation object.

The object material can be added or edited form the material selection field as shown on the left hand side of Figure 10. The drop down menu allows the user to change or

define the material of the selected object or objects. It also allows the user to create a new material. The first step of creating a new material is choosing the represented colour as shown on the right hand site of Figure 10. The parameter editing menu, as shown in Figure 11, will be bought out after the colour is confirmed.

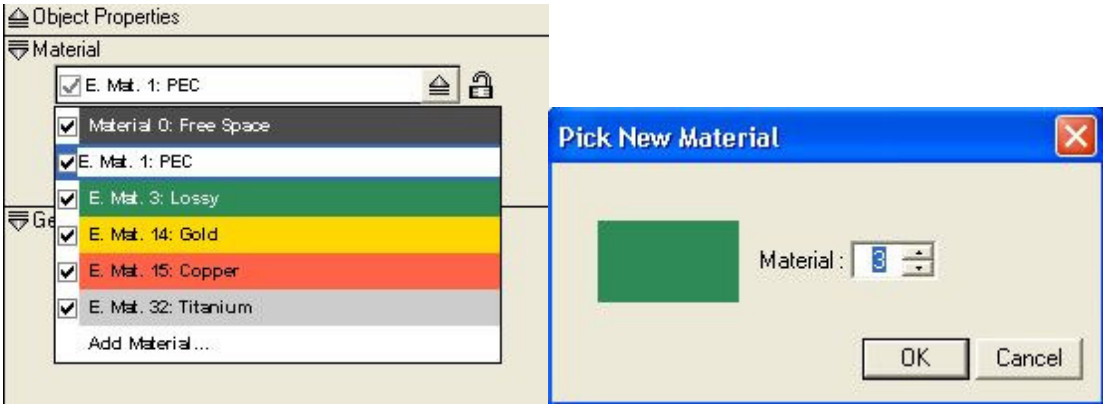

Figure 10: Material selection field and new material creating window.

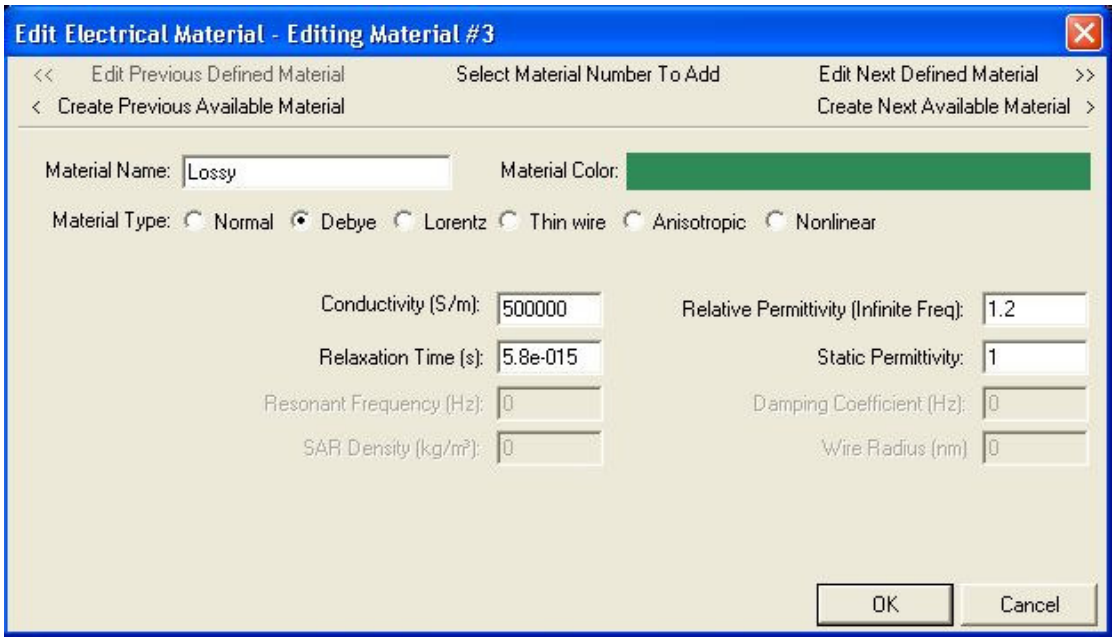

Figure 11: Material parameters editing menu.

The top two fields in the material editing window indicate the material name and colour. Below the two is the material type selection tick. There are five material types to choose from, where *Normal*, *Debye* and *Lorentz* are the three common types.

The *Normal* type models the material with only the basic parameters. To define a *Normal* material requires conductivity, relative permittivity and SAR density. SAR stands for specific absorption rates [38]. The *Normal* material type is used when the material properties do not change with frequency.

All the simulation objects in this project are modelled by the *Debye* material type, which is used for frequency-dependent (dispersive) materials. The *Debye* material type requires four parameters: conductivity, relative permittivity, relaxation time and static permittivity. This material type models the materials based on the first order *Debye* dispersion. It is a material with complex permittivity which can be described by an equation with one first order pole [38].

2.4.2 Run Parameters

The simulation grid and objects were defined in the geometry setup. Once the geometry is created, the run parameter tab is available. The run parameter setup defines the properties of the source. The run parameter tab includes four sub-tabs such as waveform, source type, components/ports and outer boundary.

Waveform

The waveform setup page, as shown in Figure 12, provides the choices of waveform type for the simulation. There are five waveform types which are Gaussian, Gaussian derivative, modulated Gaussian, sinusoid and user defined. The first three types of Gaussian waveforms provide a single pulse to the simulation. In the Gaussian waveform, the user is required to define the pulse width and the surface conductivity frequency. The pulse width is the number of time steps to define the width of the Gaussian pulse input [8].

The Gaussian derivative waveform is very similar to the Gaussian one. The only difference is that the Gaussian waveform is a single positive pulse and the Gaussian derivative is a single sine wave. As written the Gaussian waveform, the Gaussian derivative requires the setting of pulse width and the surface conductivity frequency.

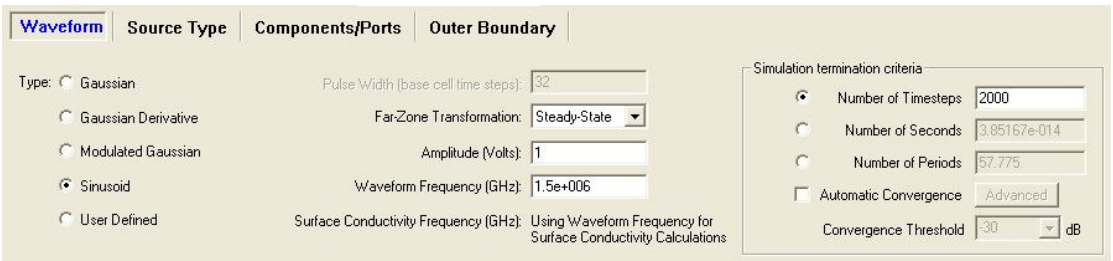

Figure 12: The waveform selection and setup.

The modulated Gaussian waveform is a sinusoidal waveform with a Gaussian envelope. There is one more requirement for defining a modulated Gaussian

waveform than the previous two Gaussian waveforms. It is the waveform frequency. For a higher waveform frequency, there are more waves in the wave envelope. This waveform frequency is limited by the cell size. This waveform is useful when a specific frequency range is desired [8].

The sinusoid waveform is used for one specific frequency. It does not require surface conductivity frequency as the waveform frequency is used for such calculation. The far-zone transformation is required to choose between the transient, steady-state and none. The steady-state is the default most common option of the far-zone transformation. It provides the most flexibility of the far-zone simulations. The transient is desired when far-zone time-domain fields required. However, the transient far-zone transformation is not available if any of the outer boundaries is perfect electric conducting (PEC) or perfect magnetic conducting (PMC).

Spatial Source Type

There are three spatial source types that can be chosen in XFDTD. They are discrete sources, plane wave and Gaussian beam. Each type is designed for specific simulations. All three of them have different setup parameters.

The discrete source is used when there is a voltage or current source as the input in the simulation. The voltage and current sources are available in the components/ports tab if the discrete source is selected. The voltage or current source is the port. And it requires at least one port in order to perform the discrete source simulation.

Plane wave source type provides a plane wave input source to the simulation. The plane wave source is polarised either in EPhi (phi) or ETheta (theta) polarisation. In phi polarisation, the electric field of the source has direction along the Y axis. As shown in Figure 13, the phi polarisation results the electric field incident amplitude in E_y to be 1.00 V/m and E_x and E_z to be 0 V/m. If theta polarisation was selected, the electric field direction is along the X axis.

In the plane wave and the Gaussian beam source types, the propagation direction can also be chosen. The incident direction panel has two fields for setting the propagation angles. The field phi controls the propagation angle along the Y axis and field theta controls the angle along X axis. If the plane wave or the Gaussian beam is selected, the amplitude field in waveform tab will be active. It allows the user to enter desired incident amplitude.

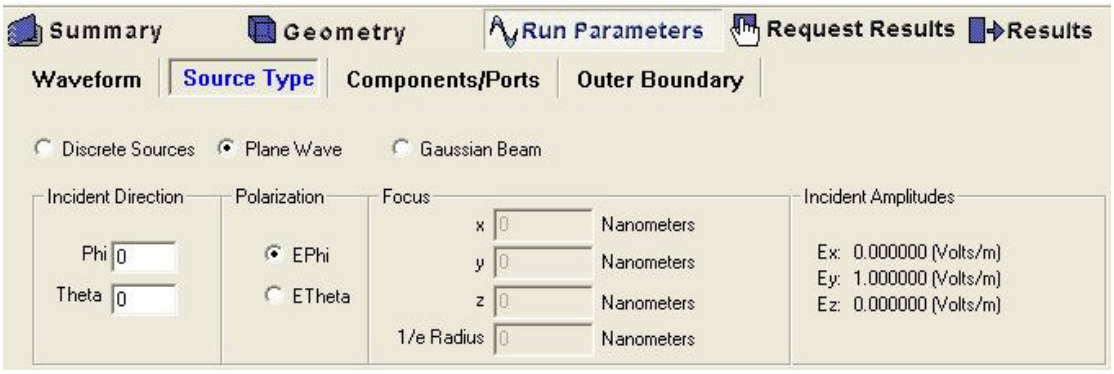

Figure 13: The source type selection window (plane wave).

The last type of source is the Gaussian beam. When the Gaussian beam is selected, the waveform can only be a sinusoid. The focus field will become available if the source type is Gaussian beam. The focus field includes the focusing spot co-ordinates and its radius.

Outer Boundary

The boundary conditions of the simulation space can be set in XFDT. The six boundaries can be defined individually. There are three types of boundary condition available. They are absorbing, PEC and PMC. And there are two types of absorbing boundary as Liao and the perfect matched layers (PML). In the simulation calculation, the boundary conditions can be mixed with absorbing, PEC or PMC, however, the two absorbing types cannot be mixed. The Liao absorbing boundary is the default boundary condition and was commonly used in simulations of this project as it models an open space that has no reflection from the boundaries.

2.4.3 Request Results

Requesting the result is the last step of setup before running the simulation. It sets up the type of measurements. There are four types of data that can be requested in XFDTD. They are near-zone data, far-zone data, transient field snapshots and steady-state data. The near-zone data and the transient field snapshots were used in the simulations of this project. The data from these two measurements were the key information for analysing the performance.

In the simulation, only the specified measurements will be recorded as the XFDTD will potentially generate massive amounts of data. For example a 50 * 50 * 50 grid contains 125,000 cells for measuring. Each cell has three components X, Y and Z in electric field, magnetic field and current field. This generates 1.125MB data in one

simulation time step. For a general 2000 time steps simulation, it could generate up to 2.25GB data. Hence, a wise placement of the measurement points is a time and resource saving method for recording the simulation results.

Save Near-Zone Data

Save near-zone data measures and saves the near-zone electric field or magnetic field quantity. The measuring point can be placed anywhere in the simulation space by entering the co-ordinates in the location field. Each measuring point will measure a component, for example E_x, of the field magnitude. There are three types of quantity able to be measured, the electric field, the magnetic field and the current. For the electric field and the magnetic field, the scattered field or total field can be chosen for measuring. Each measurement point measures one quantity at each time step during the simulation. After the simulation is finished, the series of measurements will be stored in a file with the field magnitude and respective simulation time.

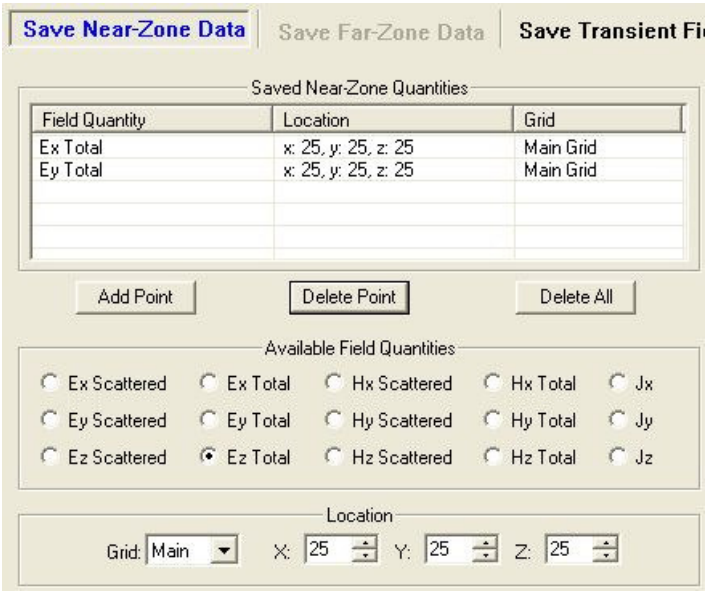

Figure 14: The save near-zone data tab for defining the measuring points.

Save Transient Field Snapshots

The Save Transient Field Snapshots tab allows the users to gather a sequence of snapshots of the desired field. As shown in Figure 15, the snapshot direction and location can be selected in the location field. This provides three directions of snapshots as XY, YZ and ZX planes. The slice number indicates the location of the snapshots that will be taken. There are three settings in the time steps field. The beginning time step indicates the first time step of taking the snapshots and the ending

time step indicates the last. The increment defines the period in time steps between any two snapshots.

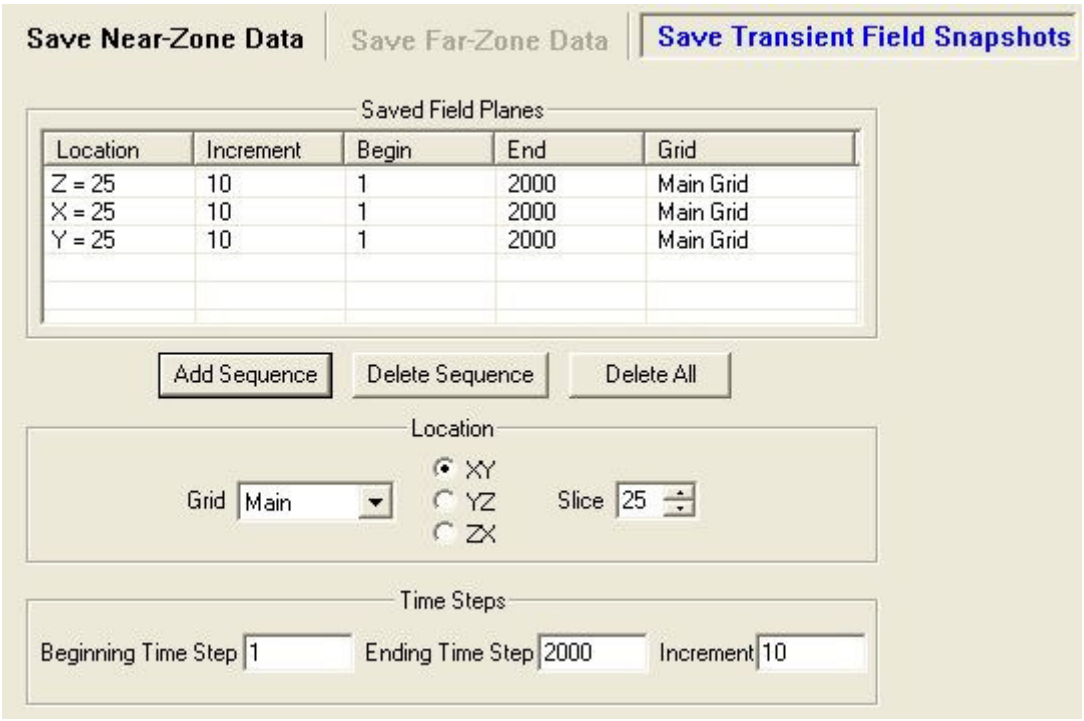

Figure 15: The save transient field snapshots window.

Each snapshot is an illustration of the 2D field profile. The sequence of snapshots creates an animation about the field variation. This result will be available from the field view command under geometry tab after the simulation.

2.4.4 Results

After all the settings are completed and saved, the simulation is ready to be performed. The *Run Calculation* sub-tab is under the results tab. The simulation starts when the *Calculate* button in the calculation window, as shown in Figure 16, is pressed. The calculation window displays the simulation progress while the simulation is running and shows a brief report after the calculation is completed.

The simulation time depends on many factors, such as the total time steps, the simulation grid size, the complexity of the simulation objects and the number of results requested. The grid size of the simulation in Figure 16 is 50 * 50 * 50 cells and the simulation lasts for 2000 time steps. There is no simulation objects present in such simulation. The requested results are shown in Figure 14 and Figure 15. The

simulation takes one minute and 30 seconds to calculate for a Pentium 4 2.8GHz processor.

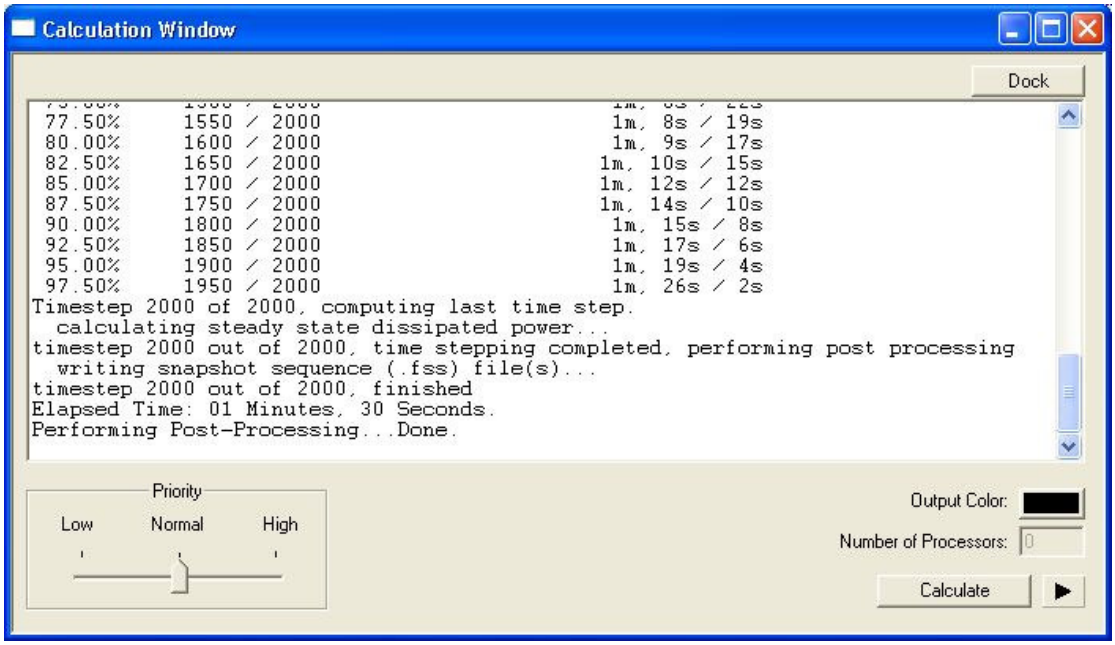

Figure 16: The calculation window showing the progress of the running simulation.

After the simulation is completed, the calculation results will be saved into files for future use. The near-zone data are saved into .g0 files. The transient field snapshots are saved into .fss files.

Transient Field View

The transient field snapshots are saved as a sequence of files. These files can then be loaded by XFDTD from the field control panel, as shown in Figure 17. All the sequences are listed in the transient field sequence. After a sequence is loaded, the *Field Sequence* control panel is enabled for playing the animation or viewing the snapshots of any sampled time step. Figure 18 is an example of the snapshot. This snapshot is taken from the XZ plane of a sinusoid plane wave source. The wave propagates along the Z axis from the positive direction towards the origin. The colour from the wave indicates the magnitude of the electric field. The colour bar below shows the magnitude scales.

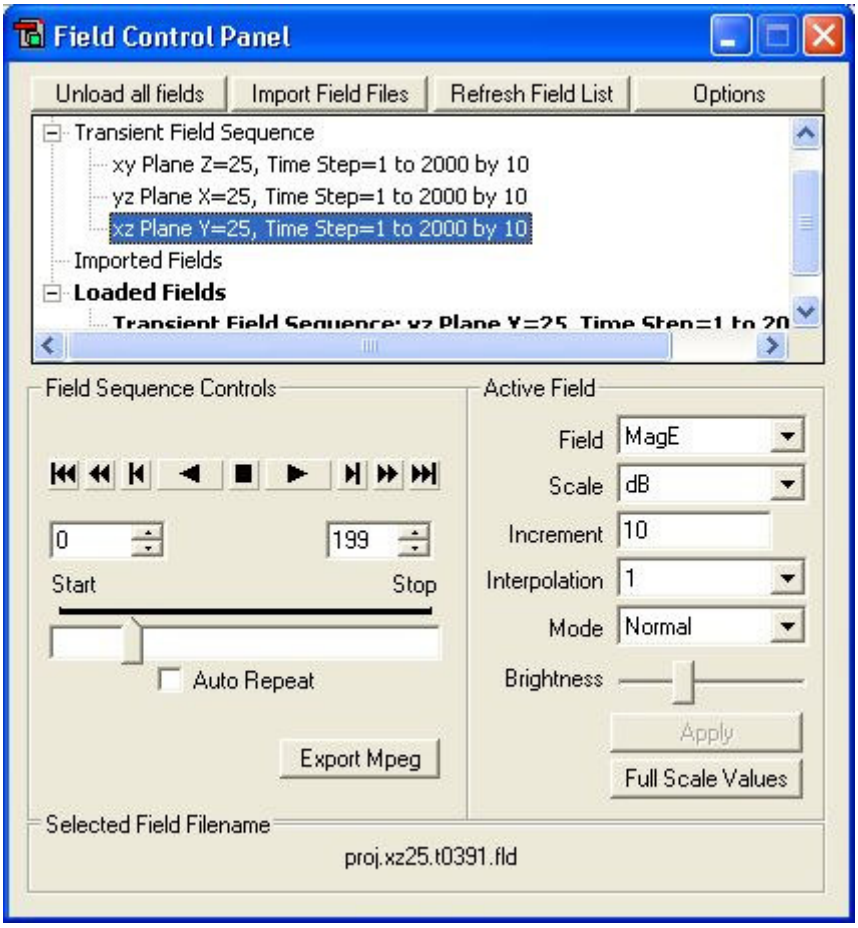

Figure 17: Field control panel for loading transient field snapshots.

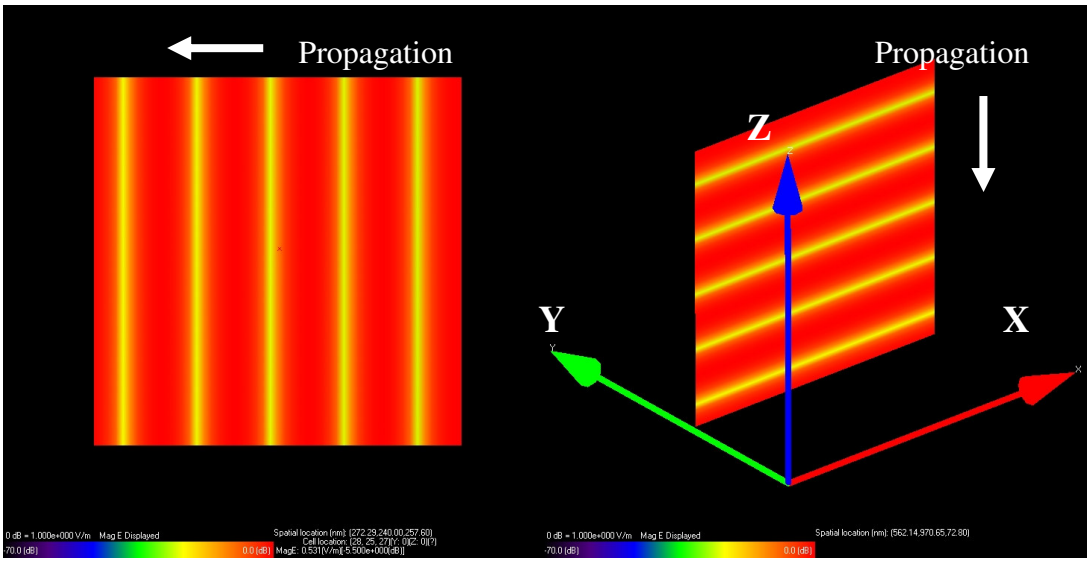

Figure 18: Transient field snapshot of a plane wave propagation.

The active field on the right hand side in Figure 17 provides the display options of the snapshots. The field selection field has the options from electric field, magnetic field and currents. Each type of field can be displayed in total magnitude or magnitude in a

single direction component. The scale field defines the display range of the magnitude. The scale can be either linear or dB. If the linear scale was selected, the colour scale bar on the bottom of Figure 18 indicates the wave magnitude in percentage of the source. Black is 0% and red is 100%. If the dB scale was selected, the colour bar shows the magnitude in dB. Black is -70dB and red is 0dB. The scale range can be adjusted from the full scale values button.

Near-Zone Data

The near-zone data are saved into a text file. The format has two fields as simulation time and field magnitudes. These data are imported into MATLAB programs for calculation and analysis. The program codes are attached in Appendix I. For each simulation, there are a number of near-zone data measurement points for analysing the field at different places. The program could load all of these near-zone data files at the same time. In order to calculate the performance of the simulation, the program requires the input data files and output data files. To the simulation, the input data file is the near-zone data of the control wave. It is the true wave propagation without any simulation object in the simulation grid. The output data file is the measured data from the simulation that does have the simulation objects. In the simulation, both E_x components and E_y components are requested for the near-zone data. Therefore the results can be used to calculate both the transmission coefficients and the crosstalk coefficients for the polarising elements that have been studied.

Figure 19 is an example of the loaded near-zone data file, plotted from the MATLAB program. The plot shows the sinusoidal plane wave propagation through the middle of the simulation grid (at point 25, 25, 25 of the 50 * 50 * 50 cells grid). The propagation took about 1fs to reach the measuring point, and the wave reached the steady-state and the maximum magnitude at about 5fs simulation time. The 2000 time steps are equivalent to 38.5fs simulation time.

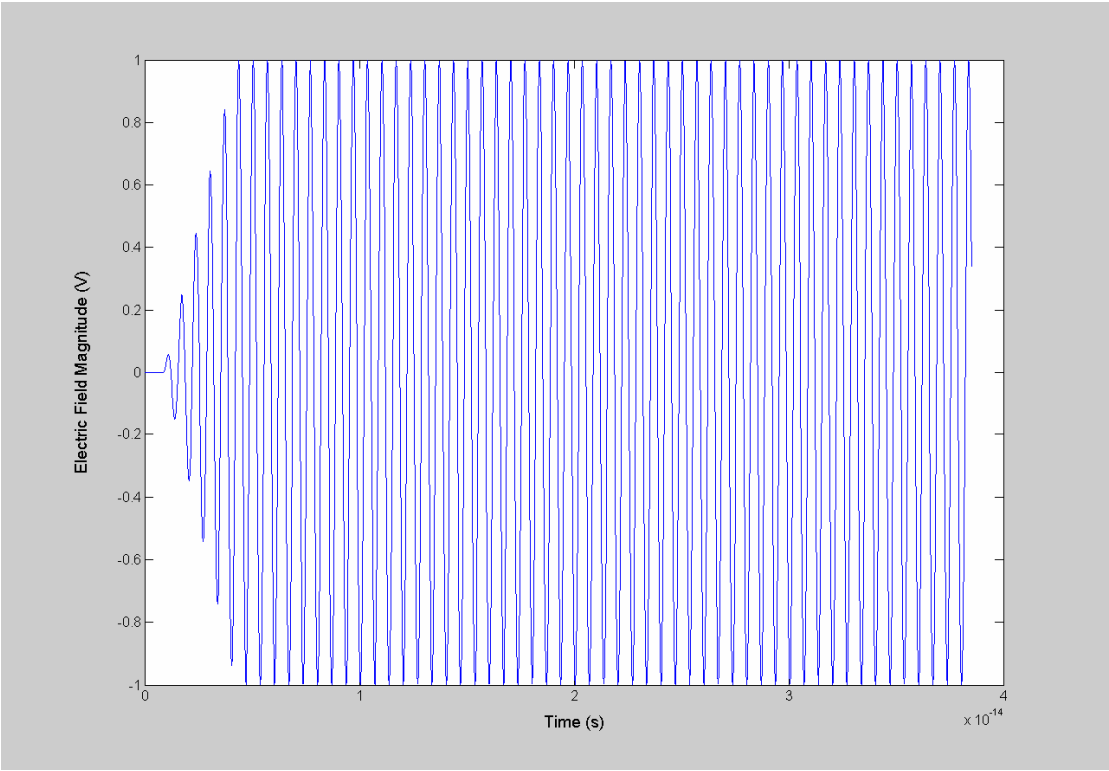

Figure 19: Near-zone data MATLAB plot.

2.4.5 Summary

XFDTD is designed specifically for simulating electromagnetic effects. The simulation grid dimension is flexible. It could be small as angstroms or big as meters. XFDTD provides several waveforms and source types. The simulations in this project use the sinusoid plane wave and Gaussian beams as the source. There are many measurements can be performed from the XFDTD simulations. The near-zone data and the transient field snapshots are two very useful tools for analysing the field effect from the simulations. In this project, the near-zone data were imported into a MATLAB program for further calculation to find the transmission and crosstalk coefficients. The coefficients are the key figures of the design performance, and will be defined and used in the following chapters.

3.0 SIMULATION PART I

The aim of the work described in this thesis was to determine the capability and efficiency of using a polarised laser and nano-scale metallic polariser structures on CD/DVD media as the data retrieving principle. This was carried out by simulating the electric field profile of the laser and polariser with XFDTD, a commercial Finite Difference Time Domain (FDTD) simulation package [59]. The simulations focus on the polarised laser transmission coefficients and polarisation cross-talk. The factors that have been varied are the polariser period, the polariser thickness, the polariser material and the polarised laser spot size.

3.1 Basic Simulation

The purpose of the first simulation was familiarisation with the simulation program and its interface. This included the concept of simulation setup, parameter setup, and post processing for determining field profiles as well as transmission and crosstalk coefficients.

3.1.1 Simulation Parameters Setup

The first step of the simulation setup was to define the simulation geometry mesh space. The grid unit was measured in nanometres and the grid type was set to be electric. Each simulation cell size was 10nm * 10nm * 10nm, which is much smaller than the wavelength used (typically 650nm). The grid size was 50 cells * 50 cells * 50 cells, which means the overall simulation space is 500nm * 500nm * 500nm.

Once the cell size and grid size were decided, the polariser was built by defining the structure dimensions. The polariser is an array of metal strips; each of them is 500nm long, 50nm wide and placed along the Y axis, as shown in Figure 20 for a 50nm period polariser. For the initial simulations, the thickness of the patterns was 10nm and the material was set to be a perfect electric conductor (PEC).

After the mesh was generated, the run parameters could be defined. The wave type was chosen to be a continuous sinusoidal wave with a frequency of 461,538GHz (corresponding to a wavelength of 650nm). The amplitude of the wave was 1 V/m as default, noting that this is not critical as no nonlinear effects are studied. The source type was set to be a plane wave with phi and theta polarisations varied. The total

simulation time steps were 2000, which was equivalent to 38fs. The outer boundaries were all defined as absorbing.

Following the setup and simulation itself, the next step was requesting the results. Transient field snapshots were saved in order to build up the electric field view after the simulation. Three sets of snapshots were taken for three orthogonal planes: the YZ plane at X = 250nm, the ZX plane at Y = 250nm and the XY plane at Z = 200nm.

3.1.2 Theta Polarisation (X Polarised)

In the theta polarisation, the electric field oscillation is perpendicular to the polariser pattern strips. The wave is expected to propagate through the polariser with a high transmission coefficient. The simulation result field view is shown in Figure 20 for a 100nm period grating after 7.5fs simulation time.

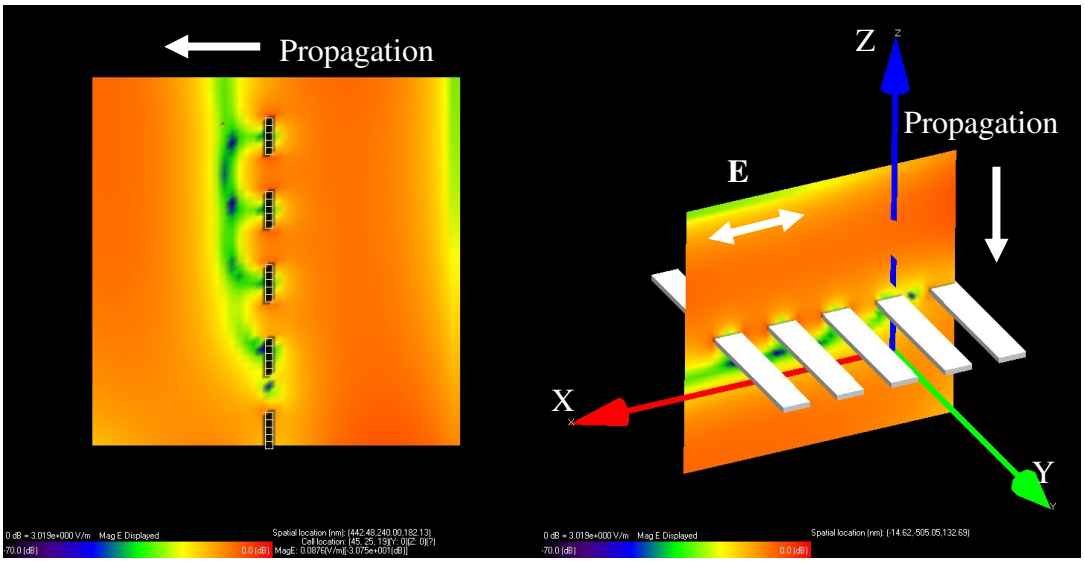

Figure 20: ZX plane field view with theta polarisation wave source. The electric field magnitudes are indicated by the colours. The colour towards red indicates high magnitude and vice versa.

Figure 20 illustrates that the magnitudes of the wave before and after the polariser are very similar. However, there is some distortion of the wave front as it passes through the polariser, as would be expected. The wave did not transmit evenly through the polariser as shown in Figure 20. This is because the polariser patterns were not placed symmetrically through the simulation field. The polariser was then replaced with a symmetrical layout, and the field plots for this situation are shown in Figure 21.

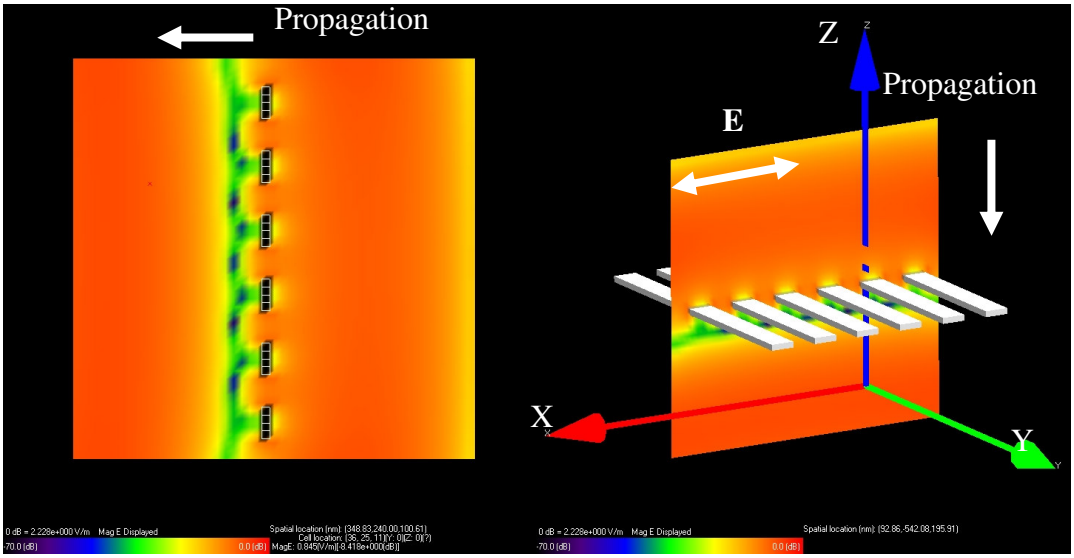

Figure 21: Theta polarisation ZX plane field view with symmetrical patterning

Figure 21 also shows the result of the theta polarised wave transmitting through the polariser without significant loss in magnitude. The wave front was distributed evenly along the simulation domain. There is identical wave pattern and colours in both sides of the wave front. This indicates there is high transmission coefficient in this polarisation as expected.

The gap between two strips was 50nm for these simulations, which is smaller than half of the incident wavelength (650nm). Therefore, there is no far field diffraction in this condition. The diffraction happens when the incident wavelength is smaller than the period of the gratings. The case where far field diffraction occurs was also simulated. The source was set to be a plane wave with a wavelength of 50nm. In order to do this, the cell size was decreased to 5nm * 5nm * 5nm and the grid size was increased to 100 cells * 100 cells * 100 cells. Therefore, the dimension of the patterns and simulation space were unchanged. The transient field snapshots were shown in Figure 22.

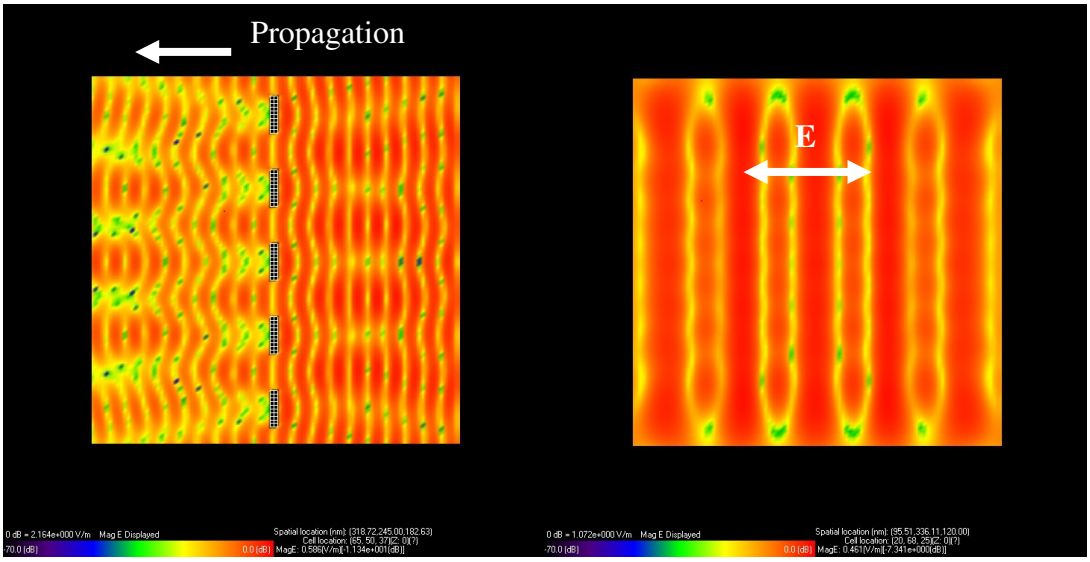

Figure 22: ZX plane and XY plane field views of theta polarised wave after 7.53001e-15 seconds simulation. There is diffraction because the incident wavelength is small.

Figure 22 shows the field view results of theta polarised incident wave with a wavelength of 50nm. There is significant far field diffraction because the wavelength was smaller than the grating period. The left hand side of Figure 22 is the ZX plane snapshot. It shows that the diffracted wave propagation spreads from the polariser. The right hand side of Figure 22 is the XY plane snapshot, which shows the cross-sectional view of the diffracted wave. The important issue to note here is that diffraction will occur if the period of the polarisers is increased above the incident wavelength.

3.1.3 Phi Polarisation (Y Polarised)

For the wave in phi polarisation, the electric field oscillates in the Y direction as shown in Figure 23, which is parallel to the polariser patterns. The expected transmission coefficient is low as the phi polarised wave excites currents along the wire, which are strongly absorbed. In addition, no phi polarised propagating waveguide mode is supported in the gaps between the wires, also contributing to the low transmission coefficient.

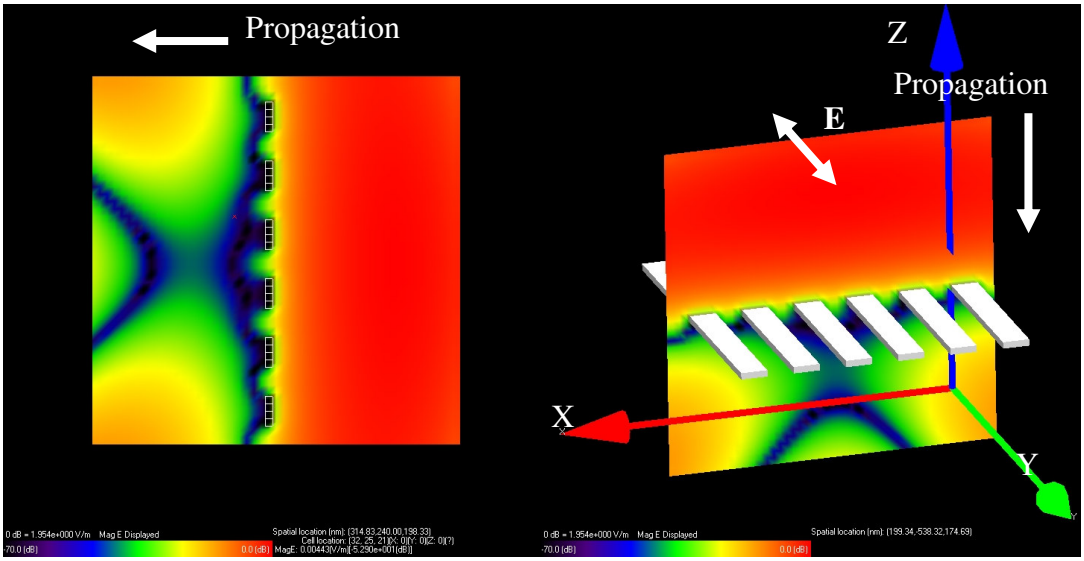

Figure 23: Phi polarisation ZX plane field view of electric field magnitudes.

Figure 23 is the ZX plane field view of the phi polarised plane wave propagation. This snapshot was taken after 1221 simulation time steps or 23.5fs. The snapshot shows that there is electric field magnitude reduction after the wave propagates through the polariser. Along the propagation direction, the field view shows red colour in front of the polariser that indicates the peak magnitude of the incident wave of approx 1.00V/m. The green and blue colours behind the polariser represent the smaller magnitudes of approx 0.30V/m. The snapshot illustrates the magnitude was lower in the middle, but stronger on the sides, which is an artefact of the artificial boundaries that must be used to surround the simulation domain.

From the same simulation, Figure 24 shows the YZ plane field view result after 23.5fs. This is strong evidence that the polariser is effective. It is notable that in the ZX plane field view the transmitted wave (the wave after the polariser) has a lower magnitude in the middle of the simulation space but a higher magnitude by the sides. But in the YZ plane, however, the emerged wave has a uniform magnitude along the Y axis. This difference can be observed more clearly from the third plane field view, shown in Figure 25.

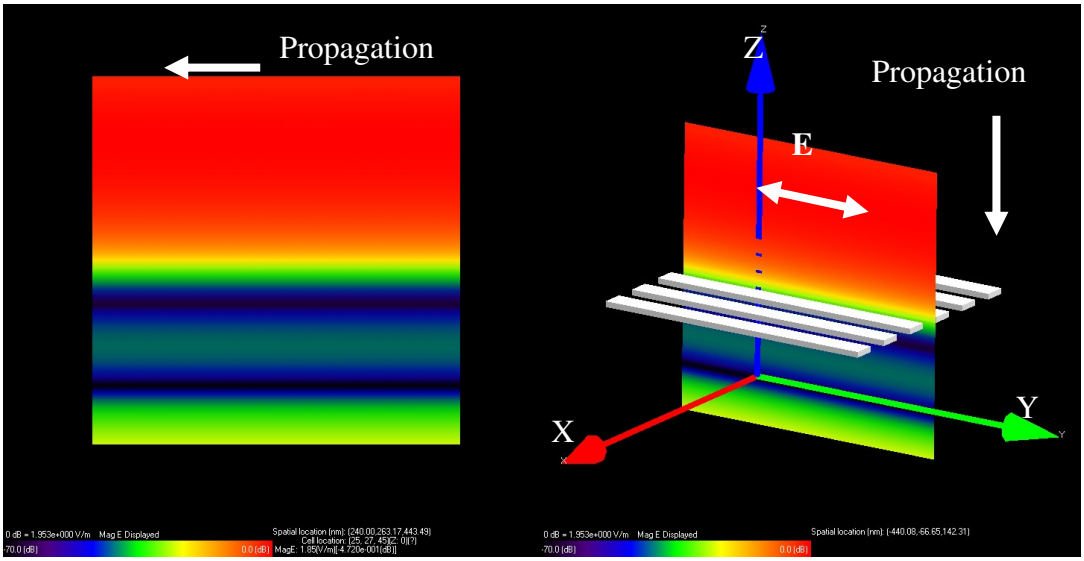

Figure 24: Phi polarisation YZ plane field view of electric field magnitudes.

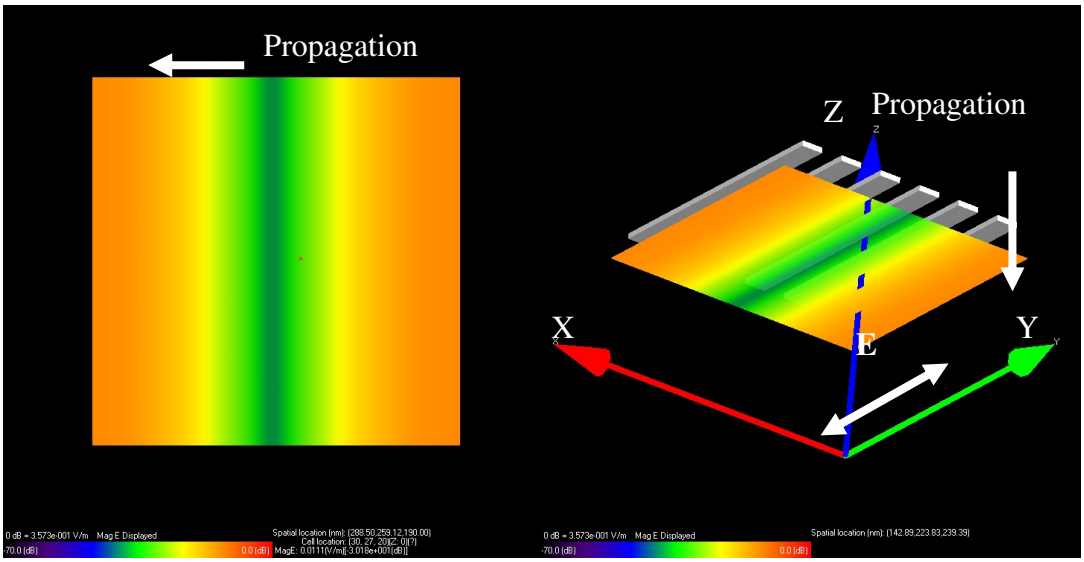

Figure 25: Phi polarisation XY plane field view of electric field magnitudes.

Figure 25 is the simulation result of the XY plane field view, also after 23.5fs. This plane view was taken at Z = 200nm, which is 50nm below the polariser. It shows the electric field magnitude after the wave had propagated through the polariser. This illustration of the result shows that the polarising effect is stronger in the middle than the two sides. Note that this is an artefact of the simulation technique as discussed earlier. The uniform magnitude along the Y axis is because the polariser orientation and the source is a plane wave.

These initial experiments simulated the electric field effect of polarised waves propagating through PEC polarisers. Both theta and phi polarisation were applied to the simulation and qualitatively returned the expected results. In the theta polarisation,

the electric field oscillation was perpendicular to the polarisers. Therefore Figure 21 shows a high transmission coefficient when the wave propagated through the polariser. Figure 23 and Figure 24 show that there is low transmission coefficient when phi polarised incident wave was applied. In this case, the electric field oscillation was parallel to the polariser gratings.

3.2 Transmission Coefficients as a Function of Polariser Period

The purpose of this experiment was to quantitatively determine the transmission coefficient when a polarised wave propagates through polarisers with different periods and orientations.

3.2.1 Simulation Parameters Setup

In this simulation experiment, the settings were very similar to the previous one. As this simulation was designed to test the transmission coefficient as a function of the polariser period, a larger simulation space was used. The overall all grid size was increased to 100 cells * 100 cells * 100 cells and the cell size remained at 10nm * 10nm * 10nm as shown in Figure 26. The wave source was kept unchanged as a plane wave at a wavelength of 650nm.

The simulation patterns were rectangular objects 1000nm long (along the Y axis) and 10nm thick. The pattern width to gap ratio was kept at 50/50. The pattern width and gap varied from 20nm to 100nm with 20nm steps.

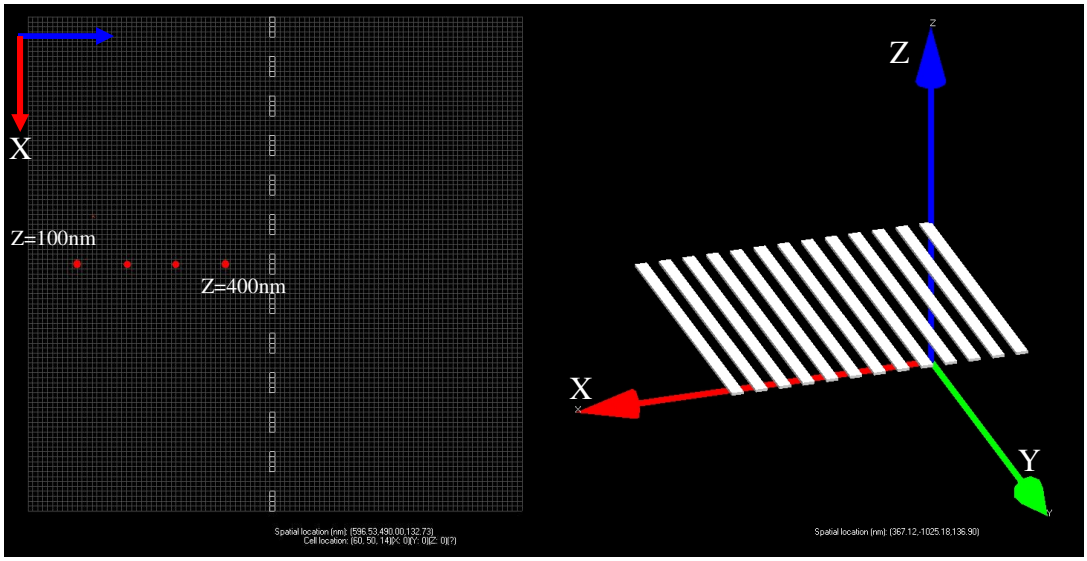

Figure 26: Simulation field space and its objects. The four red dots represent the four field near-zone field measurement points.

The transmission coefficients were going to be compared for different polariser periods, therefore quantitative measurements were required. The electric field magnitudes were gathered by saving temporal waveforms of the near-zone data. As shown in Figure 26, four near-zone data sets were measured at the centre of the XY plane for Z = 100, 200, 300, and 400nm. Each measurement recorded the electric field component E_X and E_Y in magnitude with respect to time over the whole 38.5fs simulation period.

These gathered data were then fed into pre-written MATLAB functions for data analysis (Appendix I). In order to calculate the transmission coefficient, an extra simulation of the polarised wave with no polariser was made; this simulation result data is called the control data. The transmission coefficient was then calculated by comparing the simulated data with the control data. This is shown in Figure 27.

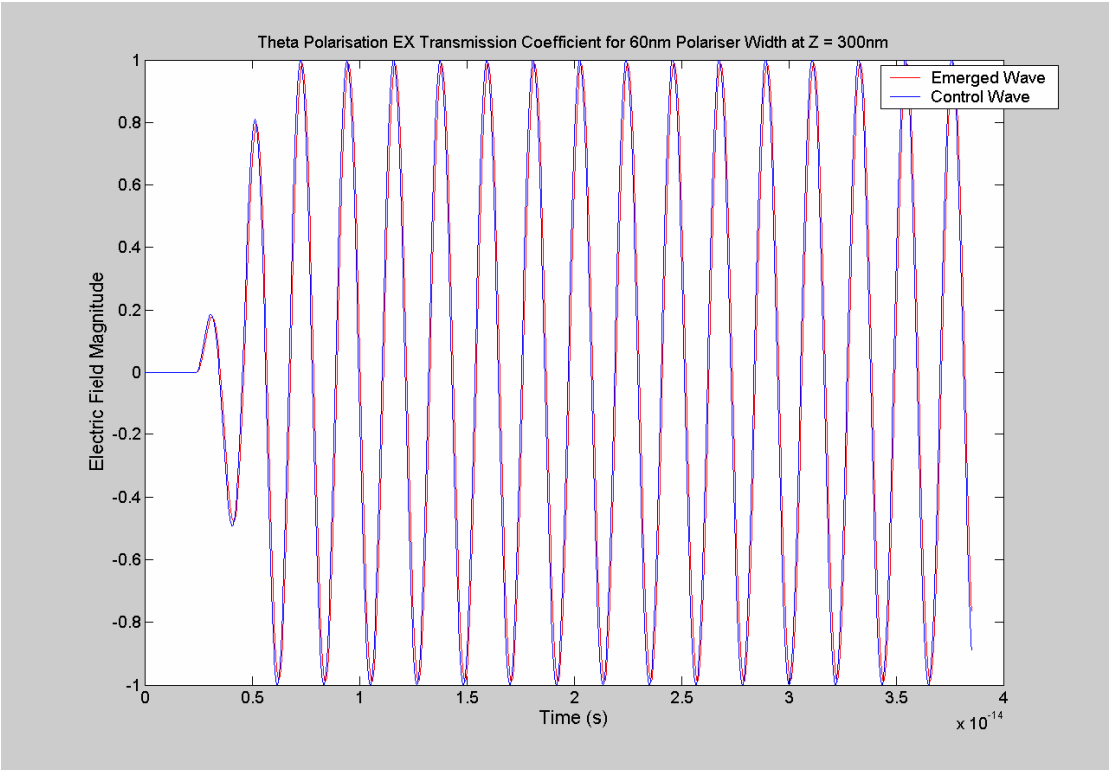

Figure 27: Theta polarisation waveform in E_X for 60nm polariser period at Z = 300nm, as well as the control data.

Figure 27 plots the measured near-zone data at Z = 300nm through the whole simulation. It shows that the wave takes about 2.5fs to propagate to the measuring point. The wave then took about 3.5fs to reach the steady state after the wave arrived there. Therefore, only the middle 1000 data points (from 10 to 30fs) are used to calculate the transmission coefficient. [Appendix I]

3.2.2 Theta Polarisation (X Polarised)

Figure 28 shows the measured transmission coefficient for the E_X electric field component (theta polarisation). The E_X results generally agree with the polarisation theory that a high transmission coefficient occurs when the incident wave is theta polarised. As for the polariser periods, the results showed that the smaller the polariser period the better transmission coefficient is. However, the differences from each period are not significant except for the measurement taken at the 400nm away from the polarisers. The transmission coefficient is lower when the grating half period is larger. This is also expected for measurements further away from the polariser.

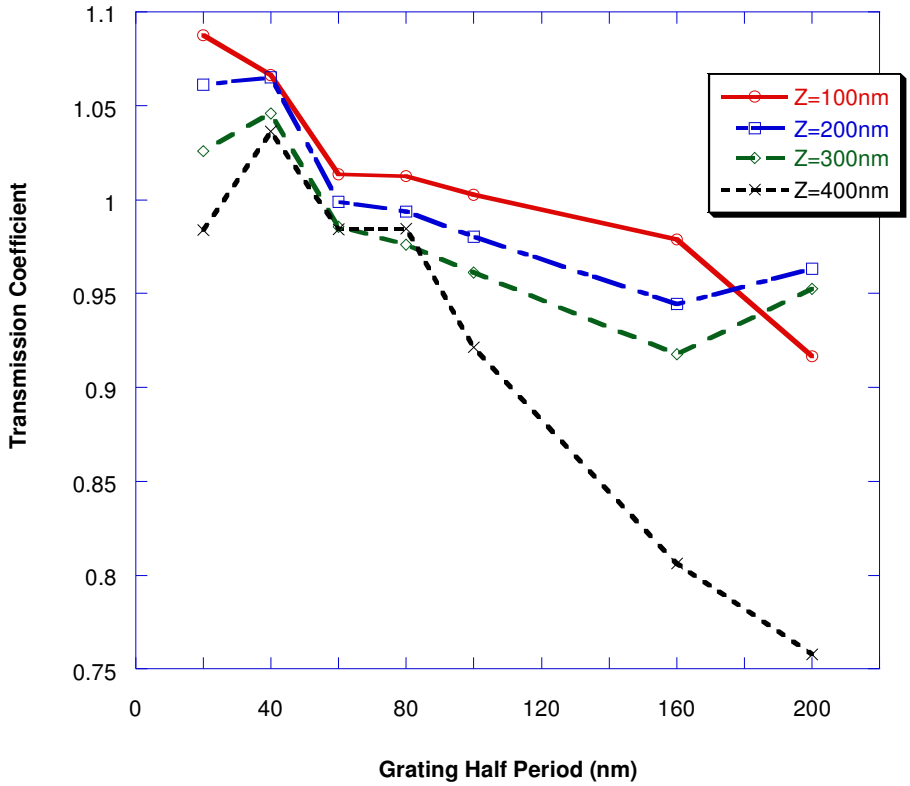

Figure 28: Theta polarisation transmission coefficients to different polariser width.

The transmission coefficient is a magnitude ratio of the transmitted wave and the incident wave. This value should be equal to or less than 1. However, there are some cases with a transmission coefficient greater than 1 in Figure 28. This is because there are wave refractions due to the polariser and small reflections from the absorbing boundaries of the simulation-space edges these cause the emerged wave to have a higher magnitude at the measuring location due to constructive interference. Also note that electric fields in the near-zone can be larger than incident fields due to field enhancements near the edge of the polarisers' metal grating lines [60].

The crosstalk coefficient was also measured and calculated. The relevant waveforms are shown in Figure 29 and results are listed in Table 3-1. Crosstalk is calculated by dividing the emerged wave E_Y component with the control wave E_X component. The crosstalk coefficient is an important indicator of the polariser performance. A large amount of crosstalk may cause errors on accessing the data via optical transmission. In this case, the crosstalk coefficients are reasonably small (less than $1*10^{-7}$) because the polariser structure is simple and the plane wave source is ideal, however this is not

always the case for some of the patterned polarisers that are discussed later. The magnitude of the crosstalk with respect to the simulation time is plotted in Figure 30.

	Polariser Half-Pitch (nm)						
Z (nm)	**20nm**	**40nm**	**60nm**	**80nm**	**100nm**	**160nm**	**200nm**
100	6.73E-08	3.73E-08	2.60E-08	3.94E-08	5.51E-08	7.11E-08	9.77E-08
200	3.53E-08	3.69E-08	5.22E-08	3.61E-08	3.84E-08	8.97E-08	8.22E-08
300	5.46E-08	3.61E-08	3.79E-08	7.92E-08	7.41E-08	1.84E-07	1.24E-07
400	3.83E-08	3.30E-08	4.11E-08	5.70E-08	5.32E-08	6.55E-08	9.94E-08

Table 3-1: Theta polarisation crosstalk coefficient.

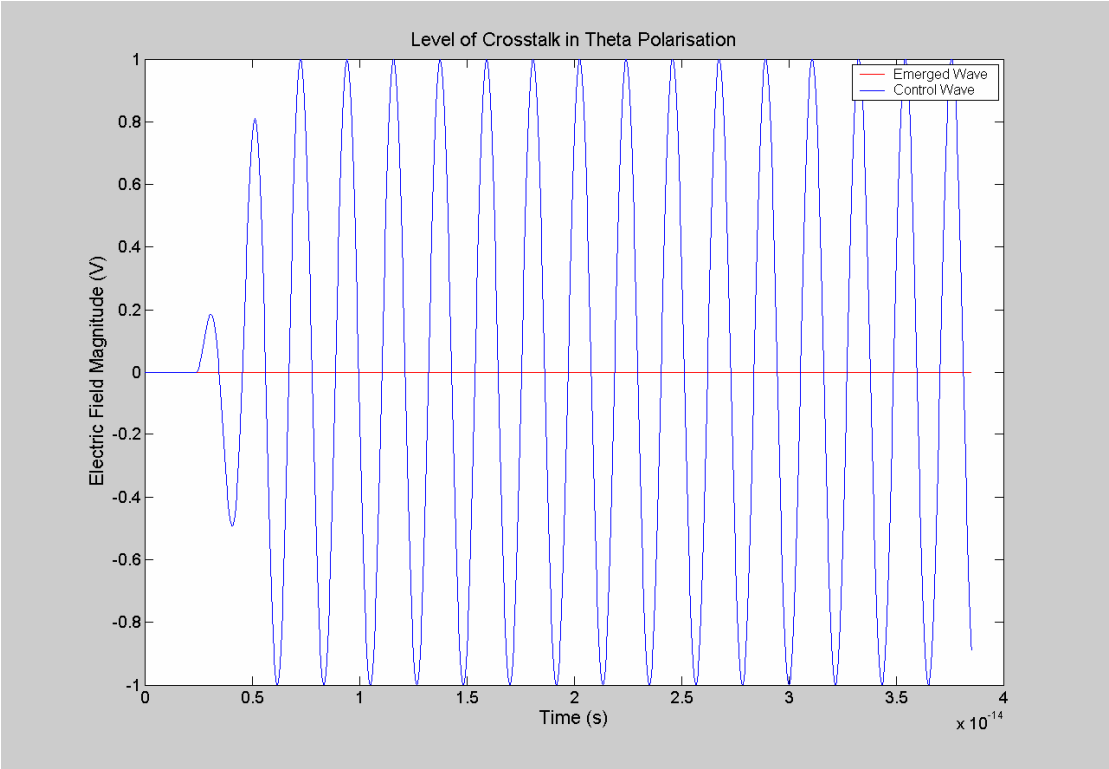

Figure 29: Theta polarisation level of crosstalk at Z = 300nm with 60nm polariser width.

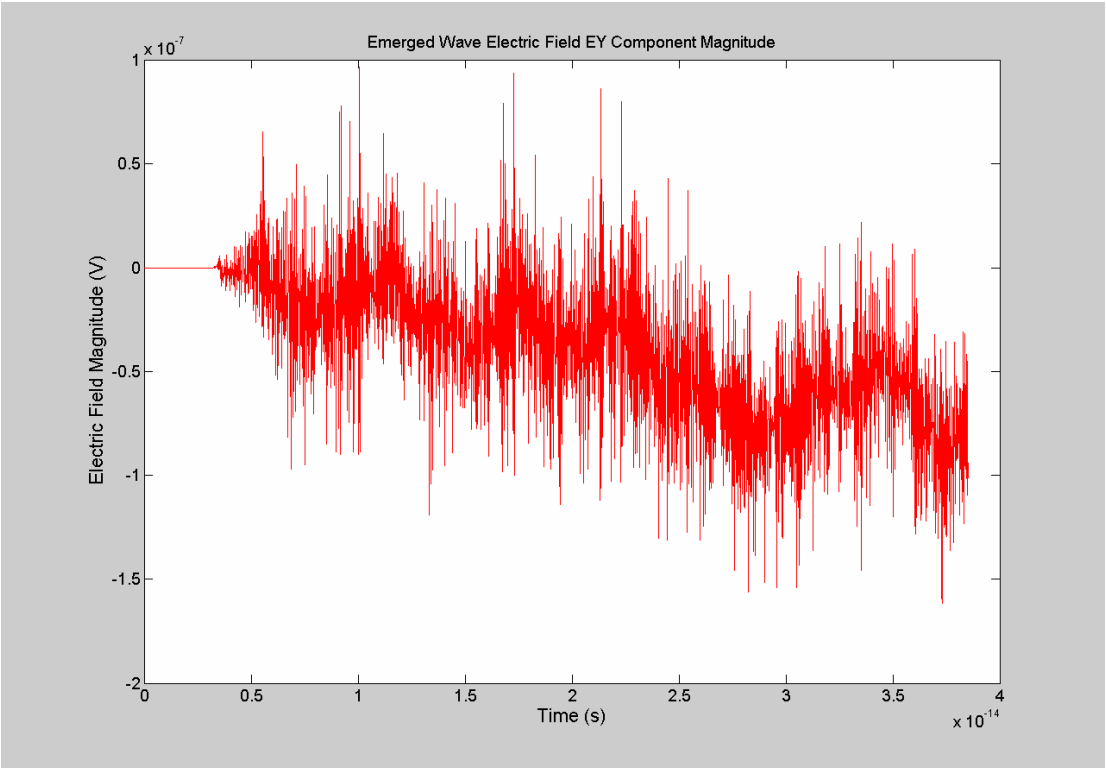

Figure 30: Theta polarisation crosstalk for 60nm polariser period at Z = 300nm.

3.2.3 Phi Polarisation (Y Polarised)

The phi polarised wave was expected to have a low transmission coefficient after propagating through the polariser. In this part of the study, simulation results were monitored is order to understand the performance with respect to the polariser period.

For the phi polarisation, the incident wave was completely polarised in the E_Y direction and E_X is 0 (there is no crosstalk). Figure 31 show that the transmission coefficients of the phi polarised wave E_Y component are low. The wave magnitude is reduced by the polariser effectively. In this case, the smaller the polariser period, the better the polarisation effect is. And once again, the ratio difference between each polariser period is not significant.

Figure 32 illustrates the control wave and emerged wave behaviour in the time domain. The plotting does not only show the reduced magnitude in the emerged wave, but also that there is a phase shift between the two waves. This was not seen in Figure 27 with theta polarisation, where the incident wave oscillation direction is perpendicular to the polariser orientation.

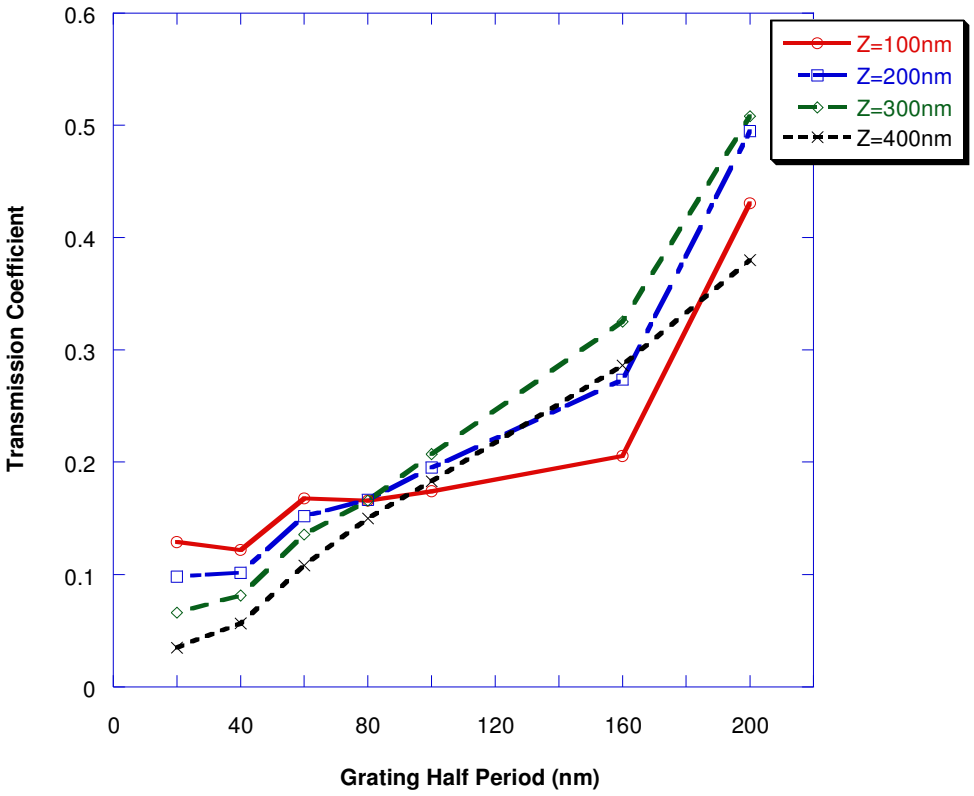

Figure 31: Phi polarisation transmission coefficients for various polariser widths.

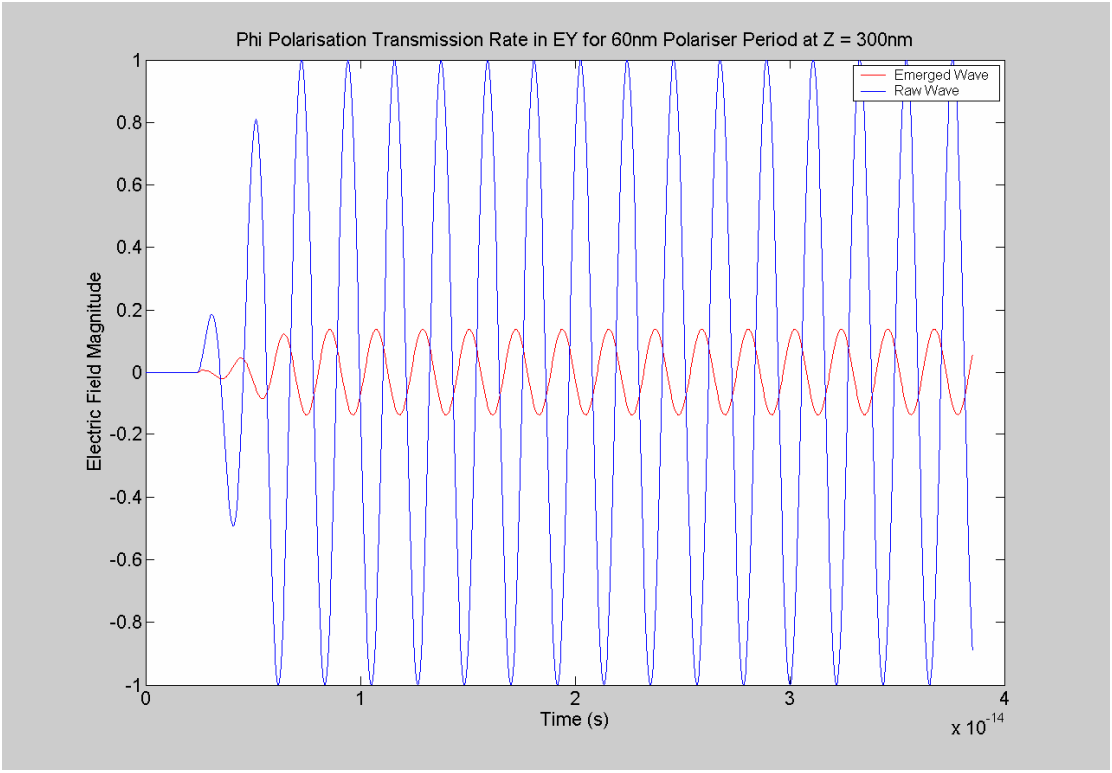

Figure 32: Phi Polarisation in E_Y for 60nm polariser period at Z = 300nm.

In this part of the simulation experiment, smaller polarised periods have a better polarisation effect. However, this effect does not vary significantly from different periods in the 20nm to 100nm range. This result proves that there is a reasonably wide range for applying the polarisation method towards CD/DVD technology.

3.2.4 Extinction Ratio

The theta and phi transmission coefficients of Figure 28 and Figure 31 have been used to calculate the extinction ratio of the single PEC polariser. The extinction ratio is calculated by the following equation;

$$Extinction\ Ratio = \frac{X\ Transmission\ Coefficient}{Y\ Transmission\ Coefficient}, \qquad (3.1.1)$$

which is usually quoted in decibel (dB) units.

Figure 33 plots the results of the extinction ratio (in dB) as a function of the grating half period. Generally, the extinction ratio is inversely proportional to the grating half period. It shows that the polarisation effect is stronger when the grating period is smaller. This also shows that grating half-periods of less than 80nm are required if the extinction ratio is to exceed 15dB.

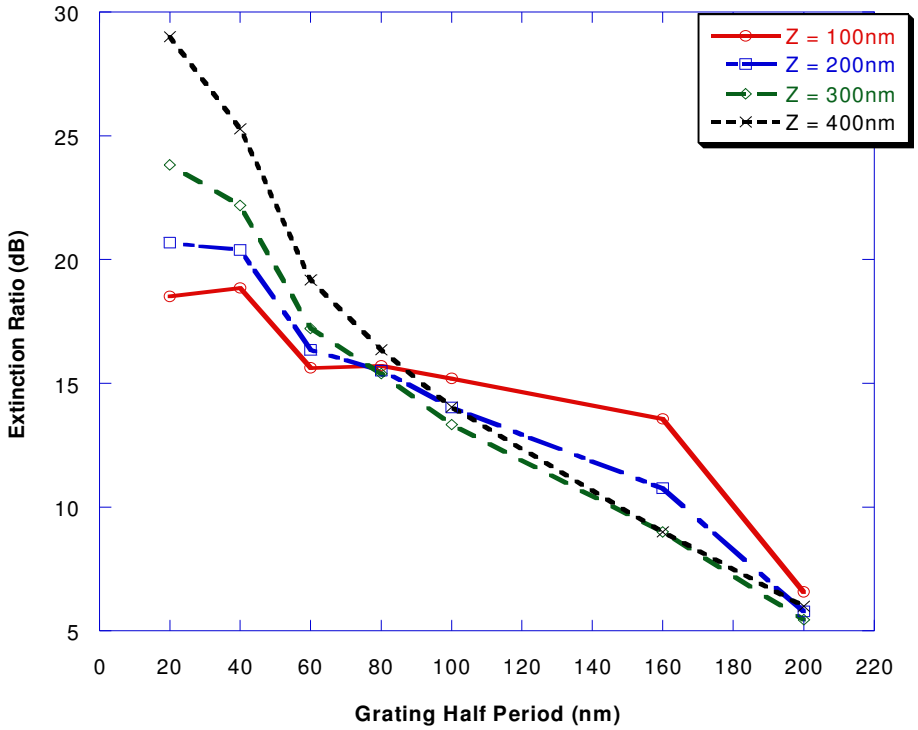

Figure 33: Extinction ratio of single PEC polariser with respect to the grating half period.

3.3 Transmission Coefficient as a Function of Polariser Thickness

Thickness is important to the DVD disc fabrication. Therefore, the polariser thickness is crucial to the application. In this part of experiment, simulations were focused on the polarisation effect from various polariser thicknesses.

3.3.1 Simulation Parameters Setup

In this experiment about the polariser thickness, the setup reproduced the previous simulation. The grid size was 100 cells * 100 cells * 100 cells. Cell size was 10nm * 10nm * 10nm. The source was a plane wave at a 650nm wavelength. The near-zone data and transient field snap shots were both being measured from the same setting.

The polariser patterns were again placed in the middle at Z = 500nm evenly and symmetrically through out the XY plane. The polariser half-period was controlled to be 40nm wide. The variable factor was the polariser thickness which ranges from 10nm to 100nm.

3.3.2 Theta Polarisation (X Polarised)

Figure 34 shows that the theta polarisation transmission coefficient is better when the polariser thickness is smaller. This transmission coefficient difference is significant but not great with these various polariser thicknesses. The results also show that the transmission coefficient is stronger at the points that are further away from the polariser.

The crosstalk was also measured in this simulation as a function of the polariser thickness. Fortunately, the crosstalk is again smaller than $1*10^{-7}$ and therefore could be ignored.

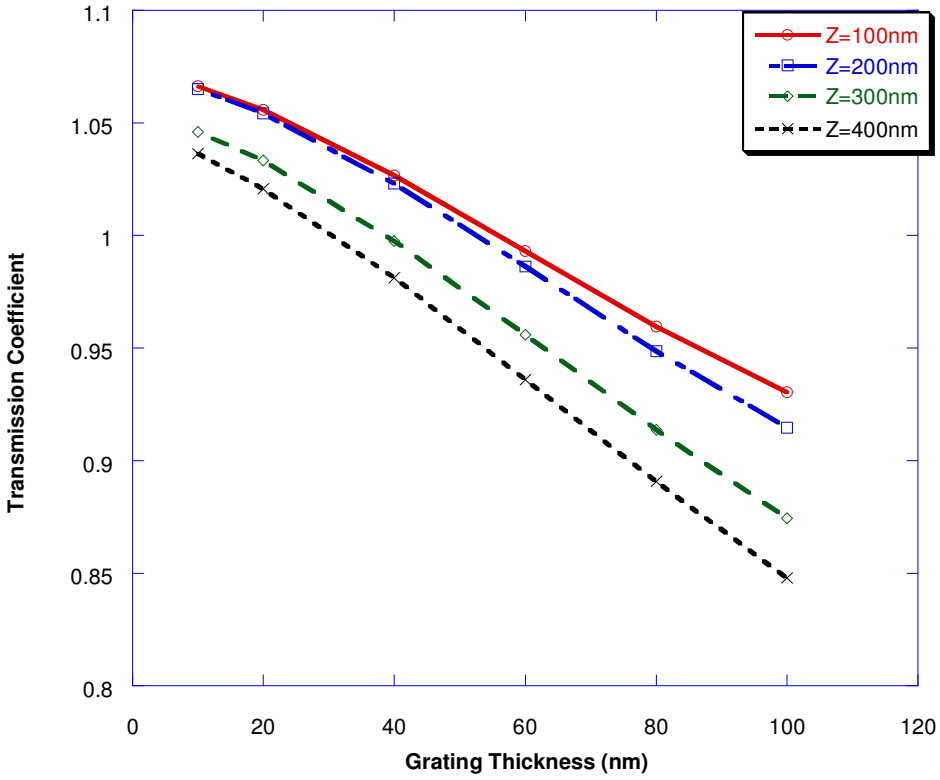

Figure 34: Theta polarisation transmission coefficients to different polariser pattern thickness.

3.3.3 Phi Polarisation (Y Polarised)

The result of phi polarisation simulation with respect to the polariser pattern thickness was analysed and is shown in Figure 35. The ratios are low as the wave was phi polarised. The transmission coefficient is higher for smaller thickness and lower for larger thickness. However, this difference is very limited as there was only 1% variation in the transmission coefficient between 10nm and 100nm thickness (based

on the measuring point at Z = 100nm which is represented by the solid line in Figure 35). Similar to the previous section, the crosstalk level for this phi polarised wave simulation was again zero.

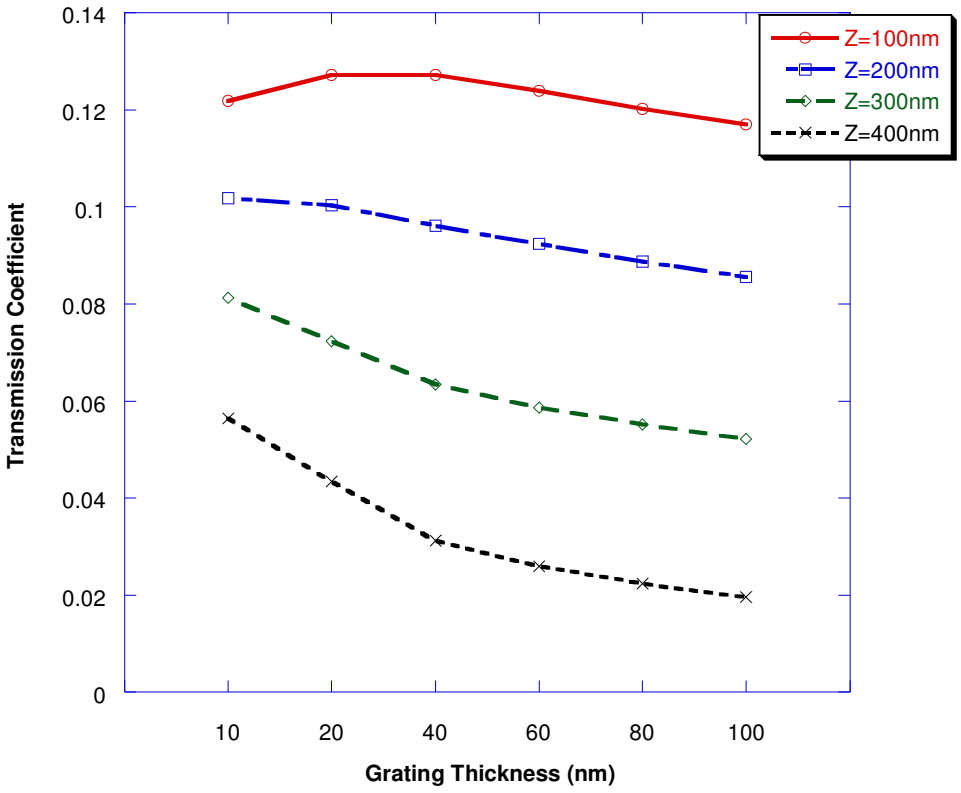

Figure 35: Phi polarisation transmission coefficients to different polariser grating thickness.

3.3.4 Extinction Ratio

The polarisation effect of the single PEC polariser is then analysed by calculating the extinction ratio as a function of its grating thickness. The results are plotted in Figure 36. The extinction ratios are generally constant with respect to various grating thickness. The only exception is when the measuring point at Z = 400nm. The dashed line in Figure 36 represents the data measured at Z = 400nm. When the polariser thickness is more than 100nm, this measuring point is so close to the polariser that the field effect is not valuable for referencing. Therefore, the extinction ratio plot suggests that the polarisation effect is not directly related to the polariser grating thickness for PEC polarisers.

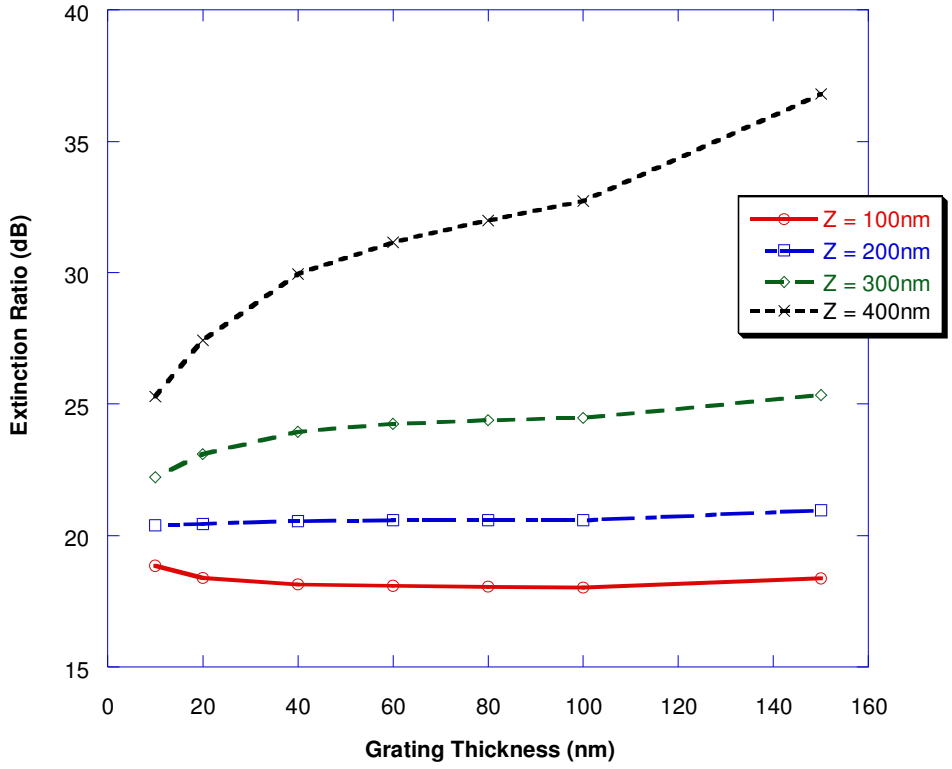

Figure 36: Extinction ration of single PEC polariser as a function of grating thickness

3.4 Transmission Coefficient as a Function of Polariser Material

This part of experiment examined the polarisation effect for different realistic polariser materials. Materials chosen for this part of the study were copper, gold and titanium, as these are common materials that can be deposited in thin film form using standard microelectronic processing technique. Also, this simulation was trying to find the major factor affecting transmission coefficient.

3.4.1 Simulation Parameters Setup

This simulation again used the same parameters as for the previous experiment. The grid size was 100 cells * 100 cells * 100 cells. The cell size was 10nm * 10nm * 10nm. The source was a plane wave with a 650nm wavelength. The near-zone data and transient field snap shots were both measured from the same setting.

The polariser patterns were 40nm in period and 40nm in thickness. Materials included PEC (as a comparison), gold, copper, and titanium. Parameter calculations

were required for using these materials in the simulation. The materials were simulated using the Debye model in the XFDTD program. The parameters included infinite frequency permittivity, static permittivity, relaxation time, and conductivity.

In order to calculate these parameters, optical properties, refractive index n and extinction coefficient k, of these materials were obtained from published data [61]. Index n, and k were used to calculate the complex permittivity, which includes the real term ε' and imaginary term ε'', where $\varepsilon' = n^2 - k^2$ and $\varepsilon'' = 2nk$. After that, the complex permittivity was then fed into a MATLAB function for finding the parameters by searching the optimised values [Appendix II].

Before finding the optical properties, the wave energy (in eV) is required to be calculated. The formula is given from [61] as

$$\lambda(\mu m) = \frac{1.2398}{E}. \qquad (3\text{-}4\text{-}1)$$

As the source wave has a wavelength of 650nm, the respective energy is 1.907eV.

The optical properties and calculated parameters of these simulated materials are listed in Table 3-2.

Materials	**Copper**		**Gold**		**Titanium**	
Optical Properties	*n = 0.21*	*k = 3.67*	*n = 0.11*	*k = 3.49*	*n = 1.57*	*k = 2.24*
Complex Permittivity	-13.4248 - 1.5414j		-12.1680 - 0.7678j		-2.5527 - 7.0036j	
Infinite Freq. Permittivity	1.1870		1.140		1.700	
Static Permittivity	-1790		-5500		-11	
Relaxation Time (s)	3.80E-15		7.00E-15		3.76E-16	
Conductivity (S/m)	4.17E+06		6.96E+06		2.99E+05	

Table 3-2: Optical properties and parameters of simulated materials.

It is significant that the optical property of gold with respect to 1.9eV was not found in [61]. Therefore, the value in Table 3-2 is the average value. At 1.8eV, Gold has n = 0.09 and k = 3.82, and at 2.0eV, n = 0.13 and k = 3.16.

3.4.2 Theta Polarisation (X Polarised)

The material parameters were inserted into the Debye model for simulation. The theta polarisation simulation results are plotted in Figure 37. This gives the transmission coefficient results of copper, gold, and titanium as a polariser with a theta polarised wave. PEC polariser results from the previous simulation are also included as a comparison. The results show, in theta polarisation, gold has the best performance as a polariser material followed by copper and then titanium. Titanium has a lower

conductivity compared to copper and gold. This results the significant transmission coefficient difference between titanium and other materials.

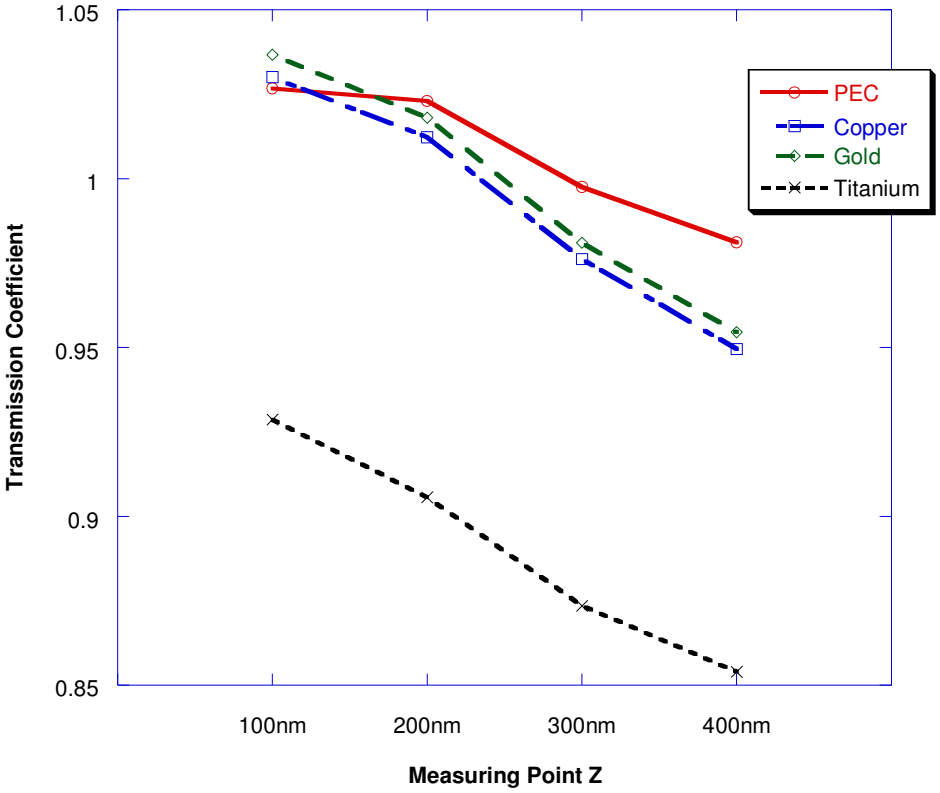

Figure 37: Theta polarisation transmission coefficients with respect to different polariser materials.

Table 3-3 also shows the crosstalk results. The crosstalk levels of these three metal materials are significantly larger than the PEC results. The crosstalk in PEC polariser had no proper wave form. However, the crosstalk in these three metal polarisers does have sinusoidal wave form with respect to time, as shown in Figure 38 to Figure 40.

Theta Polarisation Crosstalk Coefficient				
Z (nm)	**PEC**	**Copper**	**Gold**	**Titanium**
100	3.587E-08	2.840E-05	3.210E-05	2.410E-05
200	3.673E-08	3.310E-05	3.750E-05	2.690E-05
300	4.466E-08	3.920E-05	4.510E-05	2.920E-05
400	5.892E-08	4.460E-05	5.210E-05	3.250E-05

Table 3-3: Theta polarisation crosstalk coefficient with 40nm pattern thickness.

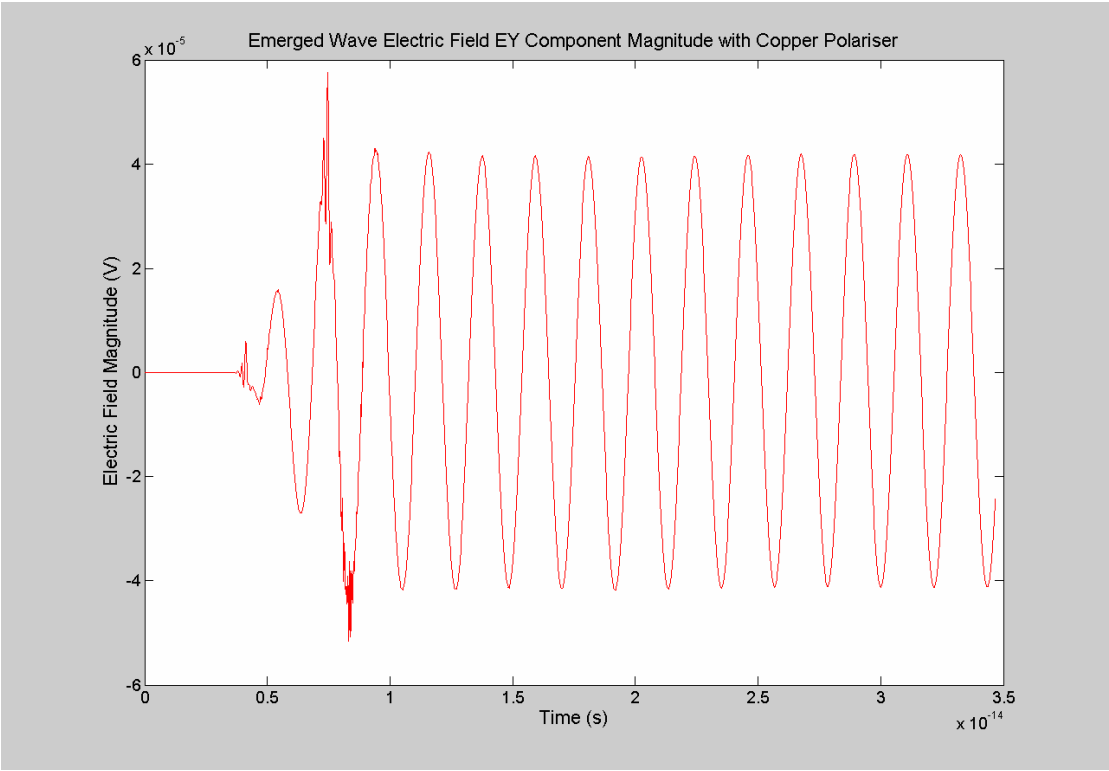

Figure 38: Theta polarisation crosstalk for copper polariser at Z = 300nm.

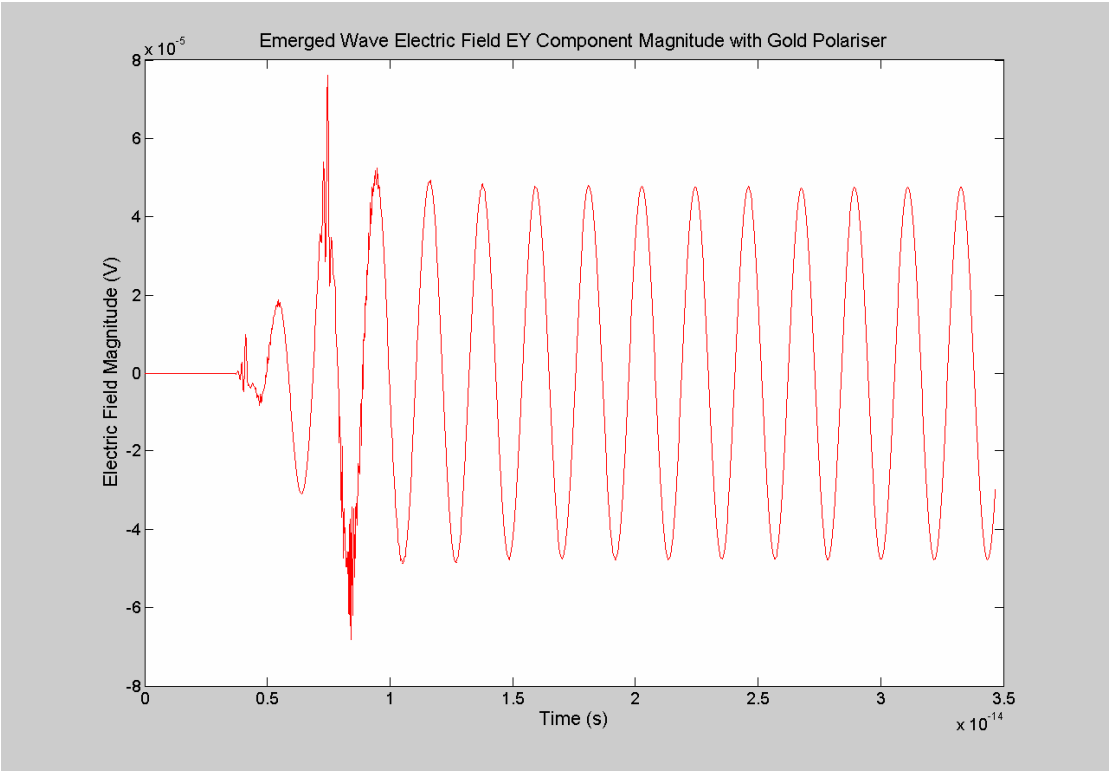

Figure 39: Theta polarisation crosstalk for gold polariser at Z = 300nm.

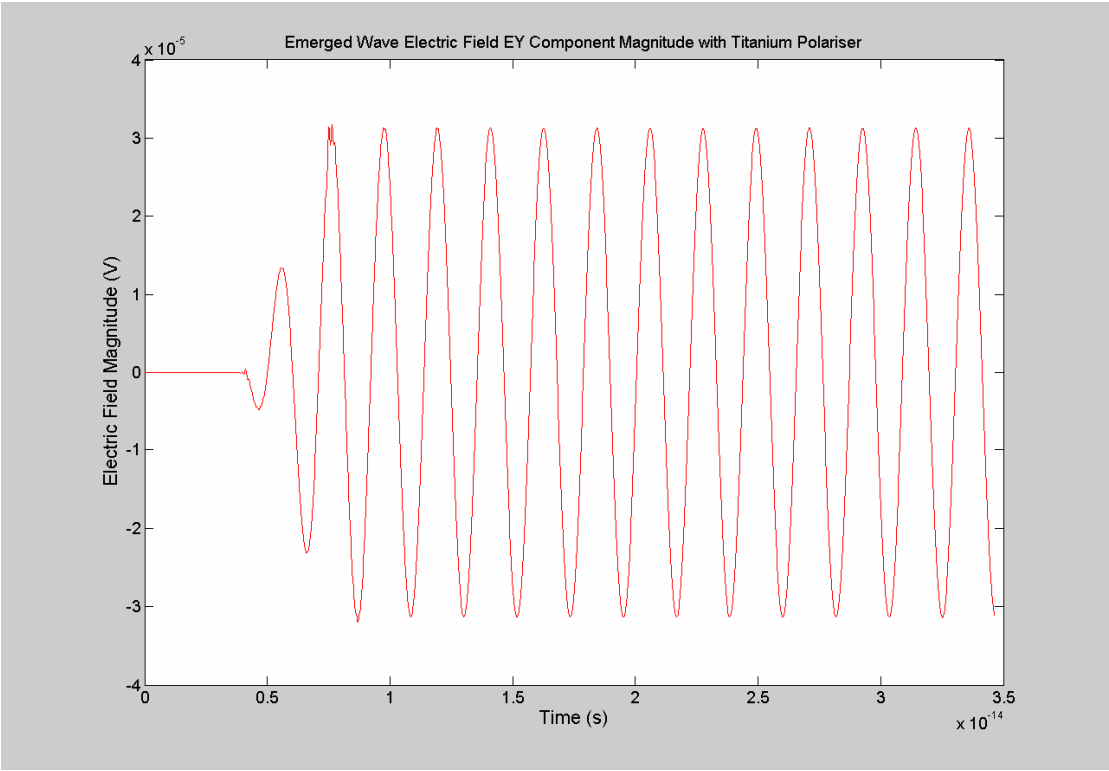

Figure 40: Theta polarisation crosstalk for titanium polariser at Z = 300nm.

In theta polarisation, titanium has a lower crosstalk level than copper and gold. As shown in Figure 38, Figure 39 and Figure 40, the crosstalk reaches the steady-state about 5fs after the wave arrives at the measuring point.

3.4.3 Phi Polarisation (Y Polarised)

The same set of metals was used as the polariser material and simulated by XFDTD for phi polarisation. The transmission results of different polariser materials in a phi polarised wave are plotted in Figure 41. In this part of experiment, Figure 41 shows that the polarisation effect in a copper polariser was the best, followed by gold, then titanium with all metals being more than a factor of two worse than the PEC polariser. The differences were significant. In phi polarisation, the titanium polariser had a transmission coefficient of almost 40%, which is unsatisfactory. However, there is no crosstalk generated from the phi polarised transmission for all kinds of polarisers.

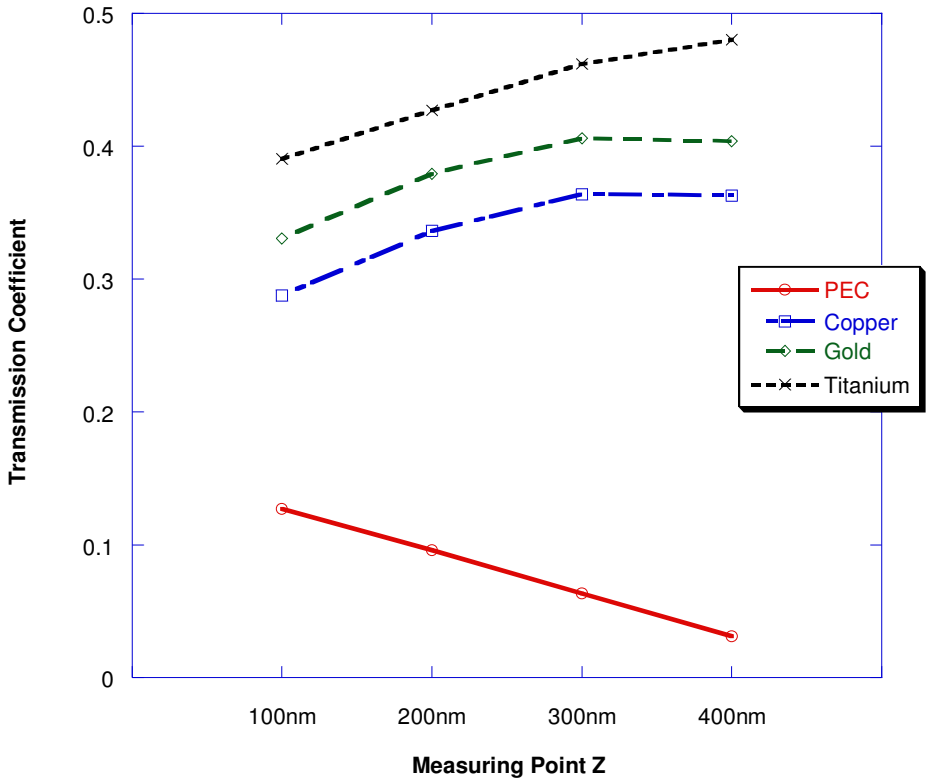

Figure 41: Phi polarisation transmission coefficients with respect to different polariser materials.

The results shown in theta and phi polarisation simulations were not consistent. Gold was the best polariser material in theta polarisation and copper was the best in phi, but there was not a major difference between these two materials. However, when the result of the transmission coefficient for a PEC polariser is compared, there is another inconsistency. The transmission coefficients in all three metal polarisers were very close to the PEC result in theta polarisation; where as in phi polarisation, the results were quite different.

The phi polarisation transmission coefficient results were quite high and unusual. It is believed that this resulted from the non-zero skin depths in these metals when compared to the PEC, which would allow significant additional field leakage. The simulation object was then modified for further tests. The polariser pattern thickness was increased to 100nm and all three materials were used in a simulation again. The fact that higher thickness reduces the magnitude was used to compensate the skin depth effects.

3.4.4 Theta Polarisation (X Polarised) in 100nm Thick Patterns

The theta polarisation was simulated again with a 100nm thick polariser in all materials. The aim of this simulation was to see if the polarisation effect improves in thicker polariser patterns in these metallic materials.

Figure 42 shows the transmission coefficient with 100nm thick different material polarisers in theta polarisation. Generally speaking, the results were satisfactory. The performance was still the best for gold, followed by copper and titanium. The crosstalk results are improved slightly for all three materials with 100nm polariser thickness. The crosstalk coefficient results are listed in Table 3-4.

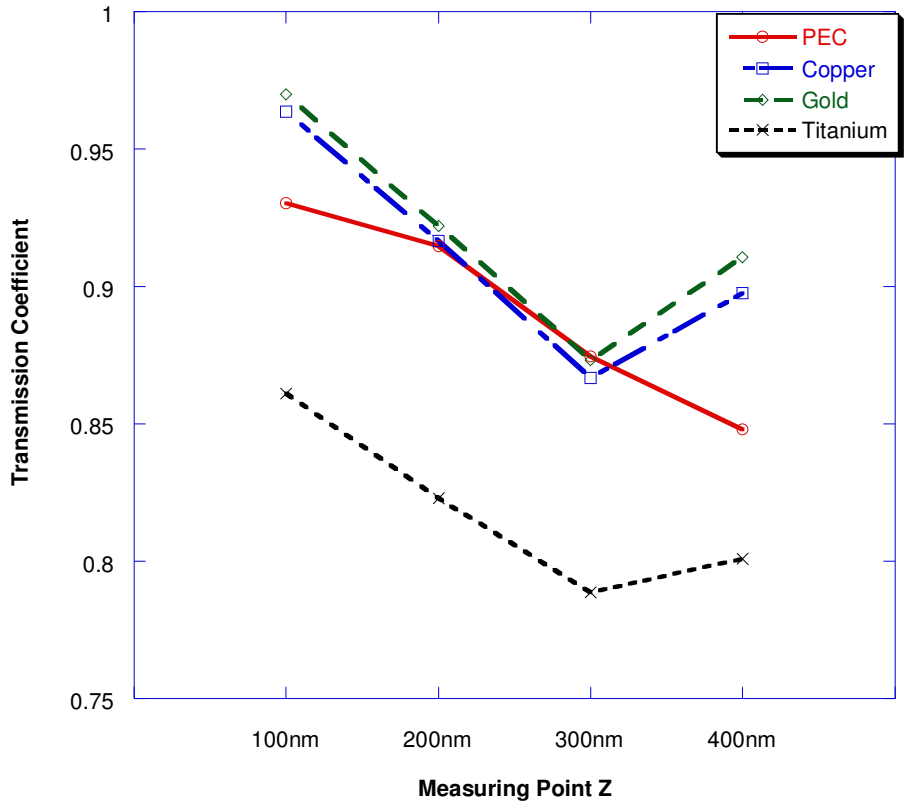

Figure 42: Theta polarisation transmission coefficients to different polariser materials with 100nm pattern thickness.

Polariser Materials				
Z (nm)	**PEC**	**Copper**	**Gold**	**Titanium**
100	6.913E-08	2.010E-05	2.240E-05	2.100E-05
200	4.419E-08	2.330E-05	2.620E-05	2.290E-05
300	4.250E-08	2.850E-05	3.200E-05	2.630E-05
400	6.738E-08	2.590E-05	3.000E-05	2.780E-05

Table 3-4: Theta Polarisation crosstalk coefficient with 100nm pattern thickness.

3.4.5 Phi Polarisation (Y Polarised) in 100nm Thick Patterns

The phi polarised simulations were also repeated with 100nm thick polariser patterns for all materials. This time, the transmission coefficient results were expected to be lowered because of the increase in pattern thickness.

Figure 43 shows promising results as the transmission coefficients are reduced significantly in phi polarisation compared to the 40nm-thick polarisers. Comparing this result with Figure 41, increased pattern thickness improves the phi polarisation effect in all pattern materials.

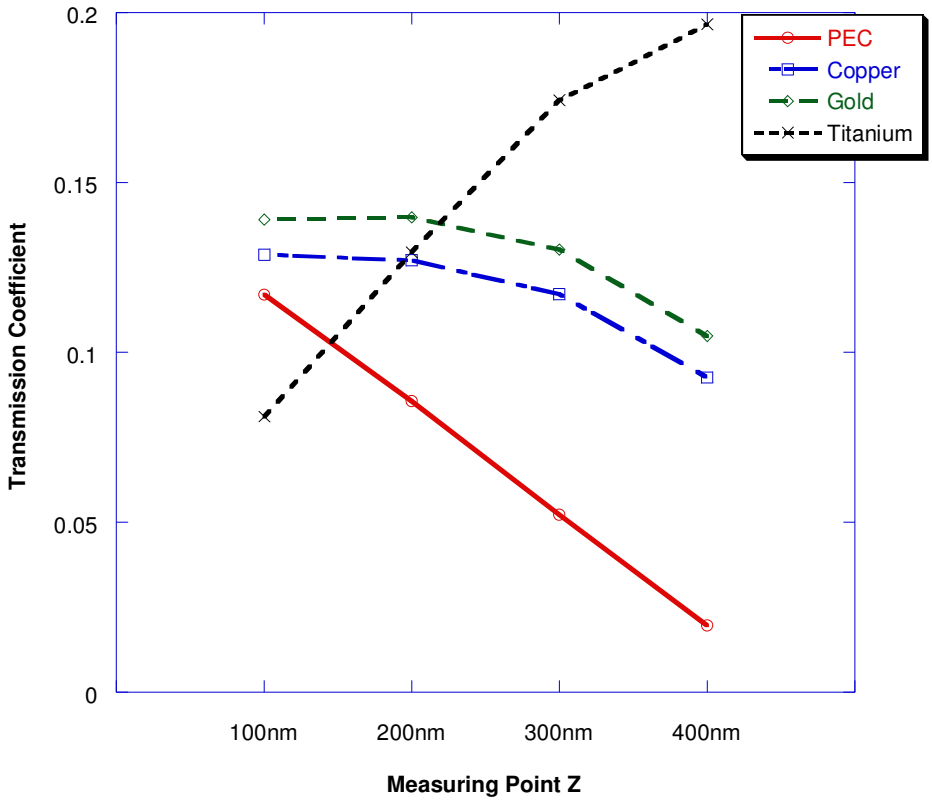

Figure 43: Phi polarisation transmission coefficients to different polariser materials with 100nm pattern thickness.

In Figure 43, copper, gold, and titanium all show less polarisation effect when close to the polariser but better results when away from it. This characteristic remains for titanium, but not for copper and gold. Although the titanium polariser showed less polarisation effect at 400nm, which is closer to the polariser (at 500nm), the wave attenuated, as is seen from the rest of the measurement points. Copper had the best polarisation effect at 400nm and then the transmission coefficient increased as the distance from the polariser increased. Gold was similar to copper but the transmission

coefficient dropped again at 100nm. Therefore, it is believed that the decreasing polarisation effect for copper and gold in the range from 400nm to 100nm was due to the near-field refraction. This refraction effect range is different for each material. The factor that affects the refraction effect range is unknown but is assumed to be related to the material parameters.

Studying the results from above indicates copper and gold are the best polariser materials with this wavelength (650nm) and pattern thickness (100nm). Titanium is not as good as copper and gold, but its performance could be optimised by changing the pattern thickness between 40nm and 100nm. Therefore, although the polariser thickness is not a major factor in PEC polariser simulation, it is useful when optimising the real material polarisation effect.

In theta polarisation, the crosstalk level with copper, gold and titanium polarisers are significant. It was not seen in PEC polariser simulations. Although the magnitudes of the crosstalk are quite low from these metallic materials, the crosstalk has a sinusoidal wave form. The crosstalk wave form takes about 0.5e-14 seconds to reach the steady-state. The level of crosstalk is reduced when the polariser thickness is increased.

3.4.6 Extinction Ratio

The polarisation effect is then measured by the extinction ratio of these polarisers. The extinction ratio of each material is calculated and plotted in Figure 44. Different materials lead to various characteristics of the extinction ratio. At measuring point Z = 100nm, PEC, copper and gold polarisers all have similar extinction ratios at about 17.5dB. Titanium has higher extinction ratio of 21dB at Z = 100nm. This plot gives more details by looking at the ratio as a function of the distance from the polariser. For the ideal material, PEC, the extinction ratio is higher when the measuring point is closer to the polariser. The extinction ratio of copper and gold are consistent through the various measuring point. The extinction ratio of titanium is higher when the measuring point is further away from the polariser.

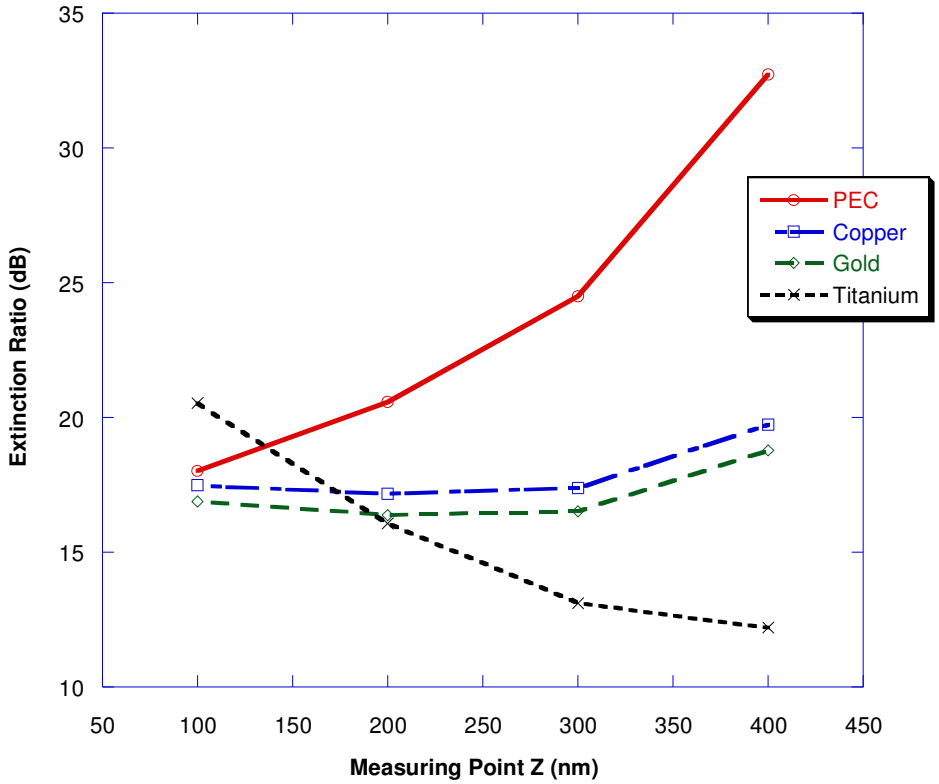

Figure 44: Extinction ratio of the single polariser with different materials.

4.0 GAUSSIAN BEAM AND FOCUSING SPOT SIZE

In previous simulations, a plane wave was used as the wave source. In practice, the laser wave is focused on to the pattern on a CD or DVD disc, in which case a plane wave does not fully model the polarisers' behaviour. It is better to apply the Gaussian beam as the wave source. (See Section 2.4.2)

In XFDTD, the Gaussian beam source has a focus spot location and radius options which were very helpful for setting up the study of the effects of spot size on polariser performance. The following experiment was divided into two parts. First, a Gaussian beam source was applied to the simulation in order to compare it with the plane wave propagation. The second part of this experiment aimed to look at the effect of varying the focusing spot size on the transmission coefficients and crosstalk parameters of metallic wire grid polarisers.

4.1 Simulation Parameters Setup

The purpose of this experiment was to observe the effect of the polariser with respect to the polarised Gaussian beam wave. The simulation parameters were copied and reproduced from the previous section. The grid size was 100 cells * 100 cells * 100 cells. The cell size was 10nm * 10nm * 10nm. The source was set to be a Gaussian beam instead of a plane wave.

The polariser pattern dimension was fixed in this simulation. Gold was applied as the polariser material. The dimensions of each of the metal strips were 1000nm long, by 40nm wide and 100nm thick. The thickness, 100nm, was chosen because it gave a better polarising effect when gold was the material used in the previous simulations.

In the first part of this experiment, a Gaussian beam source with a 500nm spot radius was applied and focused at the centre point of the simulation domain: X = 500nm, Y = 500nm and Z = 500nm. This simulation gave the result for comparison with the plane wave source simulation. In the second part of the experiment, the Gaussian beam radius was varied from 100nm to 600nm. The polarising effect and crosstalk results were observed from both theta and phi polarisations. The spot radii 100nm

and 200nm are not practical for a Gaussian beam with a wavelength of 650nm. However, these radii are included in order to test the ultimate performance limits.

4.2 Gaussian Beam Simulation

A plane wave has a uniform propagation. Its wave front is flat. Unlike a plane wave, a Gaussian beam has a focusing spot. The wave propagations before this spot and after it are symmetrical. A Gaussian beam has curved wave fronts and the focusing spot at the centre of these curves.

Figure 45 shows the Gaussian beam propagation in an empty simulation domain with a wavelength of 650nm. The Gaussian beam has the focusing spot with a 300nm radius in the centre of the field. From this the converging and diverging spherical wavefronts, before and after the focus respectively are clearly visible. Because of these spherical wavefronts the performance of a polariser may be degraded for a focused spot compared with a plane wave source, which is studied here.

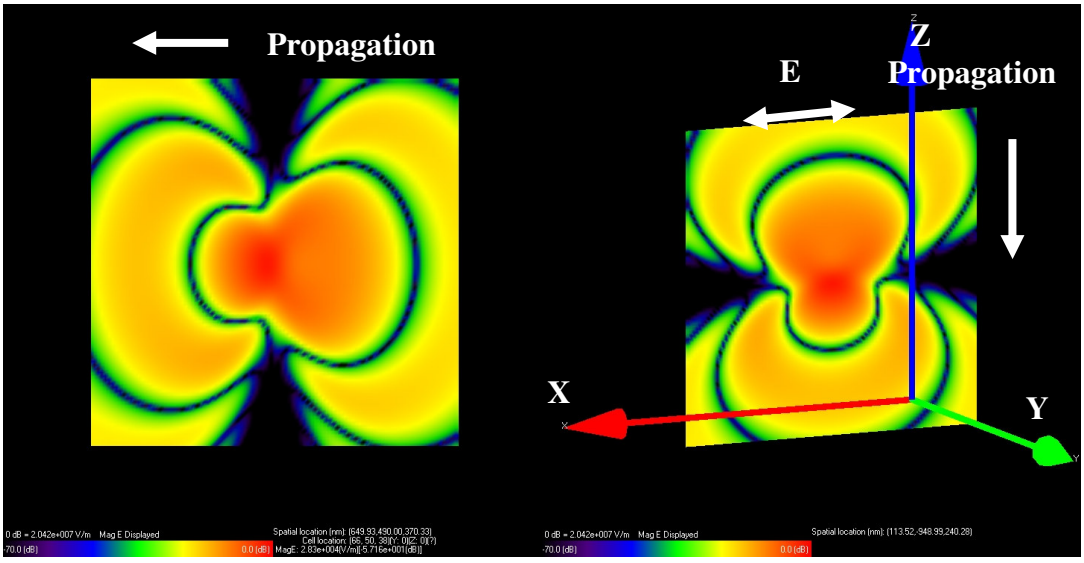

Figure 45: Theta polarised Gaussian beam with 100nm spot radius field view of electric field magnitudes.

The Gaussian beam was then applied to the simulation with a 100nm thick gold polariser. The purpose of this simulation was to compare the results with the plane wave simulations. Figure 46 is the field view of the phi polarised Gaussian beam propagation through a 100nm thick polariser. Figure 47 is the same field view, but for theta polarisation. Although the field views do not show the polarisation effect clearly, they show the Gaussian beam propagation and the focusing behaviour. The

polarisation effect is represented better by the near-zone data analysis and its extinction ratio which will be discussed later.

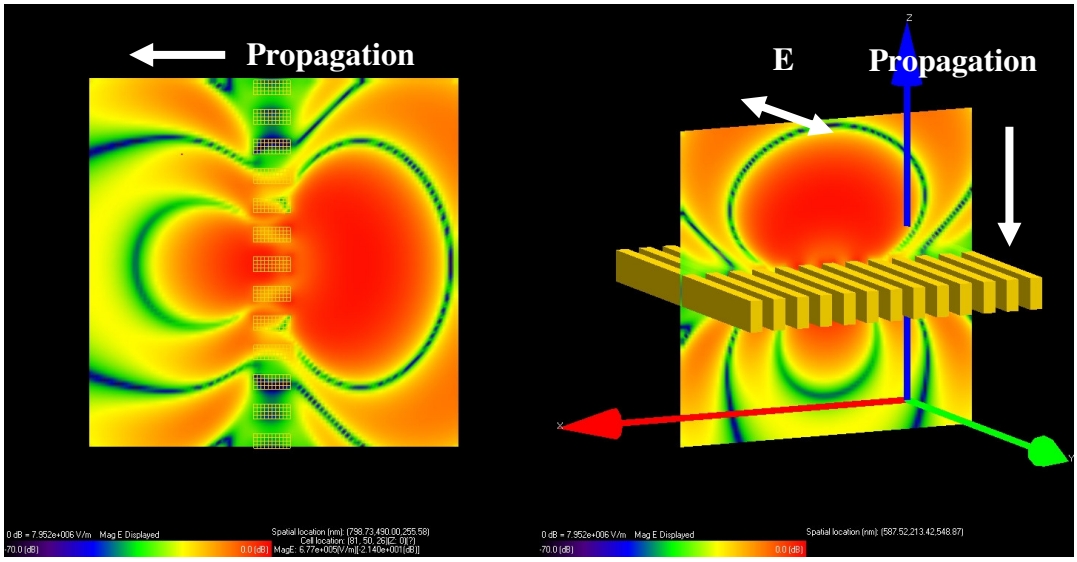

Figure 46: Phi polarised Gaussian beam in 100nm spot radius through 100nm thick polariser field view of electric field magnitudes.

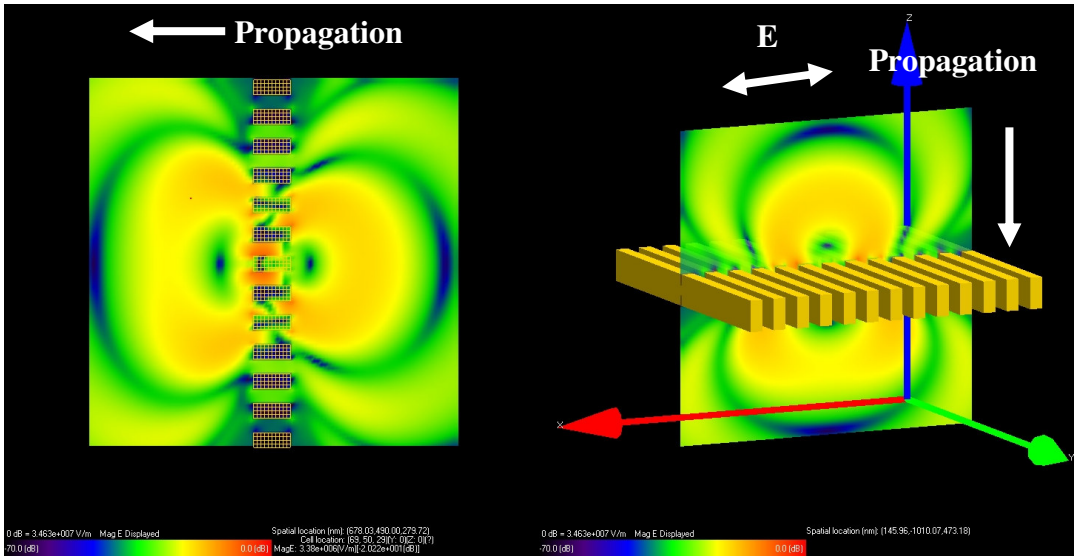

Figure 47: Theta polarised Gaussian beam in 100nm spot radius through 100nm thick polariser field view of electric field magnitudes.

4.3 Theta Polarisation (X Polarised)

The Gaussian beam theta polarisation simulation results are qualitatively similar to those for the plane wave. The transmission coefficient of the E_x component is high and the crosstalk (transfer of energy into the E_y component) is low. The near-zone results with respect to the spot radius have been used to provide quantitative comparison.

Figure 48 shows the transmission coefficient and the crosstalk of the theta polarised Gaussian beam with the spot radius from 100nm to 600nm. These results show high transmission coefficients as expected. However, the polarisation effect is not strong when the Gaussian beam spot radius is small. The transmission coefficient is greater than 0.85 when the Gaussian beam spot radius is greater than 300nm.

The transmission coefficients show reduced polarisation effect when the spot radius is smaller than 300nm. This is because the polarisation state of the Gaussian beam is not consistent at the focus spot. The Gaussian beam propagation can be modelled as a superposition of multiple plane waves from a concave surface as illustrated in Figure 49. Each plane wave component that propagates toward the focusing spot has different direction. Hence, the polarisation state of each component is different and, in particular, those incident at large angles from the normal direction will have lower transmission coefficients. This causes the reduction of polarisation effect.

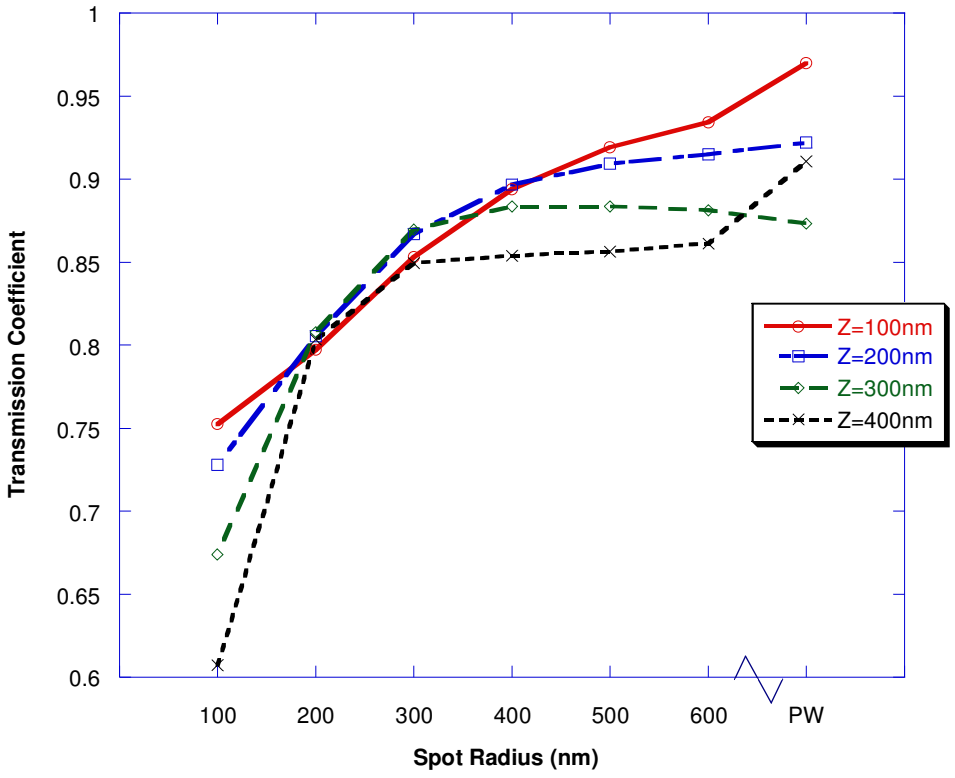

Figure 48: Theta polarisation transmission coefficients to different Gaussian beam focusing spot radius for a 100nm thick gold polariser (width 40nm, period 80nm) illuminated at 650nm wavelength. The plane wave (PW) results are shown for comparison.

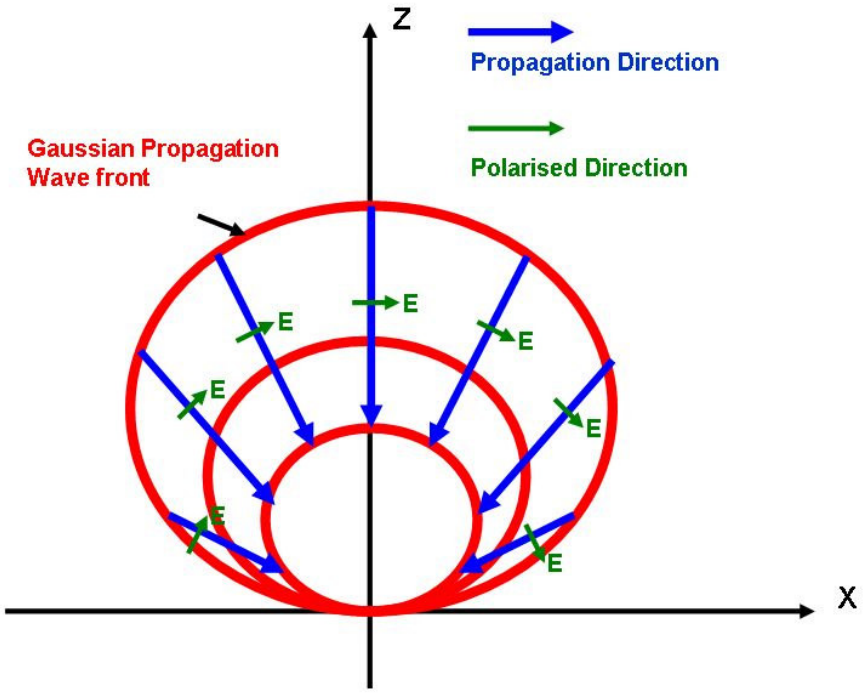

Figure 49: Gaussian beam propagation with its components and polarisation directions.

Figure 50 plots the crosstalk coefficients of the theta polarised Gaussian beam source. It is plotted as a function of the beam spot radius. The radius is in range of 100nm to 600nm. The crosstalk level is significantly higher than 0.01% when the Gaussian beam spot radius is smaller than 300nm compared with crosstalk of less than 0.007% for a plane wave illumination. In the radius range from 300nm to 500nm, the crosstalk level is decreased when the radius is increased. Also, the crosstalk level is smaller when the measuring point is further away from the polariser (Z = 100nm). However, at a spot radius of 600nm, the crosstalk is much higher for radii from 300nm to 500nm. The crosstalk level for 600nm radius is increased when the measuring point is away from the polariser. This is thought to be due to edge effects from the finite size of the simulation domain.

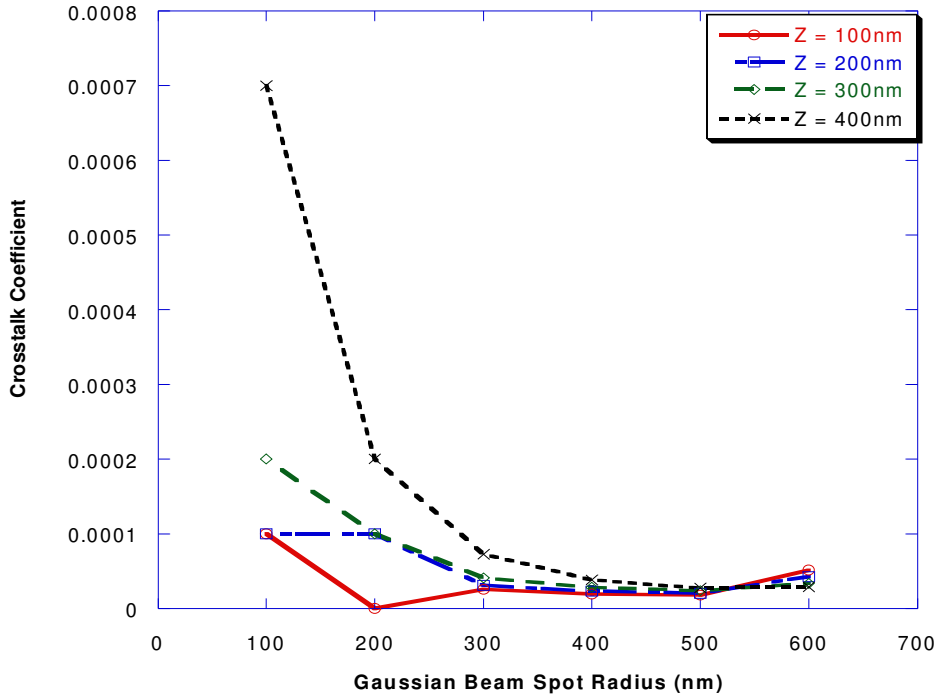

Figure 50: Theta polarisation crosstalk coefficients for different Gaussian beam focusing spot radius.

4.4 Phi Polarisation (Y Polarised)

The phi polarised Gaussian beams with various spot radii were also simulated. The near-zone electric field magnitudes were measured and analysed. The transmission coefficient of this phi polarisation is plotted in Figure 51. Similar to the theta polarisation, the polarisation effect is not strong when the spot radius is smaller than 300nm. In fact, the transmission coefficients below 300nm show a reversed polarisation effect, in which the E_y transmission is larger than that for E_x.

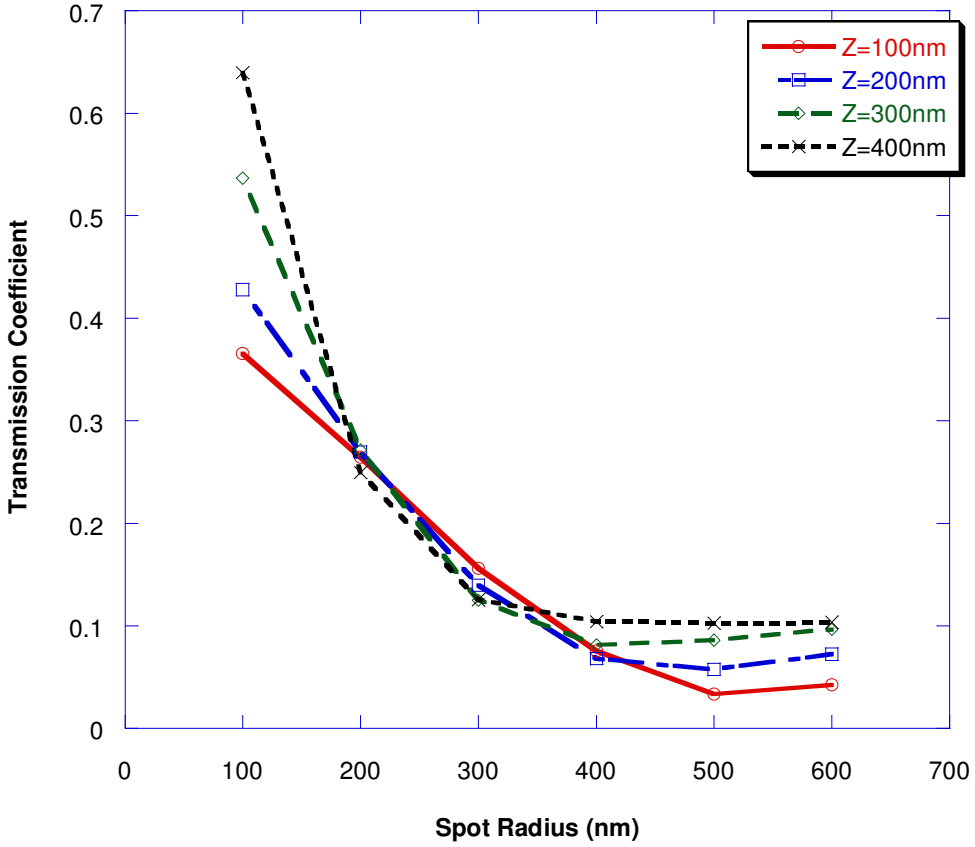

Figure 51: Phi polarisation transmission coefficients to different Gaussian beam focusing spot radius.

The crosstalk coefficients were also extracted, as shown in Figure 52. The crosstalk coefficients are plotted as a function of the beam spot radius from 100nm to 600nm. Unlike the plane wave simulations from previous sections, there is now crosstalk in the phi polarised simulation. The crosstalk level is generally larger than the results from theta polarised simulation. There is no linear relation between the crosstalk and the focusing spot radius. The crosstalk result in phi polarised simulation is the best when the spot radius is greater than 500nm which has a closer characteristic towards the plane wave than the smaller radius cases. The crosstalk coefficients of 100nm and 200nm spot radii are significantly higher than the rest. This is because the changing of polarisation state of the Gaussian beam spot at the focusing point. This is another fact that shows the polariser is no longer effective to such source spot size.

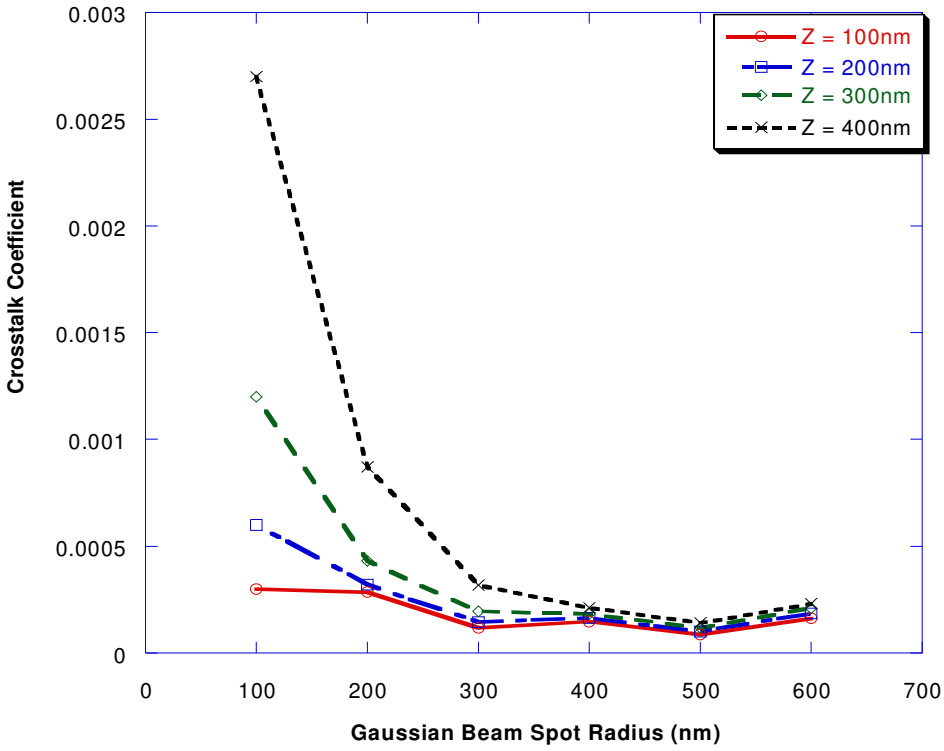

Figure 52: Phi polarisation crosstalk coefficients to different Gaussian beam focusing spot radius.

4.5 Extinction Ratio

The extinction ratios (ratio of theta transmission to phi transmission as defined in Equation 3.1.1) were calculated from the theta and phi transmission coefficients. It indicates the polarisation effect quantitatively. The extinction ratio is plotted as a function of the Gaussian beam spot radius in Figure 53, and the plane wave values are shown for comparison.

There is a linear relationship between the extinction ratio and the spot radius from 100nm to 400nm for all measuring points. The ratio is improved when the spot radius is increased. The best result occurs when the spot radius is 500nm. This is when the spot diameter equals the side length of the polariser. The 600nm radius shows the extinction ratio when the beam spot area is bigger than the polariser area and the reduction observed here may be affected by the finite simulation domain size rather than being a real effect.

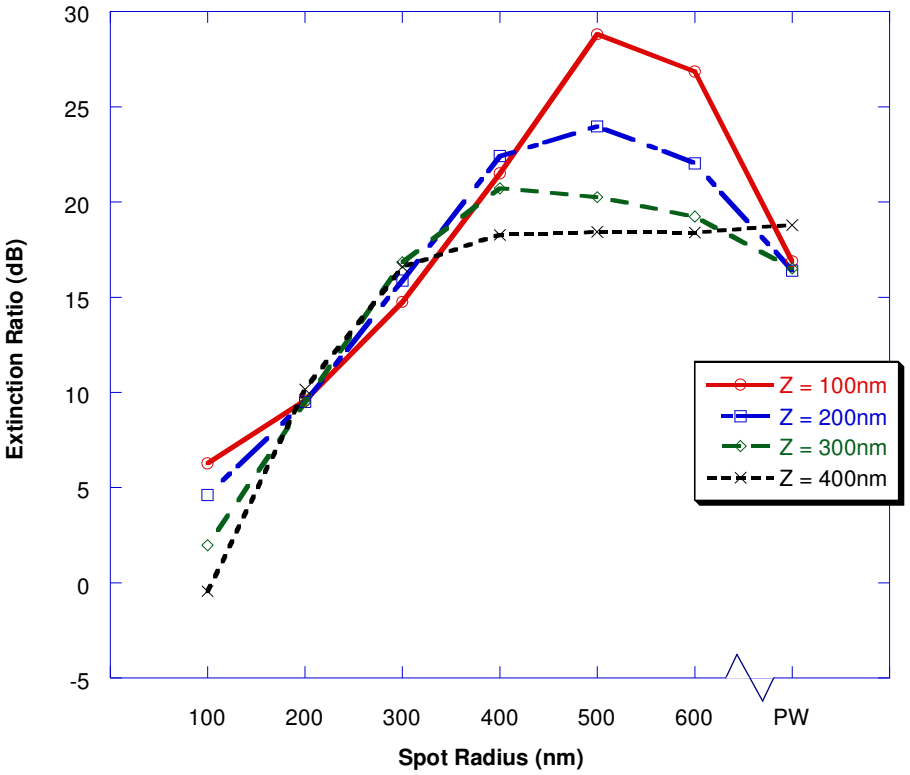

Figure 53: Extinction ratio of the single polariser as a function of the Gaussian beam spot radius.

4.6 Summary

The results suggest that the polarisation effect is better when the spot radius is bigger and close to the plane wave. So for the polarisation effect to be significant, the spot size area is required to be large enough. In this case, at least 300nm of Gaussian beam spot radius is required to get a near-field extinction ratio greater than 10dB. The optimal spot radius is when the beam close to the plane wave propagation. In this case, at 500nm radius, the polariser has the maximum effective area to the transmission. However, the polarisation effect is limited by the Gaussian beam spot radius. For the radius smaller than 300nm, the transmission coefficient can even show a reversed polarisation effect, which is interesting but not useful for the application of interest in this study.

5.0 TWO DIMENSIONAL POLARISER ARRAY SIMULATIONS

Chapter Three introduced the polarisation effect of a single metallic polariser pattern. There were high transmission coefficients for theta polarisation and low transmission for phi polarisation when the polariser was placed vertically. These simulation results show the compatibility of the polarisation effect with the CD/DVD technology. However, in order to achieve double or quadruple the data storage capacity, it is necessary to expand the simulations and study geometrical arrangements of polariser sub cells.

In the current CD/DVD technology, there is only one bit of data which can be accessed within one optical source spot. The idea of increasing the data storage capacity is to allow multiple data bits to be accessed within this one optical spot. Therefore this chapter covers simulation the experiments which were focused on two dimensional multi-polariser array patterns. The pattern was a two-by-two array of metallic polarisers. Each polariser sub cell has a vertical or horizontal orientation.

5.1 Basic Simulation

The first simulation of the multi-polariser array pattern was a basic and simple simulation. The purpose was to discover the effect of this polariser array and its interference level.

5.1.1 Simulation Parameters Setup

Similar to the single polariser simulation, the first step was the simulation geometry setup. As the pattern was a two-by-two array of polarisers, the grid size was doubled in the X and Y axes. The grid size then became 200 cells * 200 cells * 100 cells. The cell size remained as 10nm * 10nm * 10nm and gave the overall space to be 2000nm * 2000nm * 1000nm.

In this simulation, the pattern was made of the four polarisers described in the previous chapter, as shown in Figure 54. Each of these polarisers' wires had dimensions of 1000nm long, by 40nm wide, by 40nm thick. For convenience, these two-by-two polariser sub cells were numbered in quadrants as shown in Figure 54. For Q11 and Q22, the polarisers were placed vertically. For Q12 and Q21, the

polarisers were placed horizontally. This orientation helped the analysis of the interference between any two adjacent polarisers. The pattern material was PEC in this basic simulation.

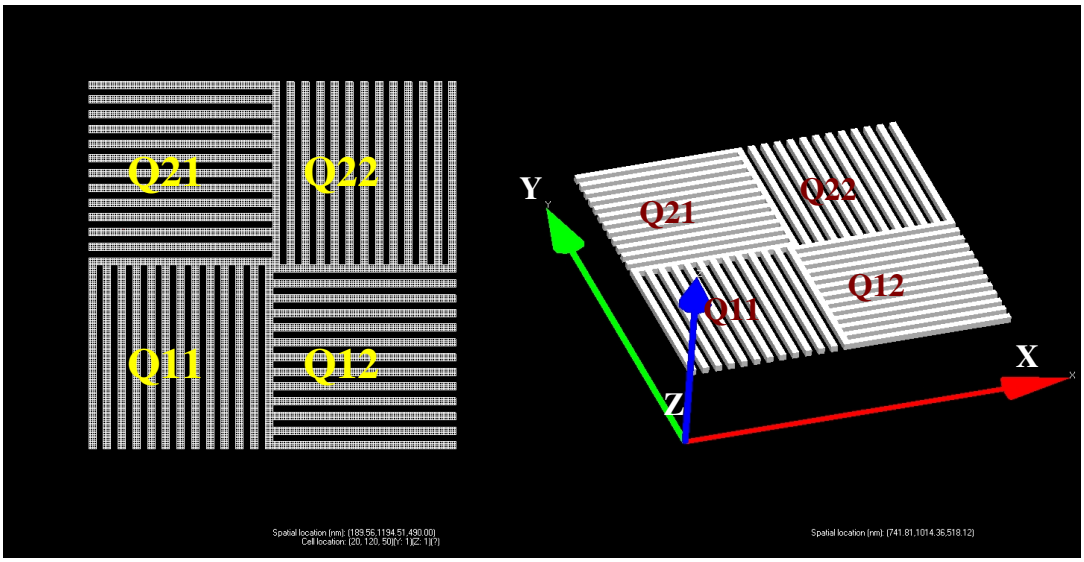

Figure 54: The multi-polariser array pattern.

The wave source in this simulation was again a plane wave with a 650nm wavelength. The plane wave was used instead of a Gaussian beam because of its simplicity in this basic simulation. Only a theta polarised wave was used in this simulation because both polariser orientations are degenerate due to the symmetry of the system. The study of the polarisation effect resulting from parallel and perpendicular transmissions could be observed from any two adjacent polarisers.

There were three sets of transient field snapshots taken in this simulation: XY plane at Z = 250nm, YZ plane at X = 500nm and ZX plane at Y = 500nm. The XY plane snapshots show the electric field after the incident wave has propagated through the polarisers. The YZ plane and ZX plane were taken through the middle of Q11, Q21 polarisers and Q11, Q12 polarisers respectively. These two sets of snapshots show the incident wave propagation and transmission for both polariser orientations.

The near-zone data was also taken in this simulation. Four sets of data were measured under the centre of the polariser sub cells Q11 and Q12. They were located at Z = 100nm, 200nm, 300nm and 400nm. These data sets observed the transmission after the incident wave propagated through the polarisers, which were located at Z = 500nm.

5.1.2 Simulation Results

The theta polarised plane wave propagated along the Z axis, and Figure 55 shows the field view of this propagation through the multi-polariser array after 22.55fs. It was taken at Y = 500nm and through the polariser Q11 and Q12. Since Q11 and Q12 have different orientations, the ZX plane snapshot shows both polarisation effects in one. At Q11, the theta polarised plane wave was perpendicular to the vertically orientated polariser and there is a high transmission coefficient. At Q12, the incident wave is parallel to the horizontally orientated polariser and there is a low transmission. More detail of the near-zone data are shown in Figure 56.

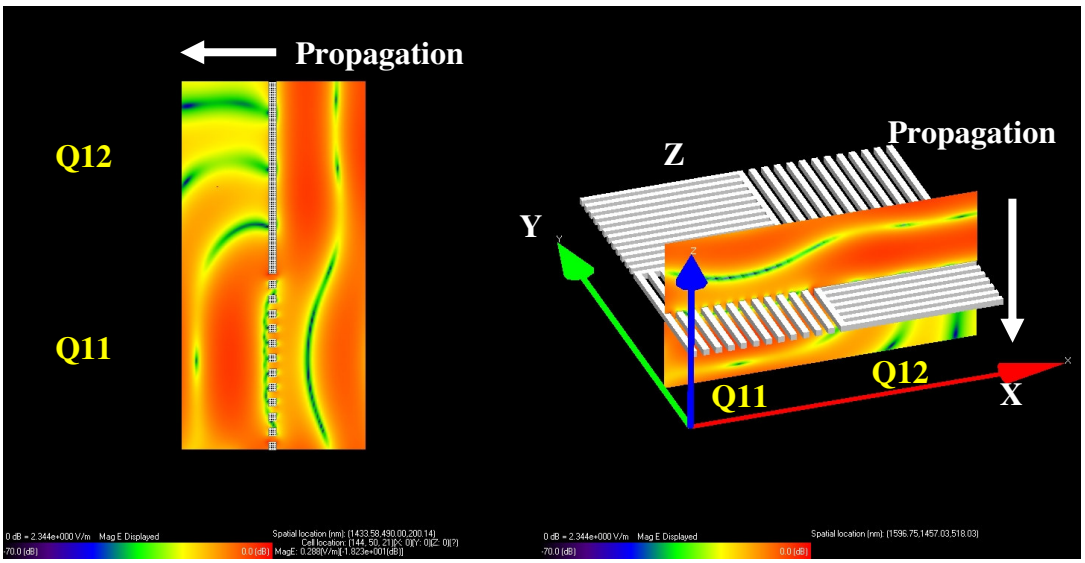

Figure 55: Theta polarised plane wave propagation through the PEC multi-polariser array pattern.

Figure 56 shows quantitatively that the transmission coefficient of E_X is high in Q11 and low in Q12. These results agree with the polarisation theory. However, for both polarisations the transmission coefficients are higher than for the uniform polarisers discussed in Chapter 3. This is because of the diffraction and also the interference from the adjacent polarisers. Note that the Q11 transmission coefficient is also greater than one.

The intra-cell crosstalk for each cell has also been determined, and there are shown in Figure 57. The crosstalk levels from both polarisers are much higher than the average in previous simulations however we note that crosstalk levels are less than 10%, and are always much less than the transmission of the desired polarisation. More details about the interference and crosstalk effects will be discussed in the later sections.

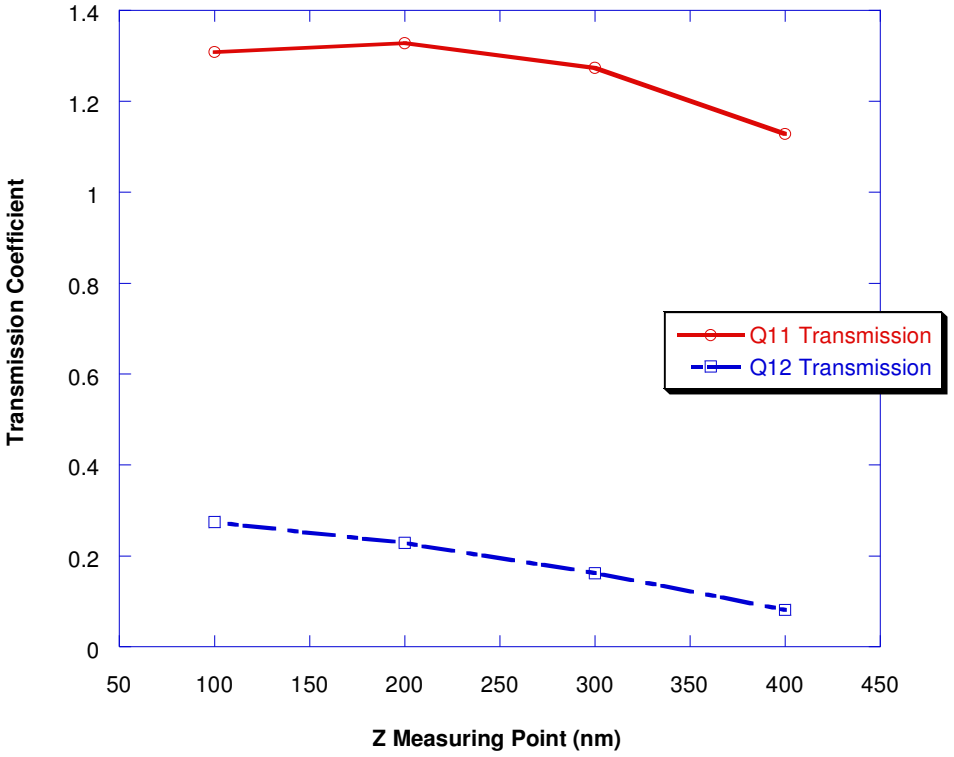

Figure 56: Transmission coefficient of the multi-polariser array pattern.

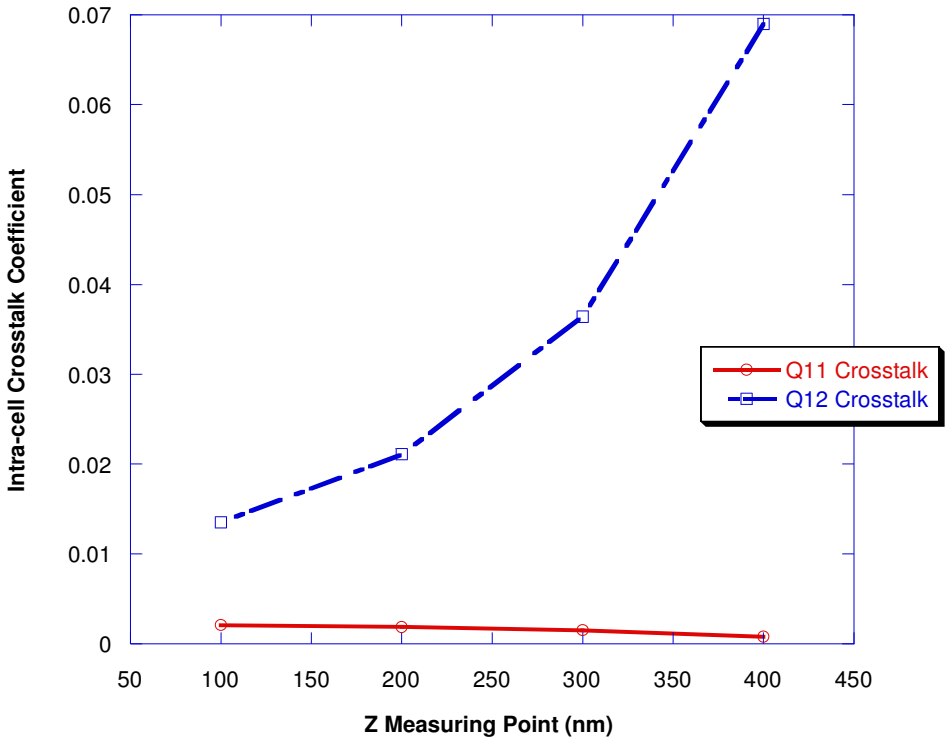

Figure 57: Intra-cell crosstalk coefficient of the multi-polariser array pattern.

5.2 Material Simulation

From the previous section, the basic simulation results show that the polarisation effect agrees with the theory in the multi-polariser array patterns. This section describes simulation of the polarisation effect with respect to different polariser materials. The transmission coefficients and crosstalk were simulated and compared between gold, copper and titanium polarisers.

5.2.1 Simulation Parameters Setup

This simulation used the same parameter settings as the basic simulation in the previous section. The pattern was also the multi-polariser array. The quadrants in this two-by-two array were numbered Q11, Q12, Q21 and Q22, the same as in the basic simulation. The simulated polariser materials included copper, gold and titanium. The parameters of these metals were calculated in Chapter Three and are re-used here.

5.2.2 Simulation Results I (40nm Thick Polarisers)

All three metal materials were used in the simulation as the polarisers. The PEC results are also included as a comparison. In this simulation, the polariser pattern was 40nm thick.

Figure 58 shows the strong polarisation effect of the E_X component transmission coefficient from all materials in Q11. All three materials performed well in this wave polarisation and pattern orientation. However, the transmission coefficients are higher when the distances are further away from the polariser. This indicates there was interference caused by diffraction and crosstalk.

The E_Y component was also measured in Q11 with the theta polarised wave as the intra-cell crosstalk as shown in Figure 59. The crosstalk levels of these three materials are all below 5% of the incident theta polarised wave magnitude. However, the values are higher than the PEC result and much higher than the single polariser simulations in Chapter 3. Within these three materials, titanium has the lowest intra-cell crosstalk level in this simulation.

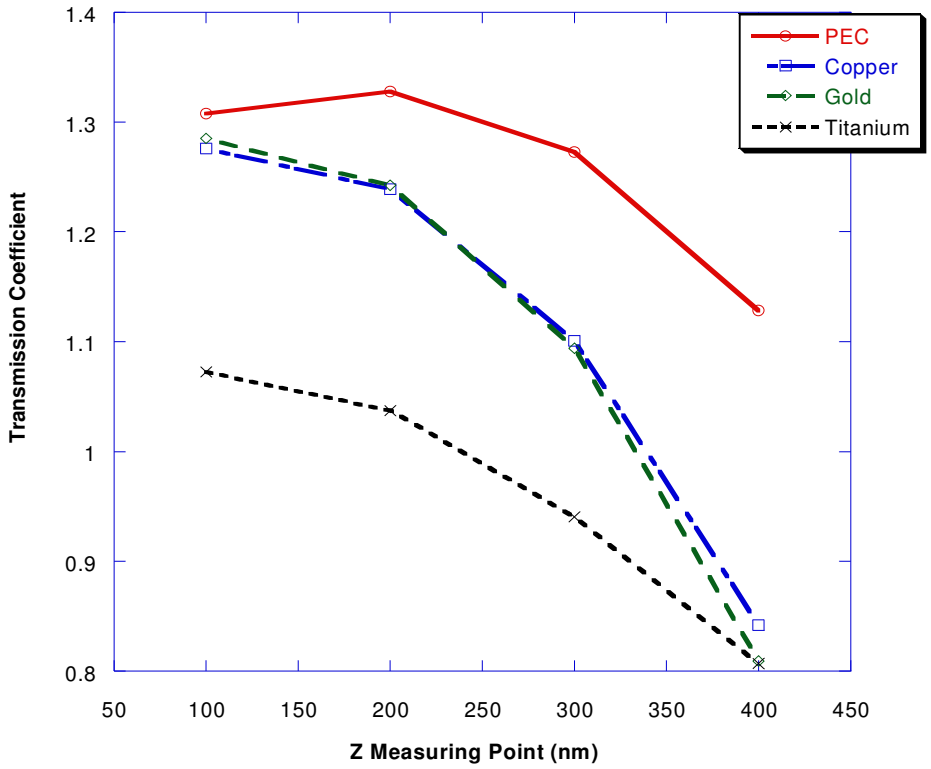

Figure 58: Transmission coefficient of Q11 polariser in multi-polariser array with different materials.

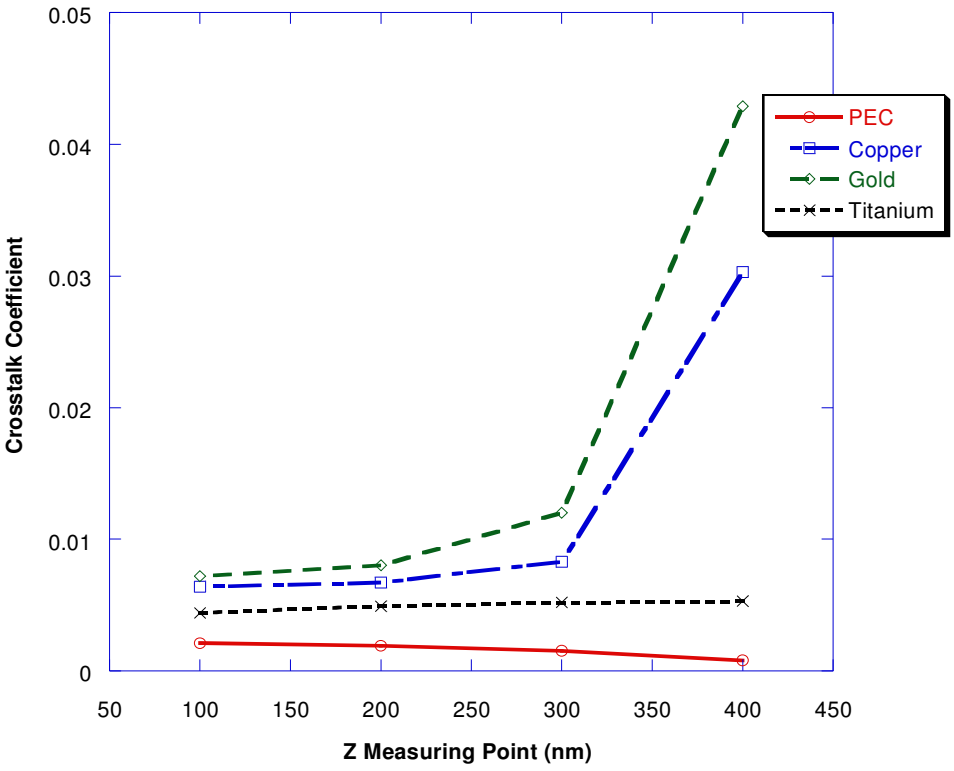

Figure 59: Crosstalk coefficient of Q11 polariser in multi-polariser array with different materials.

The transmission coefficient of the parallel transmission (sub cell Q12) is shown in Figure 60. The results of the three realistic metals are not satisfactory as the coefficients are higher than 30%. The three metals have similar results when the measuring points are at Z = 100nm and Z = 200nm. At Z = 300nm and Z = 400nm, titanium shows different characteristics compared to copper and gold. The transmission coefficient of titanium is increased when the measuring point is closed to the polariser.

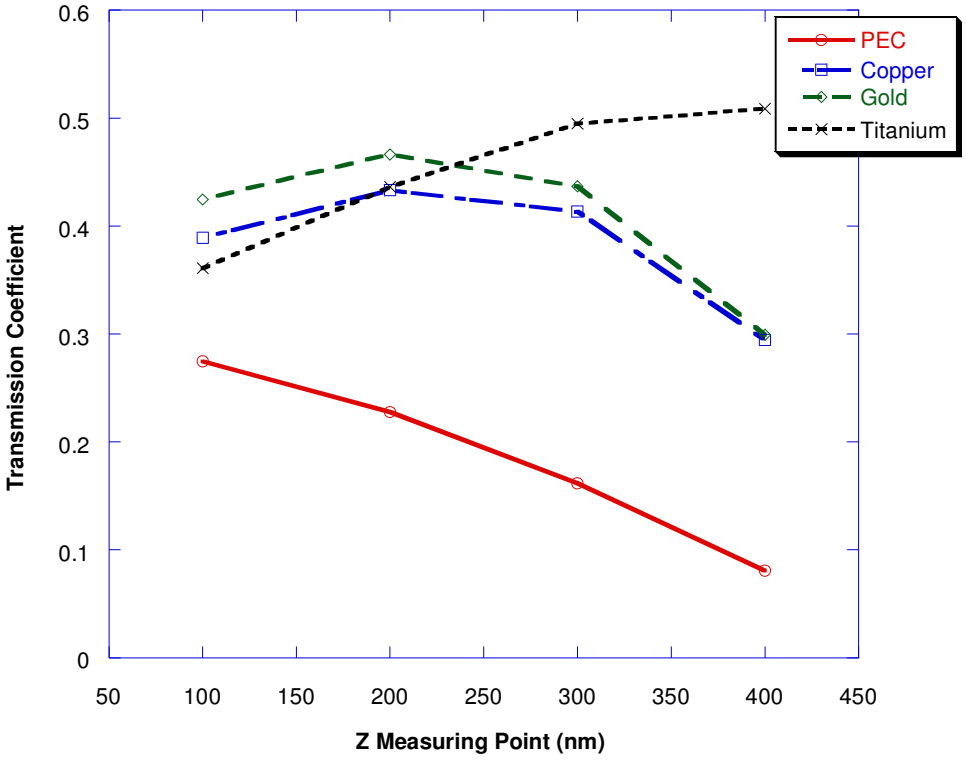

Figure 60: Transmission coefficient of multi-polariser array in Q12 with respect to different materials.

Figure 61 shows the intra-cell crosstalk coefficient of parallel transmission with respect to different materials. The crosstalk in Q12 is higher than the results in Q11. Copper and gold both have a crosstalk level of around 1% of the incident wave. Titanium has the lowest crosstalk coefficient within the three metals except at Z = 300nm. Its crosstalk coefficient does not vary with the Z measuring point significantly and is about 0.5% of the incident wave magnitude

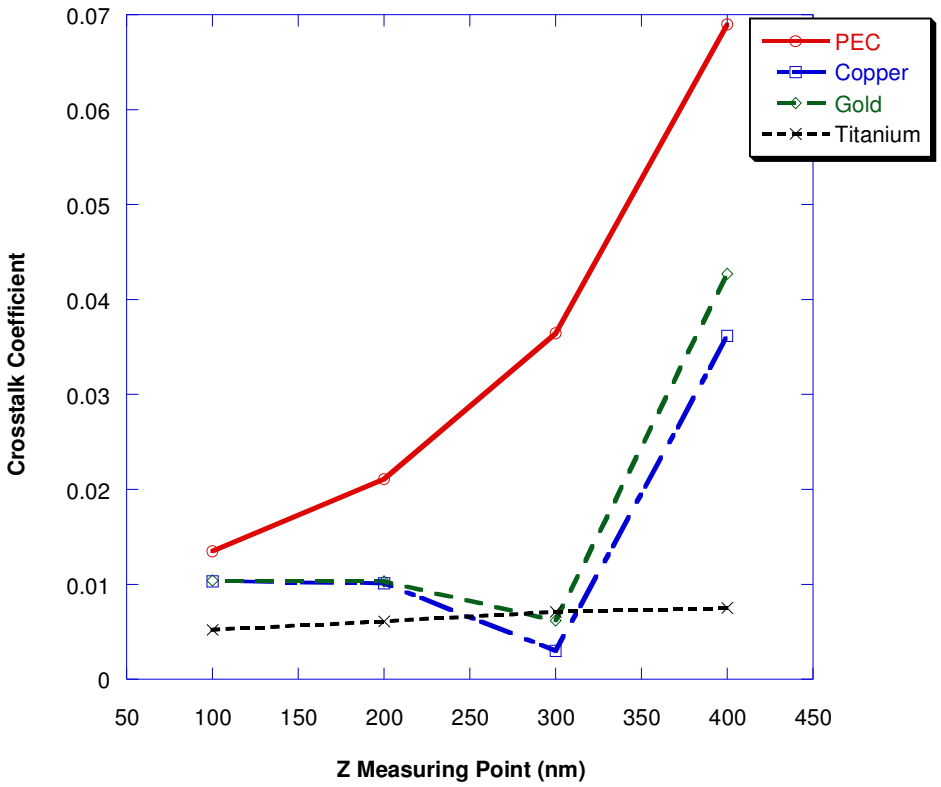

Figure 61: Crosstalk coefficient of multi-polariser array in Q12 with respect to different materials.

5.2.3 Inter-cell Extinction Ratio I (40nm Thick Polarisers)

There was only theta polarised incident wave used in the multi-polariser array pattern simulation. Therefore the extinction ratio was calculated differently from the single polariser pattern case. As the multi-polariser array is a symmetrical pattern, the theta polarisation effect in polariser Q12 can therefore be recognised as the phi polarisation effect in polariser Q11. The inter-cell extinction ratio is then calculated as:

$$Inter-cell\ Extinction\ Ratio = 20\log\left(\frac{Q11\,Transmission\,Coefficient}{Q12\,Transmission\,Coefficient}\right) \quad (5.2.1)$$

Figure 62 plots the extinction ratio of the multi-polariser array pattern with respect to different materials. The pattern thickness was 40nm. The order of the result follows the order of the conductivity. In this case, the PEC polariser has the best result and titanium is the least effective. All materials show approximately linear relationships with the distance between the measuring point and the polariser. The extinction ratio of the PEC polariser is increased when the distance of the measuring point is decreased (moved away from the polariser). However, the characteristic of titanium

is totally reversed. The extinction ratio of titanium is increased when the distance is also increased. For copper and gold polarisers, the extinction ratios are quite stable through the different measuring points.

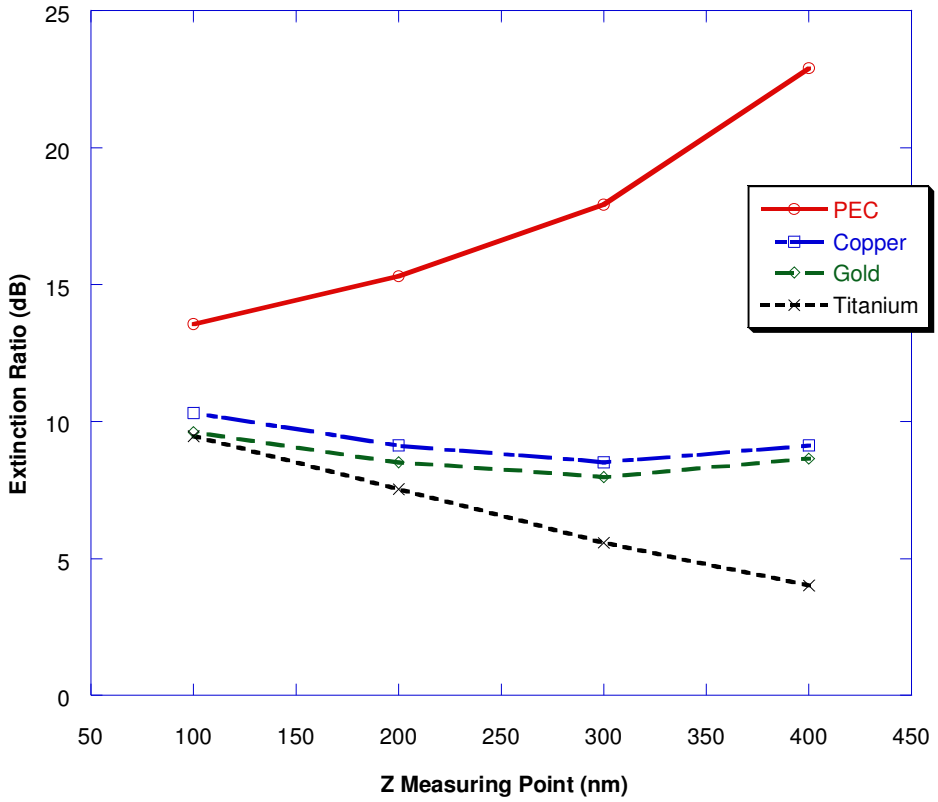

Figure 62: Crosstalk ratio of the multi-polariser array pattern in different materials with 40nm polariser thickness.

Copper and gold have better polarisation effects than titanium. These two high conductive metals result higher transmission coefficient to the desired polarisation. Figure 62 shows that the extinction ratios of copper and gold are about 10dB, which should be acceptable for CD/DVD recording media. For titanium, the extinction ratio is close to 10dB at Z = 100nm but decreases as the measuring point moves close to the polariser. This result will be compared with the 100nm thick pattern simulation in the next section.

5.2.4 Simulation Results II (100nm Thick Polarisers)

The 40nm pattern thickness was not an ideal dimension for the single polariser simulation. Unfortunately, the extinction ratio of a multi-polariser array pattern was worse than for a single polariser. Therefore, the pattern thickness was increased to

100nm and the simulation was repeated. The thicker polarisers were expected to have a better polarisation effect and reduced crosstalk.

Figure 63 is the result of E_X component transmission coefficient (sub-cell Q11) when the polariser thickness was increased to 100nm. The transmission coefficient relationships are quite similar to Figure 58 and Figure 63. The difference is that the transmission coefficient of the 100nm thick pattern is reduced by about 10% from the 40nm case.

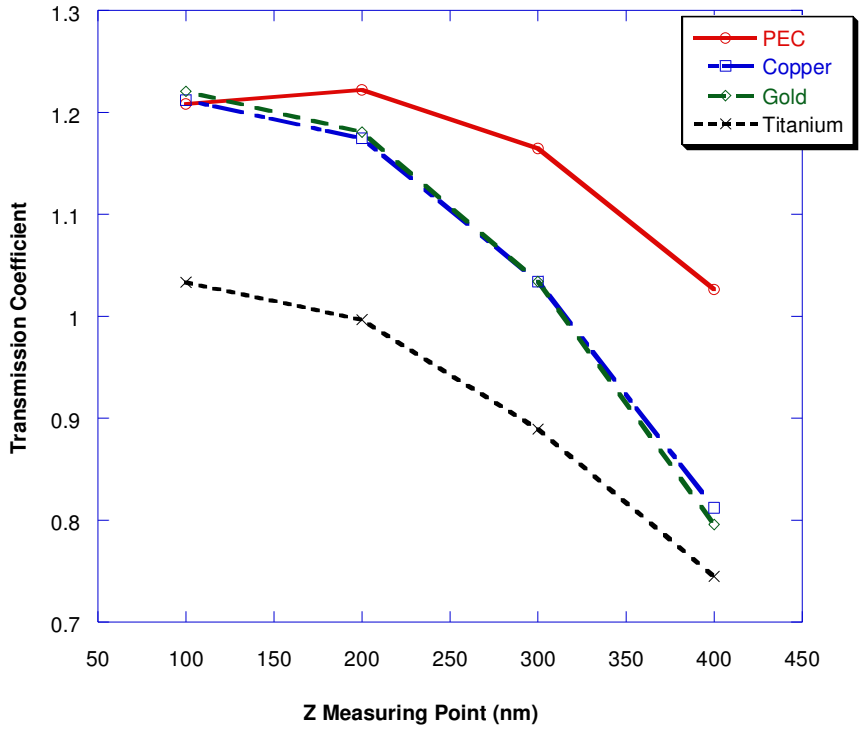

Figure 63: Transmission coefficient of multi-polariser array in Q11 with respect to different materials and 100nm polariser thickness.

Figure 64 shows the intra-cell crosstalk coefficients at Q11 in 100nm polarisers, which are slightly better than the results for 40nm thick polarisers. Copper and gold have reasonable crosstalk coefficients within the measuring point from Z = 100nm to 300nm. However, at Z = 400nm, the crosstalk coefficients are very high. This is because the measuring point is very close to the polariser. Unlike copper and gold, titanium has the crosstalk coefficient constant through the different measuring points.

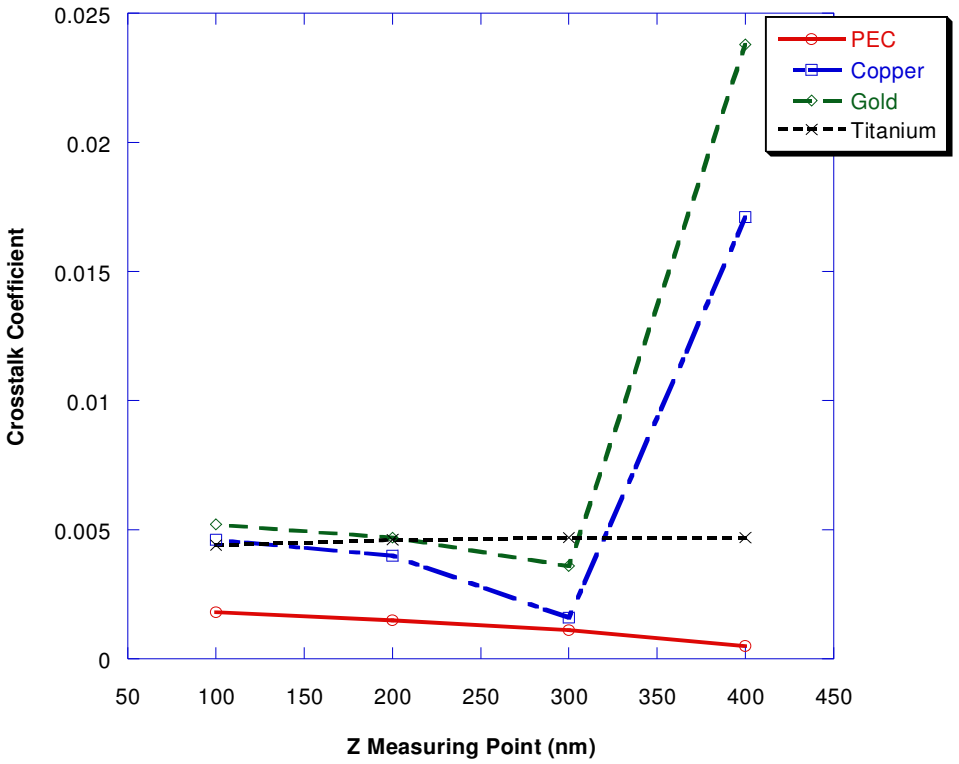

Figure 64: Crosstalk coefficient of multi-polariser in Q11 array with respect to different materials and 100nm polariser thickness.

Figure 65 shows the transmission coefficients in Q12 for 100nm thick polarisers. By comparing Figure 60 and Figure 65, the results of the 100nm thick pattern are improved significantly. There is average 20% drop of the transmission coefficient from the 40nm thick pattern simulation. Titanium has the most improvement and the best result in the transmission coefficient at Z = 100nm and 200nm. This increases the polarisation effect of the titanium polariser strongly, which will be discussed in the next section with the extinction ratios.

As shown in Figure 66, the intra-cell crosstalk levels in Q12 are slightly higher than in Q11 with the theta polarised wave. However, the crosstalk of copper and gold are improved significantly from the 40nm case. For titanium, the results in 40nm and 100nm cases are similar. Its crosstalk coefficients are lower than copper and gold and show stable values with different measuring points.

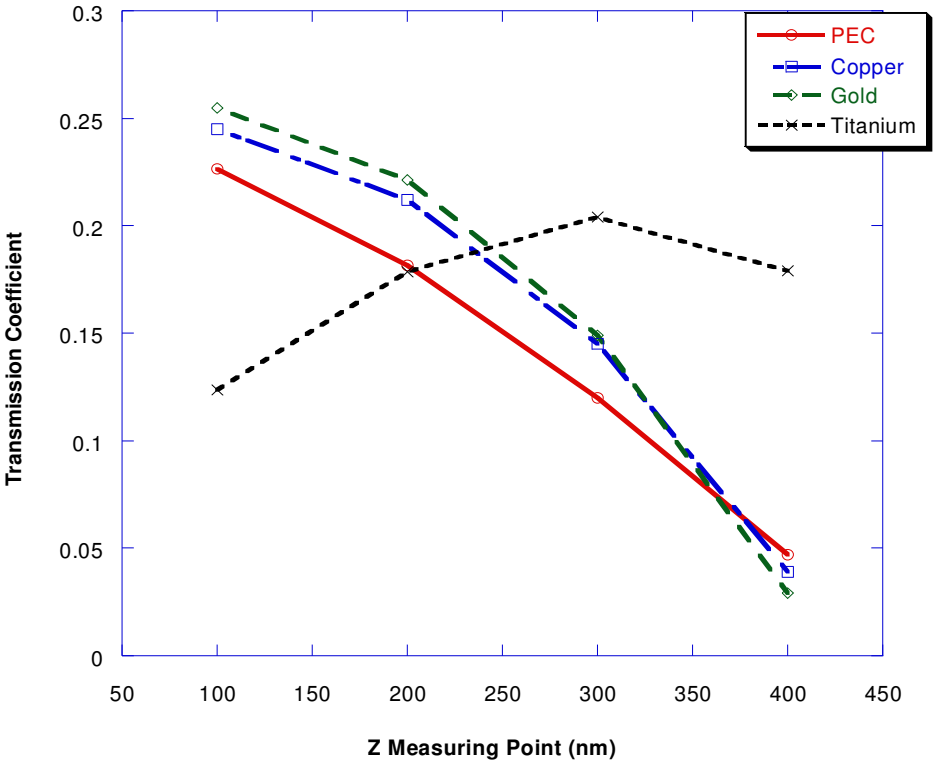

Figure 65: Transmission coefficient of Q12 polariser in multi-polariser array with different materials and 100nm polariser thickness.

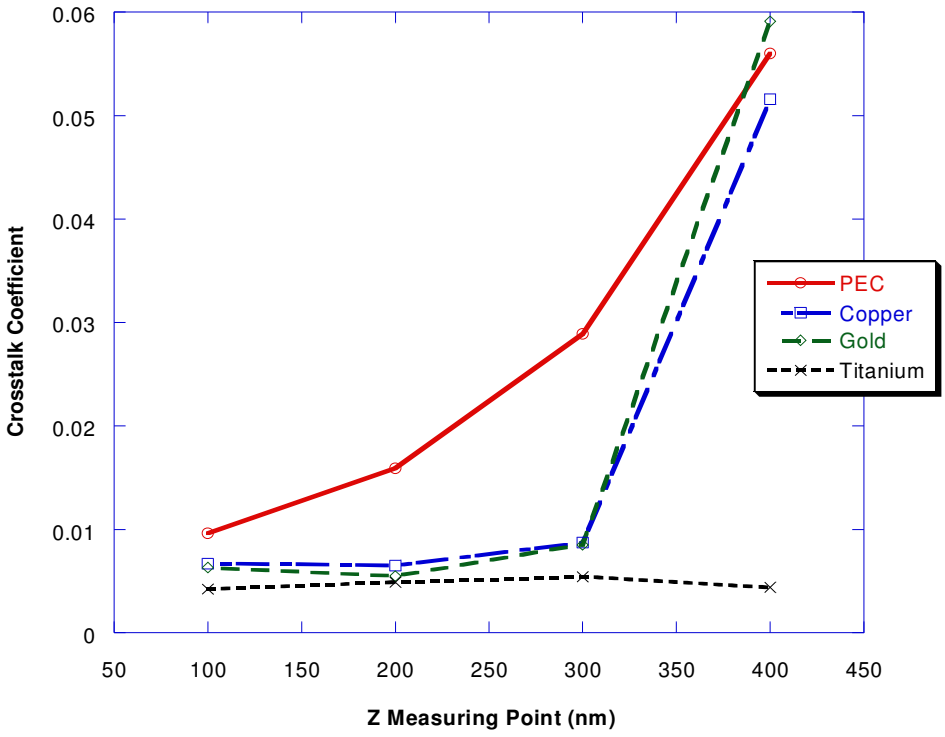

Figure 66: Crosstalk coefficient of Q12 polariser in multi-polariser array with different materials and 100nm polariser thickness.

In this multi-polariser array pattern simulation, titanium was the best material for the polariser. From the optical properties table, titanium has lower conductivity and a smaller relaxation time than copper and gold. These result in the polarisation effect having less crosstalk in titanium polarisers.

By comparing the results from the single polariser simulation and this multi-polariser array simulation, it is clear that the transmission is much higher in the latter for both perpendicular and parallel transmissions. This is because the reflected waves propagate from the nearby polarisers and contributes to the crosstalk. It is a serious problem to the multi-polariser array pattern as there are different polariser orientations. The high transmission emerged wave may propagate to the next polariser and cause the low transmission emerged wave to have a higher magnitude. This problem could be solved by choosing a low conductivity material, like titanium, or by improving the polariser structure.

5.2.5 Inter-cell Extinction Ratio II (100nm Thick Polarisers)

Figure 67 is the inter-cell extinction ratios of the multi-polariser array pattern with 100nm thickness. The order of the ratios no longer follows the order of the material conductivity. At Z = 100nm, the extinction ratio of titanium is better than all other materials. At Z = 200nm, the results of copper, gold and titanium are all similar. At Z = 300nm and 400nm, the extinction ratio of titanium is lower than copper and gold. However the results were all improved, especially for titanium, as the polariser thickness was increased and in all cases the extinction ratio is greater than 10dB.

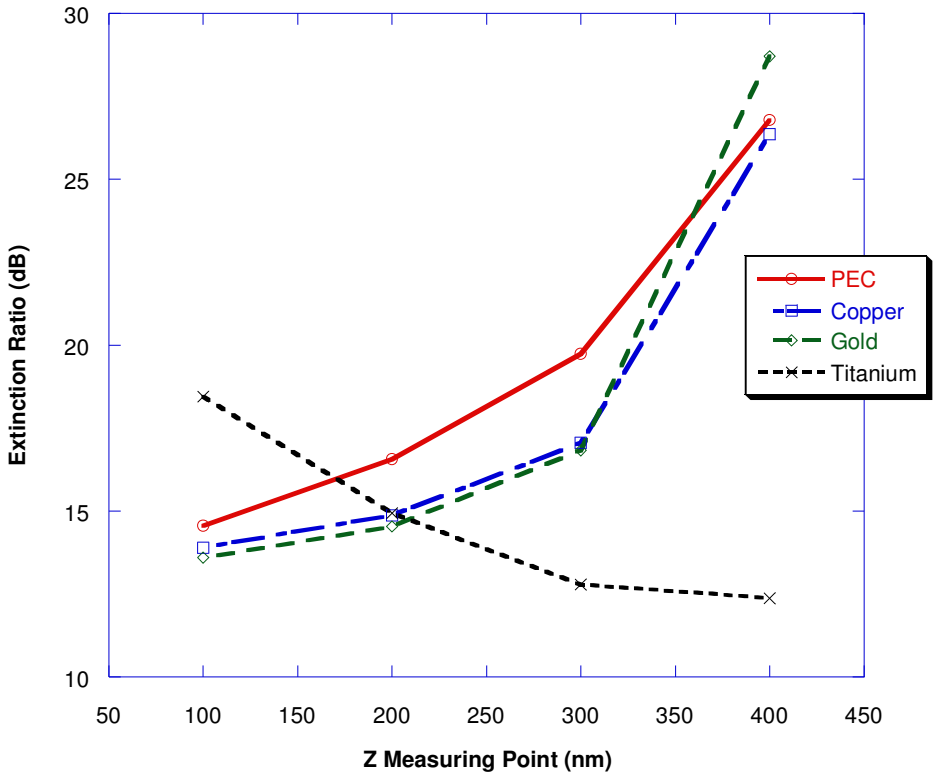

Figure 67: Extinction ratio of the multi-polariser array pattern in different materials with 100nm polariser thickness.

5.3 Multi-polariser Pattern with Solid Borders

There is significant increasing of interference in the grating polariser array pattern than the single pattern case. A major component of the interference is from the neighbouring polarisers. One possible solution to this is to place a border between the grating polarisers. The effect of adding borders to the sub-cells was hence studied to see if the way in which the edges are terminated significantly affects the performance.

The grooved polariser pattern was applied to the multi-polariser array simulation. Like the ordinary multi-polariser array simulation, the grooved polarisers were placed as a two-by-two array and defined as four quadrants, as shown in Figure 68.

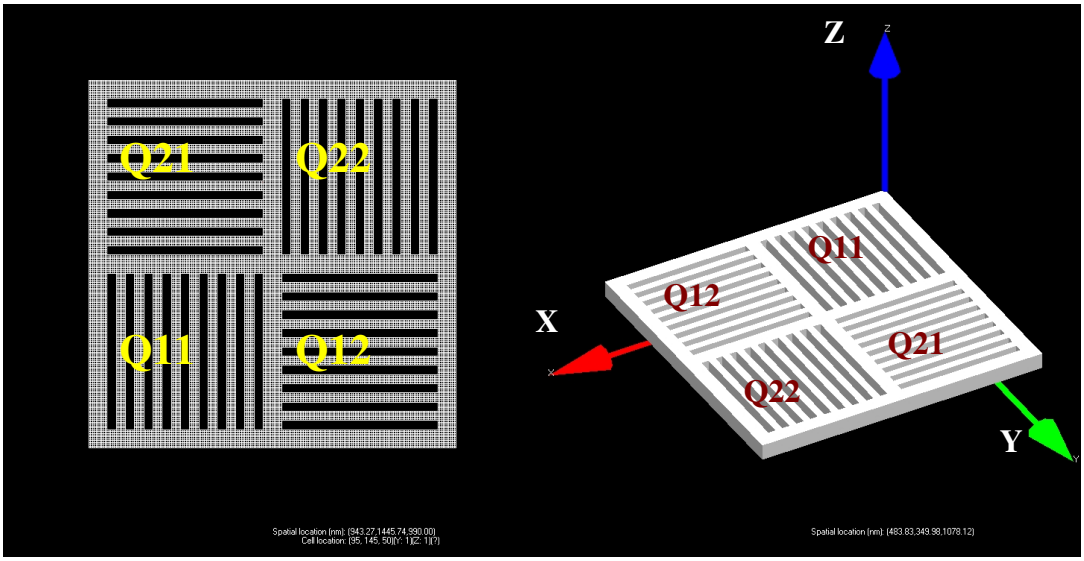

Figure 68: Multi-polariser array groove pattern.

In this section, the purpose of the experiment is to observe the performance of the multi-polariser array with groove polarisers.

5.3.1 Perpendicular Transmission Results

In quadrant Q11, the theta polarised incident wave oscillation direction is perpendicular to the polariser orientation. The simulation result of Q11 is plotted in Figure 69 and Figure 70 with respect to all materials.

In Figure 69, the transmission coefficients of all three metals are higher than the ordinary array pattern case. However, the crosstalk coefficients of copper and gold in Figure 70 are also increased. This indicates that the grooved polariser patterns cause more diffraction and interference than the ordinary polarisers. The only exception is the titanium. Its crosstalk is decreased slightly from the ordinary array pattern. Because of titanium's low conductivity, it has a lower crosstalk effect than the other two metals.

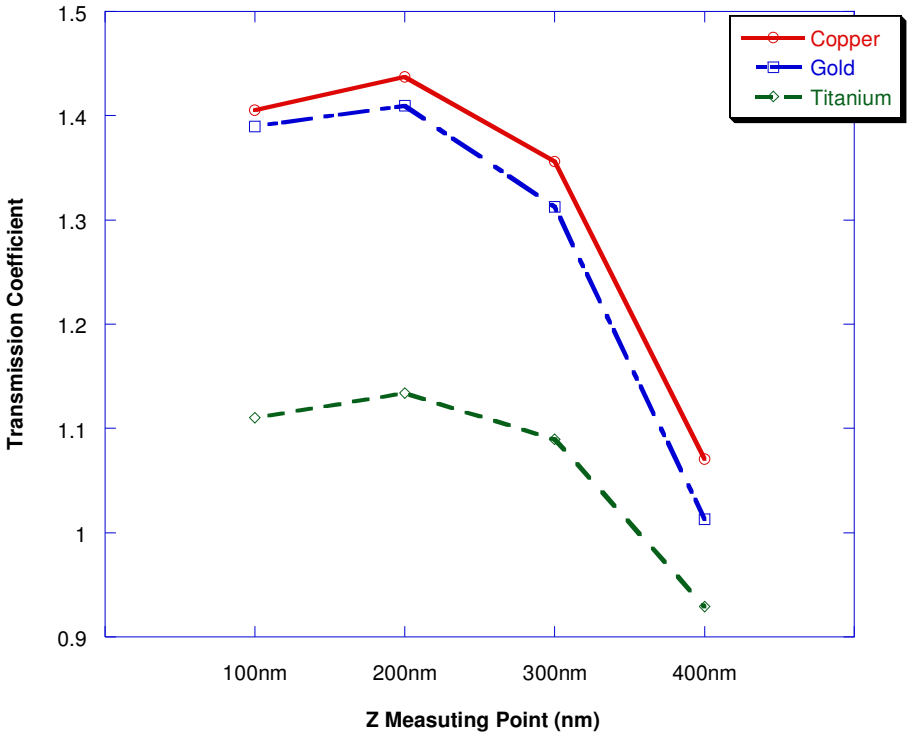

Figure 69: Transmission coefficients of the theta polarised wave with different materials of the multi grooved polarisers array pattern at Q11.

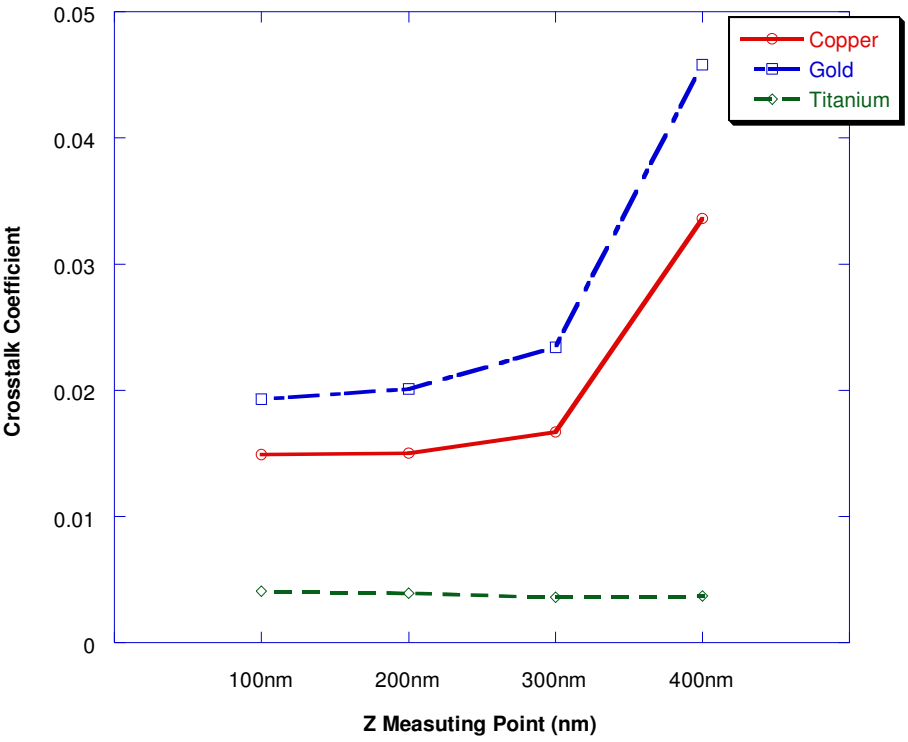

Figure 70: Crosstalk of the theta polarised wave with different materials of the multi grooved polarisers array pattern at Q11.

5.3.2 Parallel Transmission Results

The theta polarised wave has oscillation direction parallel to the Q12 polariser orientation. The transmission coefficient is low in this polariser sub-cell. The transmission coefficients and crosstalk coefficients are plotted in Figure 71 and Figure 72 respectively.

Figure 71 plots the transmission coefficients of all three metallic materials when a theta polarised incident wave is applied to the Q12 polariser sub-cell. The plot shows that titanium has a different characteristic from copper and gold when the measuring point Z is in the range of 200nm to 400nm. At Z = 100nm, titanium has the transmission coefficient as 33%, copper and gold are above 35% and 40%. The coefficients are much higher than the ordinary polariser case.

Figure 72 show the crosstalk effect in Q12 sub-cell. All three metals have lower crosstalk coefficients in this sub-cell than the Q11 case, but the results of copper and gold are much higher than the ordinary polariser simulation except titanium. However, the characteristics are similar to the Q11 case and the ordinary polariser case. Figure 72 shows that the crosstalk coefficient of titanium has the linear relationship with the measuring point distance from the polariser. Copper and gold are similar but have the crosstalk increased enormously at Z = 400nm. Overall, titanium has the lowest crosstalk coefficient within the three materials and its result is not worse than the ordinary polariser case.

Both the transmission and crosstalk coefficients of all three materials are higher in the grooved pattern simulation than the ordinary polariser case. The only exception is the crosstalk of the titanium polariser. The additional border of the pattern causes certain amount of components of the emerged wave to have a different polarisation state. This crosstalk is proportional to the material conductivity. Therefore a titanium polariser, which has lower conductivity than copper and gold, has lower crosstalk coefficient in the sub-cell simulations.

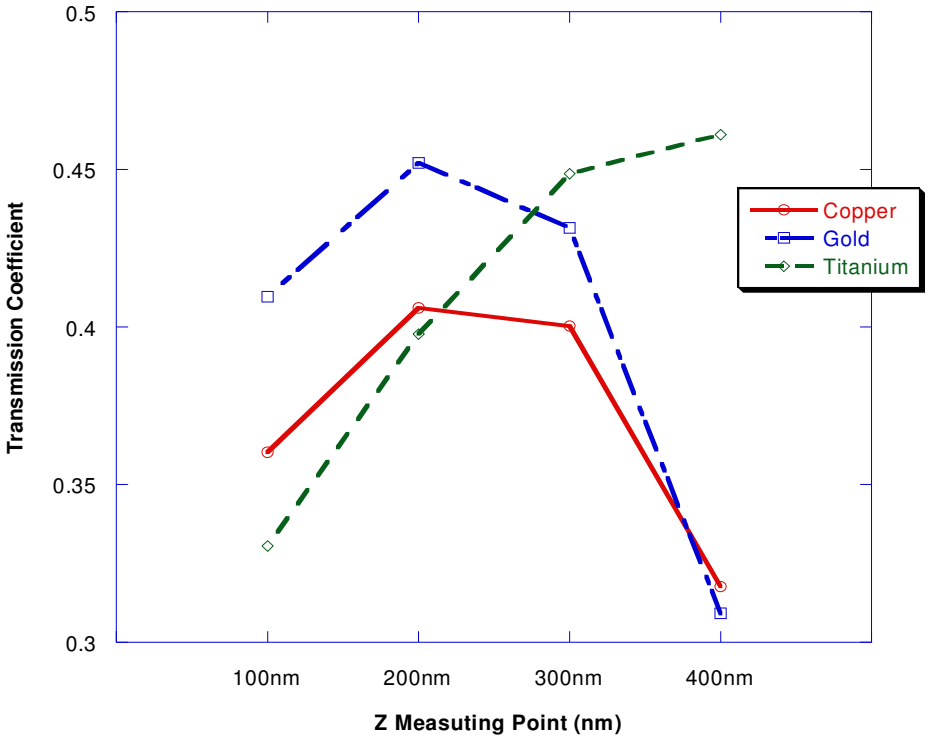

Figure 71: Transmission coefficients of the theta polarised wave with different materials of the multi grooved polarisers array pattern at Q12.

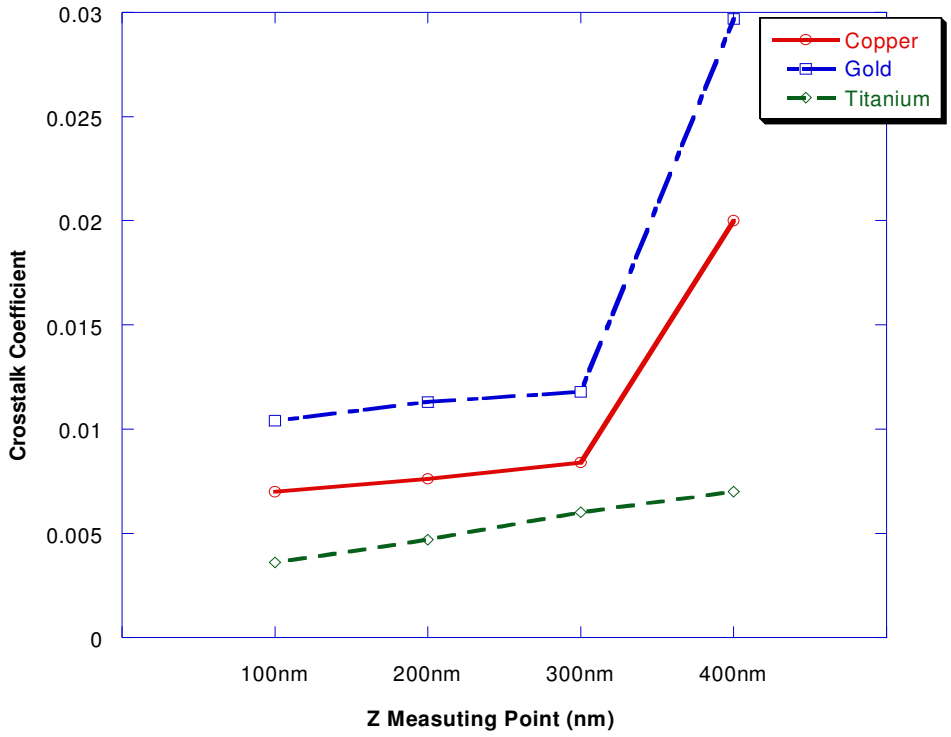

Figure 72: Crosstalk of the theta polarised wave with different materials of the multi grooved polarisers array pattern at Q12.

5.3.3 Inter-cell Extinction Ratio

The polarisation effect of the grooved multi-polariser array was analysed by calculating the inter-cell extinction ratio. The ratio was calculated by following the same method which was mentioned in Section 5.2.3. The results were based on the transmission coefficient of Q11 and Q12 polarisers with respect to the plane wave source.

As shown in Figure 73, the extinction ratios of copper and gold are quite similar. However, the titanium has different characteristic from the other two metals. For copper and gold, the extinction ratios are higher when the measuring point is closed to the polariser. The extinction ratio of titanium is increased when the measuring point is further away from the polariser. At Z = 100nm, titanium has great polarisation effect as its extinction ratio is about 20dB. By comparing the results from Figure 67 and Figure 73, the extinction ratios of the titanium grooved pattern are improved significantly from the ordinary pattern case. The extinction ratios of copper and gold polarisers are slightly lower because the higher phi polarisation transmission coefficients as shown previously.

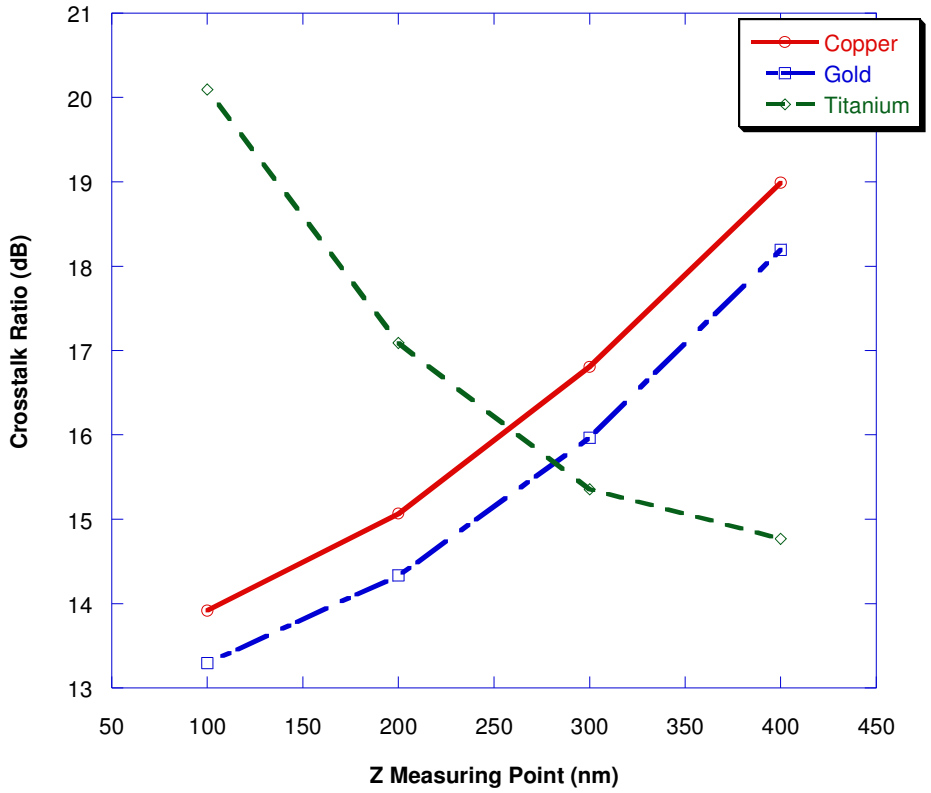

Figure 73: Crosstalk ratio of the grooved multi-polariser array in different materials.

5.4 Summary

The two dimensional polariser array simulations are important to the data accessing application on the DVD disc in this project. Unlike the single polariser simulation, each sub-cell of the two-by-two polariser pattern may have crosstalk that be generated from the neighbouring polarisers. This results in a certain amount of reduction of the polariser performance. The simulations showed that the polariser performance is related to the polariser material, orientation and structure.

In the material simulations, copper and gold have better transmission coefficients than titanium polarisers. However, titanium has a better inter-cell extinction ratio than the other two at the Z = 100nm measuring point. This is because a titanium polariser generates less crosstalk than the other materials. The groove polariser pattern is an improved design for reducing the crosstalk that is generated from the neighbouring sub-cells. The transmission and crosstalk coefficients are both increased in the multi-polariser pattern with solid borders simulation because the solid borders increase the

local crosstalk to the desired sub-cell. The only exception is the titanium polariser which has lower crosstalk because the lower material conductivity.

6.0 MULTI-POLARISER ARRAY SIMULATIONS WITH GAUSSIAN BEAM ILLUMINATION

The plane wave is a handy and ideal wave source type for using in the polariser simulations. The simplicity and unity of the plane wave propagation provides great convenience to test the polarisation effects. However, for a practical analysis of the potential usefulness of the polarisers the Gaussian beam source is required to model the real wave propagation. Unlike the case of normalized interference in the plane wave, the Gaussian beam simulation shows real crosstalk scenarios, from which realistic interference levels can be determined.

6.1 Gaussian Beam on Multi-Polariser Pattern with Solid Borders

The previous simulation had shown the transmission results of the multi-polariser groove pattern with a plane wave source. In this section, the simulation observed the transmission and crosstalk coefficients of the same pattern with Gaussian beam illumination.

The simulation geometry and parameters were set exactly the same as the previous simulation (see Figure 68). The simulation grid contains 200 * 200 * 100 cells. The pattern thickness is 100nm. The Gaussian beam source wavelength is 650nm. The experimental factor was the Gaussian beam spot radius. In this experiment, the spot radius was varied in the range of 500nm to 1000nm with respect to copper, gold and titanium polarisers.

6.1.1 Perpendicular Transmission Results

The theta polarised source wave has perpendicular oscillation direction to the polariser orientation in sub-cell Q11. All three metals were used as the polariser material and simulated individually. The transmission and intra-cell crosstalk coefficients were collected from each simulation and plotted in Figure 74 and Figure 75 as a function of the spot radius. Data was collected at Z = 100nm.

In Figure 74, the copper polariser and the gold polariser have very similar transmission coefficient curves. The titanium polariser curve has the same characteristic but a lower magnitude. All three curves have reasonable transmission

coefficient when the spot radius is larger than 700nm, and these results tend towards to the plane wave simulations when the spot radius is increased. And for radius smaller than 700nm, the coefficients are much larger than unity.

The transmission and crosstalk coefficients are abnormally high when the spot radius is smaller than 600nm. These excessive transmissions are generated by the polariser during the Gaussian beam propagation. The principle of crosstalk generation and the Gaussian beam propagation was discussed in Chapter 4. Figure 75 shows the relation between the crosstalk coefficient and the spot radius. The coefficient is lower when the radius is larger and close to the plane wave. All three materials have similar crosstalk level but titanium is slightly lower than copper and gold.

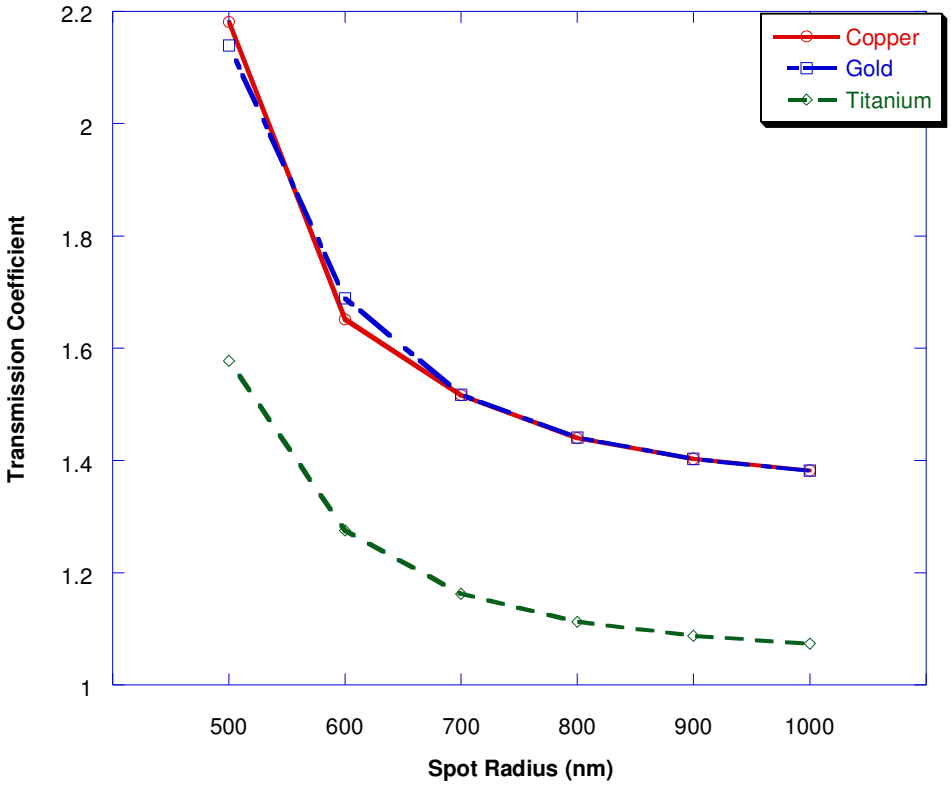

Figure 74: Gaussian beam transmission coefficients in sub-cell Q11 at Z = 100nm.

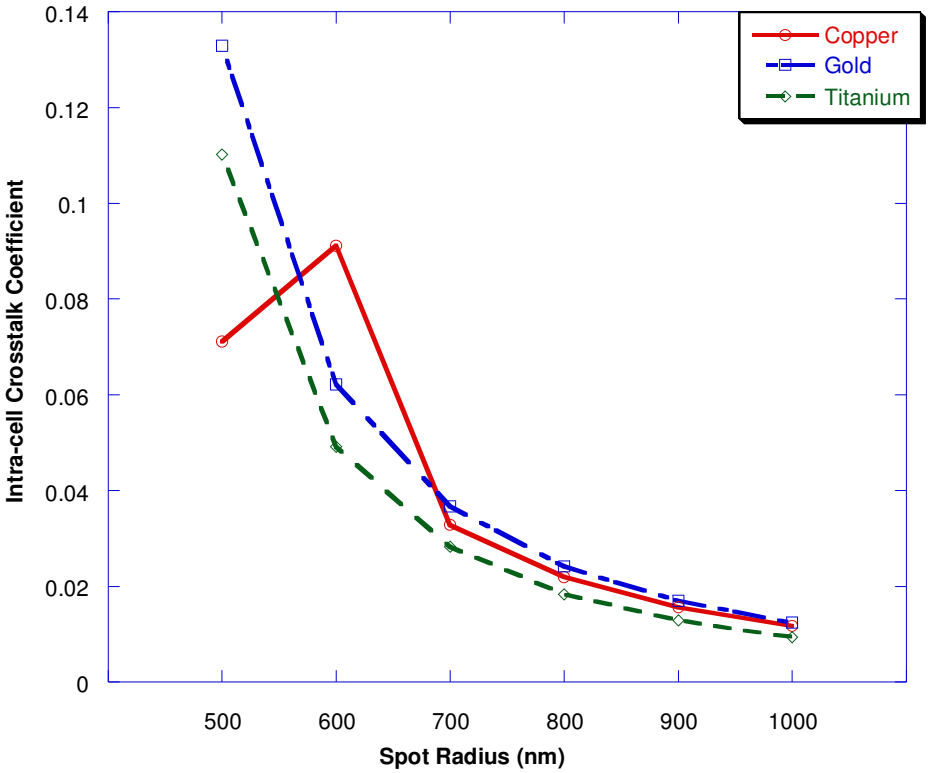

Figure 75: Gaussian beam crosstalk coefficient in sub-cell Q11.

6.1.2 Parallel Transmission Results

The data collected in the sub-cell Q12 are the results of parallel transmission, where the source oscillation direction is the same as the polariser wire orientation. The transmission and the crosstalk coefficients are plotted in Figure 76 and Figure 77.

The copper and gold polarisers have higher transmission coefficients than titanium in the parallel transmission simulation, as shown in Figure 76. The coefficient of the titanium polariser is around 20% lower. This result is similar to the previous simulations. However, when the radius is smaller than 700nm, the copper and gold transmission coefficients are so high that the structure does not show the appropriate polarisation effect. The result is better and more stable when the radius is larger than 700nm. The larger the radius is the better the polarisation effect is.

Figure 77 shows the crosstalk coefficients of the three polariser materials in the sub-cell Q12. Copper and gold polarisers have very similar results when the radius is larger than 700nm and titanium polariser has lower crosstalk levels. High crosstalk coefficients when the radius is smaller than 700nm results in further reduction of the

polarisation effects. This suggests that the polariser is effective only when the source spot radius is greater than 700nm.

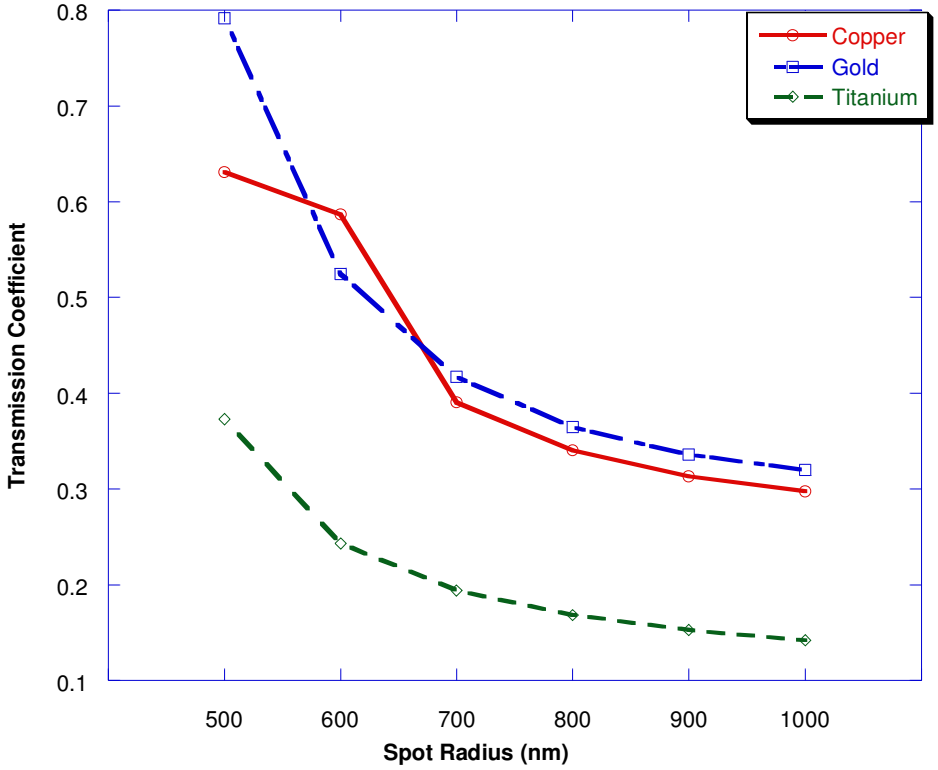

Figure 76: Gaussian beam transmission coefficient in sub-cell Q12.

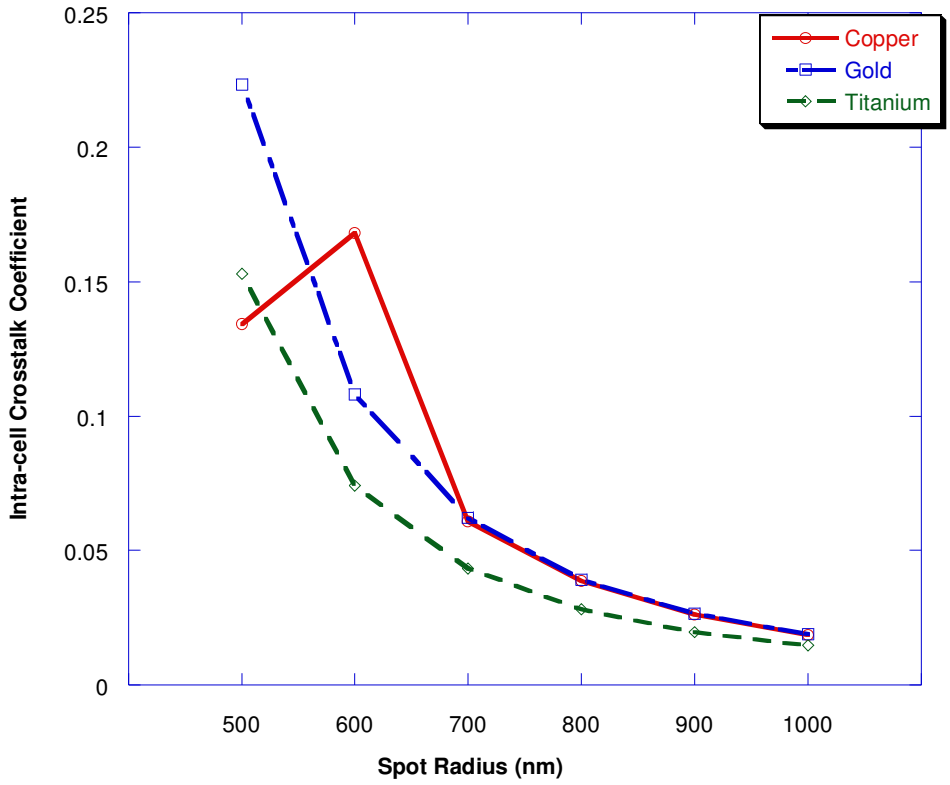

Figure 77: Gaussian beam crosstalk coefficient in sub-cell Q12.

6.1.3 Inter-cell Extinction Ratio

The transmission coefficients generally show the polarisation effect of the multi-polariser groove array pattern. The perpendicular transmission has high coefficient in the sub-cell Q11 and the parallel transmission has low coefficient in the sub-cell Q12. However, the crosstalk ratio, defined in Equation (5.2.1) indicates the polarisation effect more quantitatively. The inter-cell extinction ratio (in dB) of the multi-polariser groove array pattern is calculated and plotted in Figure 78 as a function of the spot radius.

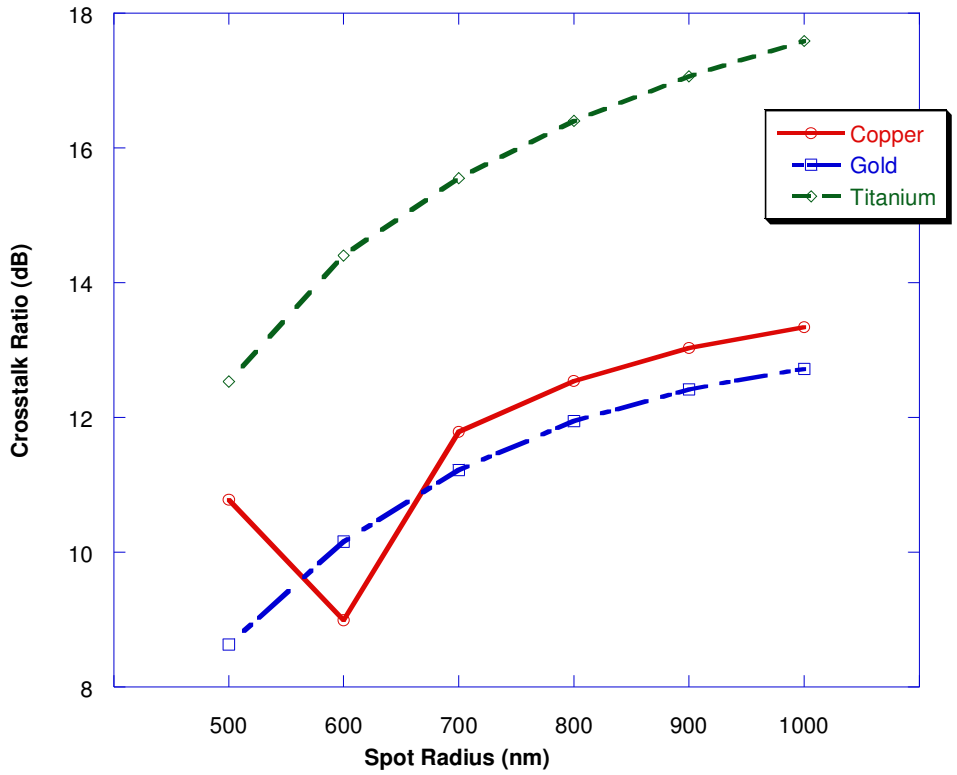

Figure 78: Crosstalk ratio of the multi-polariser groove array pattern with Gaussian beam source.

Two key factors are shown in the plot in Figure 78. Firstly, titanium has a better and higher extinction ratio than copper and gold through the entire spot radius range. Secondly, the ratio is better and higher when the spot radius is greater. The lower conductive material such as titanium has lower crosstalk coefficient and better extinction ratio.

6.2 Two by Two Array Hybrid Material Polariser Simulation

All the previous simulations used a single material polariser for testing the polarisation effect. The simulation in the last section shows that the titanium polariser has better polarisation effect than copper and gold because it results less crosstalk from its low conductivity material. However, copper or gold polarisers do have better transmission coefficient than the titanium polariser. This leads to the idea of using a hybrid-material polariser which may have a high transmission coefficient such as gold and a low crosstalk coefficient such as titanium.

This hybrid material polariser simulation uses exactly the same simulation setting as the multi-polariser groove pattern case. For the material, the polariser wires of each

sub-cell are made of gold for high transmission coefficients. The frame which separates each sub-cell is made of titanium in order to reduce the crosstalk from the adjacent polariser sub-cells. The pattern is shown in Figure 79.

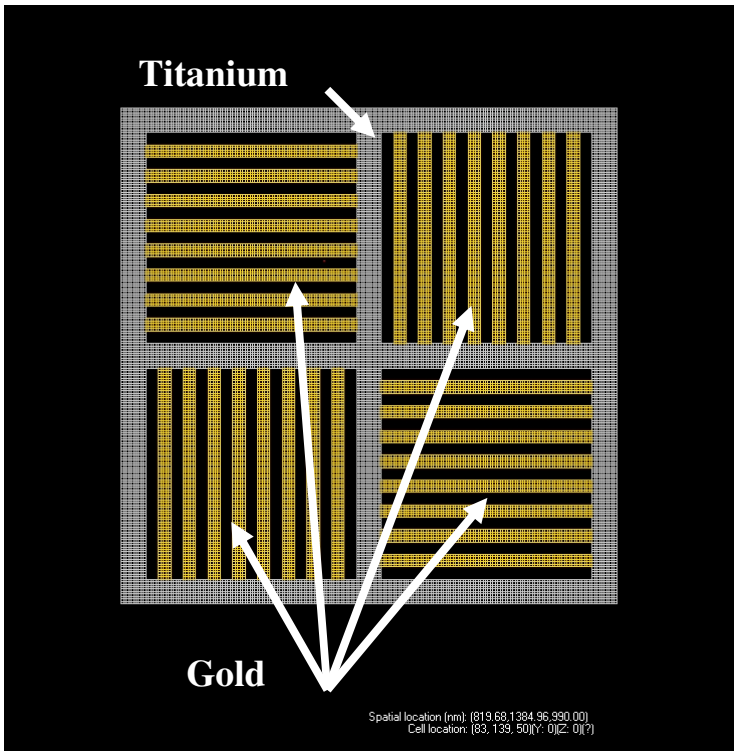

Figure 79: The hybrid material multi-polariser array pattern with gold wires and titanium frame.

6.2.1 Perpendicular Transmission Results

In the single material simulation, copper and gold have higher transmission coefficients than titanium because the higher crosstalk. Figure 80 shows the perpendicular transmission coefficients of the hybrid material polariser and compares these with the three single-material polarisers. The hybrid material has the transmission result higher than titanium, and close to the two high conductive metals, copper and gold.

There is reduction in the transmission coefficient, but it is not matched by a reduction of crosstalk. As shown in Figure 81, the hybrid material has even higher crosstalk coefficient than all three metallic materials. The titanium frame increases the crosstalk level of the perpendicular transmission, which was not expected.

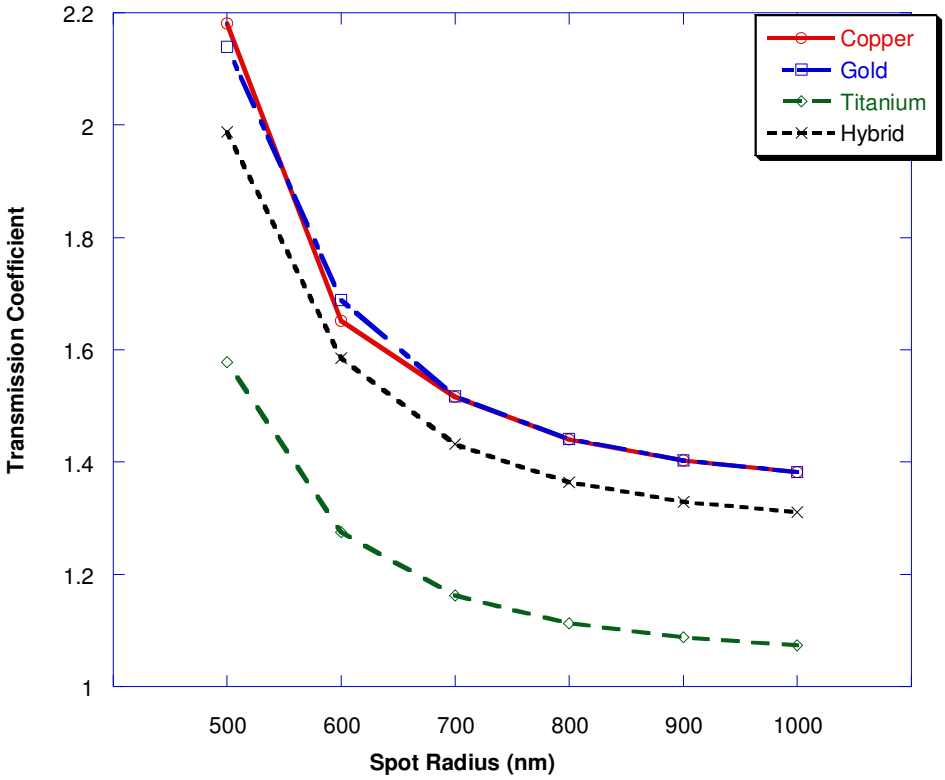

Figure 80: The hybrid material polariser transmission Coefficient on Q11 sub-cell.

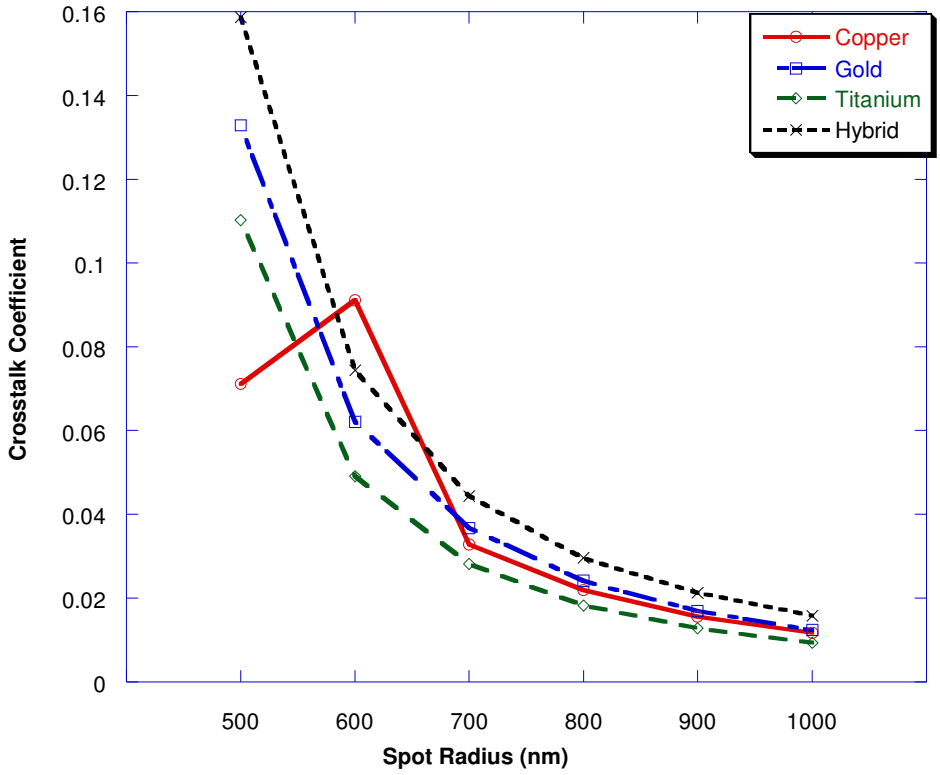

Figure 81: The hybrid material polariser crosstalk coefficient on Q11 sub-cell.

6.2.2 Parallel Transmission Results

Figure 82 shows the transmission coefficient of the parallel transmission of the hybrid material polariser. The result has been improved from the gold and copper materials but still not as good as titanium. Quantitatively, it is about 15% higher than titanium and about 5% lower than gold. However, the result is satisfactory when the spot radius is greater than 700nm.

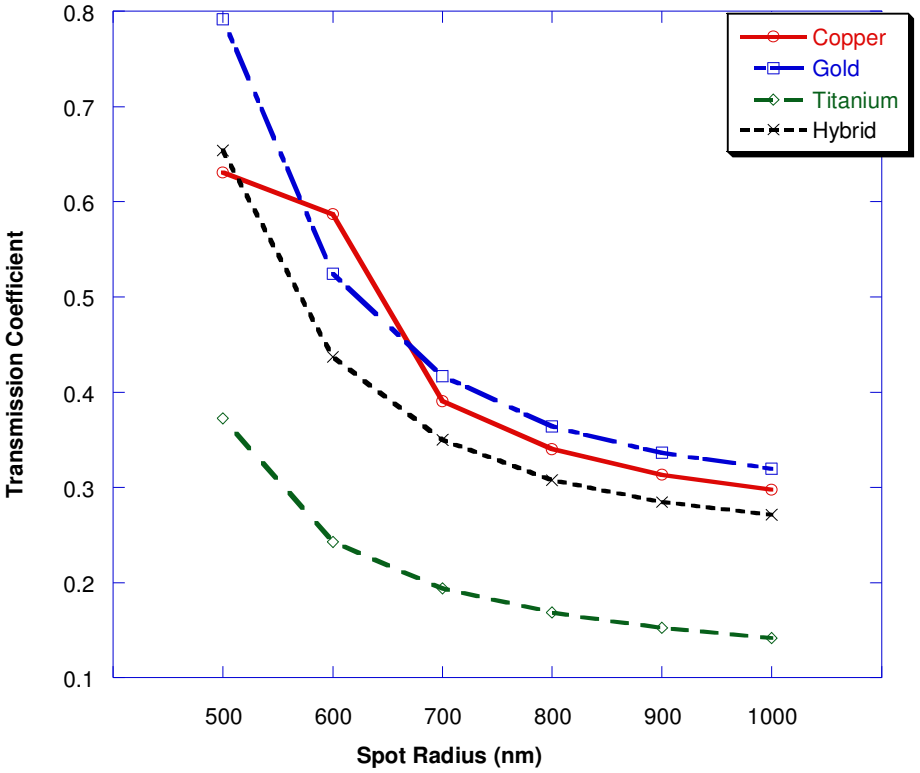

Figure 82: The hybrid material polariser transmission Coefficient on Q12 sub-cell.

The crosstalk coefficient plot in Figure 83 does not show that there is a significant improvement in the crosstalk of the hybrid material polariser. The coefficient of the hybrid material is very close to the gold polariser result. Hence, the titanium frame does not reduce the undesired crosstalk significantly.

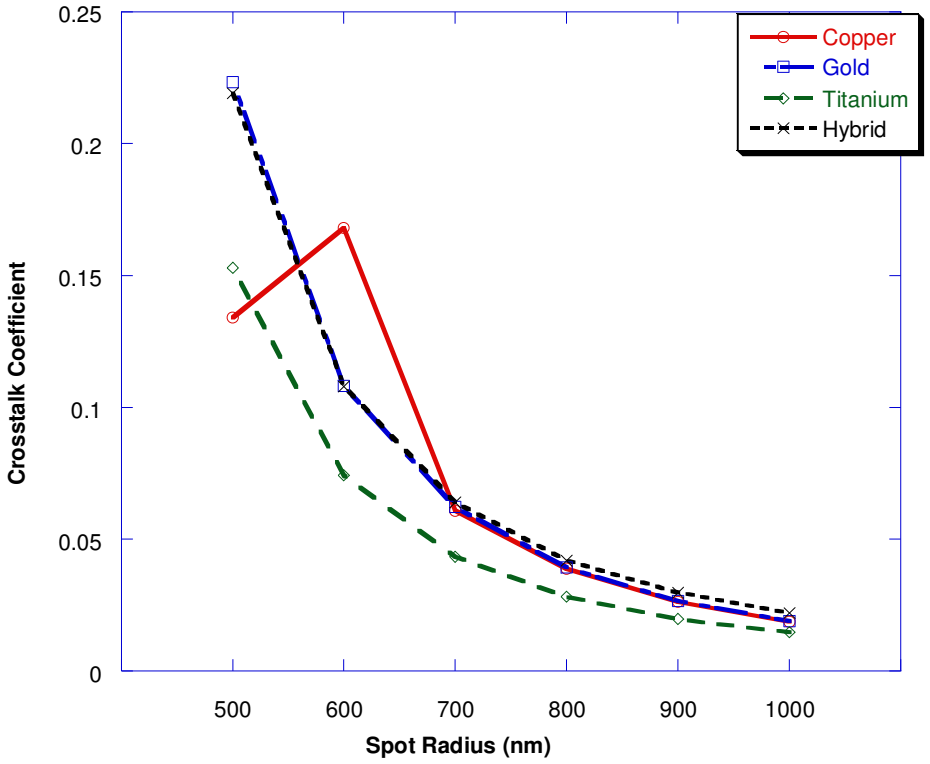

Figure 83: The hybrid material polariser crosstalk coefficient on Q12 sub-cell.

6.2.3 Inter-cell Extinction Ratio

The inter-cell extinction ratio as shown in Figure 84 gives more detail about the performance of the hybrid material polariser. Because of the reduction in transmission coefficients on both transmission orientations, the extinction ratio is higher than copper and gold. However, it is about 3 to 4dB lower than the titanium result. The only helpful information from this simulation is that the low conductive metal, such as titanium, may perform better as the polariser material, and that the effort that would be required to fabricate a complex hybrid polariser would not be necessary.

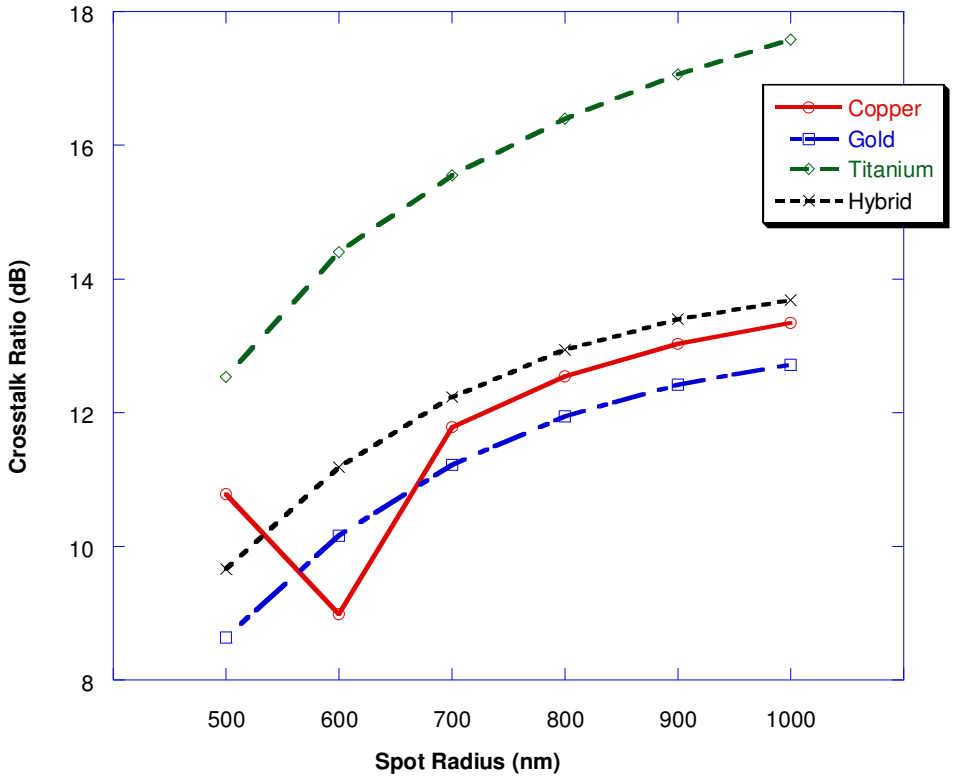

Figure 84: The hybrid material polariser crosstalk ratio.

6.3 Three by Three Array Polariser Simulation

The two by two multi-polariser simulations had represented some aspects of the performance of the polariser pattern for used in CD and DVD data storage technology. However, the crosstalk is a key problem about the optical data recognition sensitivity. Especially the interference from the neighbouring polarisers is a major issue to the transmission coefficient of the desired sub-cell. In this section, the aim is to look at the transmission and interference for neighbouring sub-cells with various polarisation orientations around the desired polariser.

The pattern in this simulation is a three-by-three multi-polariser groove array. It is basically an extended version of the two by two groove pattern that was used in the previous sections. The pattern structure is shown in Figure 85. The sub-cell Q22 is the desired sub-cell and also the centre of the Gaussian beam spot. The rest of the labelled sub-cells are the measuring points for analysing the interference effect, and they cover all possible nearest-neighbour position and orientation combinations.

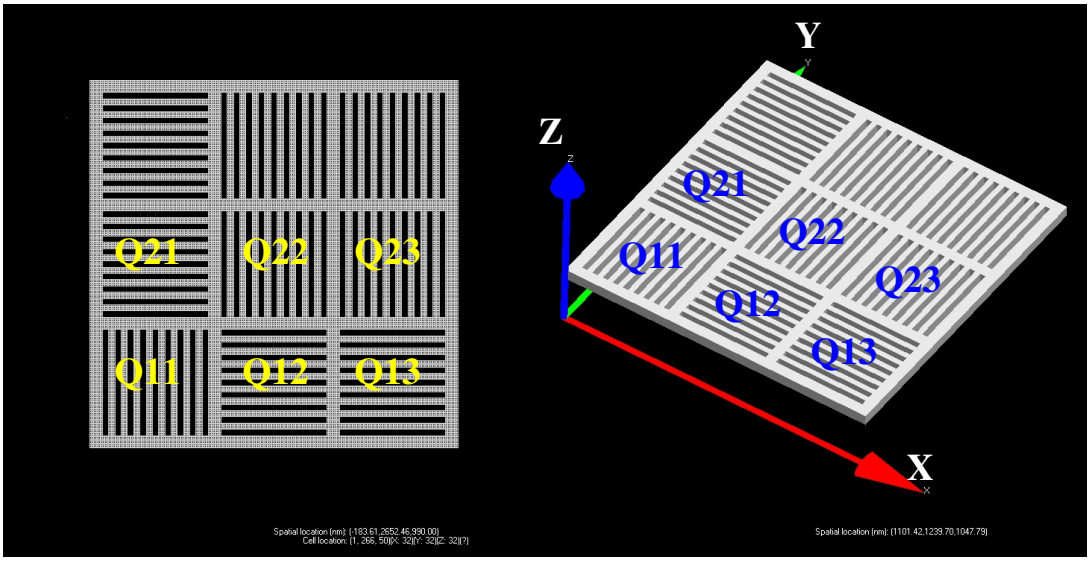

Figure 85: The three by three multi-polariser array simulation pattern and its sub-cell orientations.

6.3.1 Simulation Result

In this simulation, a theta polarised Gaussian beam was applied with various spot radii. The radius range was varied from 500nm to 1500nm in 250nm steps. The source was focused at the centre of the pattern and the Q22 polariser was the desired sub-cell. There were two vertically orientated measured sub-cells around the desired sub-cell, Q11 in diagonal and Q23 in adjacent positions. There were also three horizontally orientated sub-cells measured around the sub-cell Q22, they were Q12 and Q21 in adjacent and Q13 in diagonal positions. The measurements are plotted in Figure 86 as a function of the spot radius. The plane wave result is also included for comparison.

The ratios in Figure 86 were calculated differently from previous cases. The aim of this simulation is to examine the interference effect of the neighbouring sub-cells to the desired polariser so the sub-cell transmission coefficients are divided by the desired sub-cell control wave intensity. This is indicated by the legend label in Figure 86. The solid line represents the transmission coefficient of the desired sub-cell Q22.

The three curves in the bottom of Figure 86 (Q12, Q13 and Q21) are the results of the parallel transmission sub-cells. The curves have linear relationship with the spot radius from 500nm to 1500nm as the ratio gets higher when the spot radius is larger. However, even if the source is a plane wave, the transmission ratios are less than 20%. Therefore, the transmission on the neighbouring sub-cells has limited effect on the desired sub-cell, as is necessary for this polarising scheme to work effectively.

The Q11 and Q23 curves in Figure 86 show the sub-cell transmission coefficients of the vertically oriented neighbouring polarisers. These two are also linear to the spot radius from 500nm to 1500nm. The adjacent sub-cell Q23 has slightly higher ratios than the diagonal sub-cell Q11. This is reasonable as the focus spot covers more area in the adjacent polariser than the diagonal one. When the spot radius is 500nm, the focus spot covers only the desired sub-cell; these two neighbouring polarisers have reasonably low sub-cell transmission coefficients that are about 1%. When the radius is increased to 1500nm, the sub-cell Q23 has the ratio about 60% and the sub-cell Q11 has about 50%. This result indicates that the interference effect to the neighbouring sub-cells is significant only if the spot radius is significantly greater than one sub-cell dimension. In this case, the sub-cell Q23 has strong sub-cell transmission coefficient when the spot radius is greater than 1000nm, which is equivalent to one and half sub-cell dimensions.

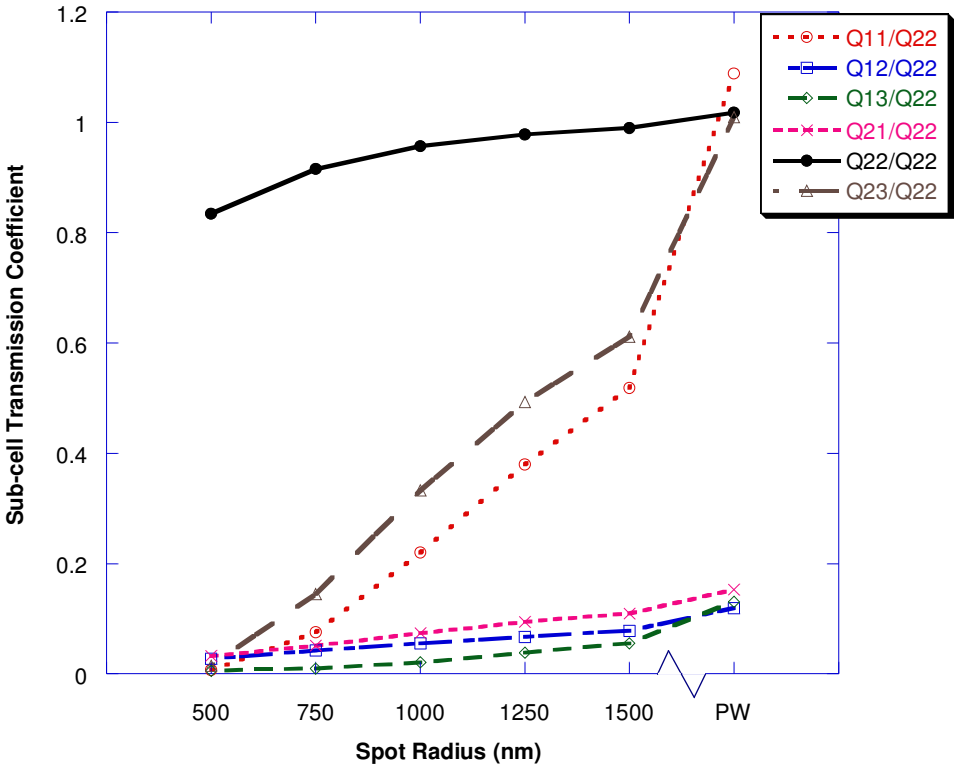

Figure 86: Transmission coefficient of each sub-cell with respect to the desired sub-cell.

6.3.2 Sub-cell Interference Ratio

There are two purposes in the three by three array pattern simulation. The first one is to observe the interference effect to the neighbouring cells. The second one is to look at the performance of the neighbouring sub-cells when a large spot size wave is applied. The sub-cell interference ratio gives great details about these two observations. It is calculated by using Equation (6.3.1).

$$Interference\ Ratio = 20\log\left(\frac{Object\ Subcell\ Ratio}{Desired\ Subcell\ Ratio}\right) \qquad (6.3.1)$$

Figure 87 plots the sub-cell interference ratios of each sub-cell polariser with respect to the desired one, Q22. Therefore, the ratio of Q22/Q22, thick solid curve, is 0dB.

At the 500nm spot radius, only the desired sub-cell is expected to have high transmission. The simulation results indicate this as all the neighbouring sub-cell interference ratios are high. The two diagonal sub-cells Q11 and Q13 have the highest ratios that are above 40dB. The three adjacent sub-cells have the ratios about 30dB to 35dB.

For the large spot radius and the plane wave, the simulations show two different results. The two vertically orientated polarisers Q11 and Q23 have the sub-cell interference ratios less than 10dB at 1500nm spot radius and about 0dB at plane wave source. The three horizontal polarisers keep high sub-cell interference ratios which are about 20dB with the large spot radius. This result shows that the polarisation effect is strong on the three by three titanium array polarisers if the spot radius is smaller than 1000nm.

The result in this simulation is important not only to the polariser pattern performance but also to the actual application on the optical disc data access. The transmission coefficient and the crosstalk to the neighbouring sub-cells can be controlled by varying the source spot radius while the polarisation effect remains high. For the spot radius 500nm, the desired illumination area is one sub-cell. The polarisation effect is significant to the desired sub-cell only and there is negligible transmission to the neighbouring sub-cells. Each sub-cell shows significant polarisation effect at spot radius 1500nm and plane wave source where the whole three by three array pattern is covered by the illumination.

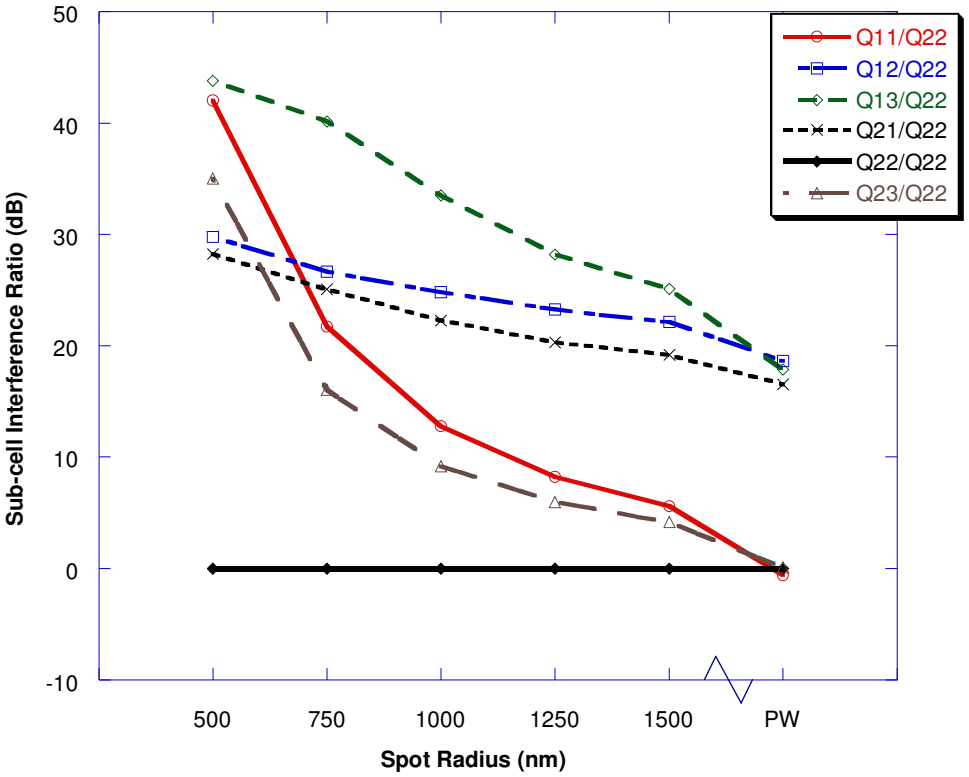

Figure 87: Sub-cell interference ratio with respect to the desired polariser Q22 in dB scale.

7.0 CONCLUSIONS

In this thesis, a technique of using polarised light source and metallic wire grating pattern to increase the optical disc data storage density was introduced. The aim of this project was to develop a capable data pattern and test its performance. The capability and performance of the grating polariser was tested by running the electromagnetic simulations with computer program, XFDTD.

The grating polariser is a new design pattern to replace the traditional data pit. The metallic wire grating is a scattering polariser with good polarisation effect to the visible light bandwidth. Simulations showed that the grating polarisers have good performance in both single or array patterns.

7.1 Background (Literature) Review

CD and DVD technologies use optical source to illuminate the data pits on the disc to fetch the digital information. With the destructive interference effect, the reflection light from the disc could be detected and digitised into signals 1 and 0. CD-ROM drive uses 780nm wavelength light as the optical source. A CD disc could normally store 700MB data in single side single layer. The data pit diameter is 830nm. DVD drive uses 650nm wavelength laser as the source. Its disc could store 4.7GB data in single side single layer. The data pit diameter is 400nm on a DVD disc.

There are many traditional methods to increase the optical disc data storage. The idea is to increase the data density on the disc surface. Using a higher frequency shorter wavelength optical source is the most common solution. The blue laser DVD technology is an example.

However, there is a limit to the source wavelength when applied into the optical data technology and this limit will soon be reached. It now requires a technique to increase the data density that is independent to the source. This thesis showed that the near field effect in nano-scale metallic wire polariser is a possible solution.

Polarisation can be divided into linear, circular and elliptical polarisations. Polarisers can therefore divide into these three categories base on its polarisation. There are dichromatic, birefringence, reflecting and scattering polarisers base on the optical mechanism. The metallic wire grating is a scattering polariser. It has good polarisation effect when its wire spacing is smaller than the source wavelength. The

grating polariser was used in this thesis as the digital data pit. Good polarisation effect results were measured from simulations with plane wave and Gaussian beam source propagation.

The finite-difference time-domain method of electromagnetic calculation was purposed by Yee in 1966 to solve the Maxwell curl equations. FDTD is a great technique for computational calculation. A stable FDTD simulation requires significant cell size, time step size and boundary condition. There are several ways to model the dispersive materials such as Debye, Drude and Lorentz media in FDTD.

XFDTD is electromagnetic simulation program developed by Remcom Incorporated. XFDTD v6.2 was used for polarisation simulation in this project. It supports nano-scale simulation grid dimension and customised setting in material parameters. After version 6, XFDTD supports Gaussian beam source illumination. It was very helpful to this project for simulating the laser beam focusing propagation.

7.2 Simulation Review

The simulation was performed to test the polarisation effect of the metallic wire grating polariser to the light source. The source was either a plane wave or a Gaussian beam with a 650nm wavelength, which is the same as the DVD drive laser. The simulations tested wire dimensions, wire spacing, polariser materials and source beam spot radius.

The basic simulation tested the performance about a 500nm * 500nm polariser with 50nm wide and 10nm thick wire grating. This metallic wire grating polariser has good polarisation effect to a polarised wave with 650nm wavelength. The grating period is related to the polariser performance although the difference is barely significant. The smaller the period is, the better the polarisation effect is as long as the grating period is smaller than the source wavelength. A good polarisation effect requires high coefficient in perpendicular (theta) transmission and low coefficient in parallel (phi) transmission [2]. The grating thickness is linearly related to the perpendicular transmission coefficient but less significant to the parallel transmission.

[2] Theta (horizontal) polarised light has vibrating direction perpendicular to the vertical oriented grating. Phi (vertical) polarised light is parallel to this grating.

The relationship is an inversed proportion. The larger the grating thickness is, the smaller the coefficient is.

The polariser material simulation is important to this project. The simulations show that titanium has different characteristics from the other materials. It has lower conductivity than copper, gold and PEC, hence it has lower transmission coefficient than the other materials. However, titanium also has lower crosstalk coefficient than others as an advantage of low conductive metallic material.

Gaussian beam illumination was applied in the simulations to model the laser beam. It has focusing parameters for adjusting the focusing spot radius and coordinates. The spot radius has significant influence to the polariser performance. When a Gaussian beam spot is too small, the polarisation state of the propagation that close to the focusing spot may have inconsistency and therefore reduce the performance.

The two dimensional polariser array simulations are the major part in this thesis. The two by two polariser pattern represents one data pit on the optical disc. This pattern has potentially four bits of digital information under one focusing spot. The simulations show that there is crosstalk from the neighbouring sub-cells to the desired polariser bit. This crosstalk reduces the polarisation effect and the polariser performance, however by keeping the laser spot radius above 700nm the inter-cell extinction ratio of greater than 15dB can be maintained.

Copper, gold and titanium were applied as the polariser materials in the two dimensional polariser array simulations. The two by two polariser array pattern generates higher amount of crosstalk than the single polariser case especially for copper and gold. Titanium polarisers have lower transmission and crosstalk coefficients but higher extinction ratio than the other materials.

In the two dimensional polariser pattern simulations, a major portion of the crosstalk comes from the neighbouring polariser sub-cells. In order to reduce this inter-cell crosstalk, the two by two polariser pattern with solid borders was applied in the simulation. The result shows that performance improves for titanium polariser but deteriorates for copper and gold. In the Gaussian beam source simulations, titanium had much better performance than the other two materials. The lower conductivity, which generates lower crosstalk coefficients, is the key factor.

The two by two hybrid material polariser consisted of gold made polariser gratings and titanium made solid borders. The purpose of this pattern was combining the advantage of high transmission coefficient from the high conductivity material and the low crosstalk coefficient from the low conductivity material. However, the performance is not as good as the titanium single-material pattern.

A titanium three by three polariser array with solid border was simulated to test the effects from the Gaussian beam spot size to the neighbouring polariser sub-cells. When the spot radius covered only the desired sub-cell, all the neighbouring polarisers have sub-cell transmission coefficient less than 5%. When the spot radius is greater than 1500nm, the vertical orientated neighbouring polarisers have sub-cell transmission coefficient around 50% to 60%; the horizontal orientated neighbouring polarisers have the coefficient less than 10%. To reduce this interference to better than 15dB a spot radius smaller than 1000nm must be used.

Based on these findings, spot radii in the range 700-1000nm would be suitable for the improved data storage method presented here, with 500nm square sub-cell dimensions. This corresponds to a data storage density of 400MB/cm^2 and lens NA in the range 0.45 to 0.85, compared with current DVD technology.

The specifications of the DVD disc and the disc from this project are listed in Table 7-1. DVD disc recording area is calculated to be 0.0112m^2. Although the new disc data pit and track pitch are both larger than the respective in the DVD disc, there are four significant data bits in each pit. An eight bits (one byte) data occupies 1000nm * 1000nm * 8 / 4 = 2e-12m^2. Hence the capacity of the new disc is calculated to be 5.5GB.

	DVD	This Project
Numeric Aperture (NA)	0.6	0.6
Laser Wavelength	650nm	650nm
Laser Spot Size	1083nm	1083nm
Pit Diameter	400nm	1000nm
Track Pitch	740nm	1000nm
Capacity	4.7GB	5.5GB
Bits per Track Pitch	1	4

Table 7-1: Technical comparison of DVD and Metallic polariser array pattern disc.

The data storage density improvement from the new disc is only marginal mainly because the size of the pit diameter. Due to the optical reading mechanism, the pit

diameter cannot be less than the spot radius in order to prevent the crosstalk from adjacent data pits.

7.3 Future Development

This thesis introduced a solution for increasing the CD/DVD data storage density without reducing the source wavelength. Computational simulations were experimented and the results confidently support the theory. However, physical evidence is required for this to be studied further. This includes sample fabrication of the data track, data pit blocking effect investigation, and source illumination experiment.

Sample Fabrication

Producing the grating polariser data track samples will require nano-fabrication technology. There will be two stages of this research and development: first, fabrication on SiO_2; second, fabrication on transparent material substrate. The samples from the first stage will be used for observation of the fabrication performance. The samples from the second state will be used for the illumination experiments.

There will be three types of sample fabricated for testing: the single polariser with solid borders; the two by two grooved polariser array; and the data track with series of array patterns. Based on the simulation results, titanium will be chosen as the grating polariser material.

Titanium could be coated on the sample by using the chemical vapour deposition (CVD) technique. The fabrication process will be performed by using the electron beam lithography (EBL). The pattern will be in nano-scale and the finest feature is expected to be 40nm. EBL is capable of fabricating patterns in such dimension. The fabricated sample will then be observed by the atomic force microscope (ATM).

Fabrication on transparent material requires more advanced technology than on SiO_2. The substrate material influences the fabrication process and its performance. Possible materials are glass and transparent plastic. Plastic will be preferred as it is similar to the disc material. Fabrication on glass substrate may require additional packaging process when mounting the patterns onto the disc.

Blockage Investigation

This part of experiment will research on the blocking of the data pit. The purpose of blocking the data pit is to stop the transmission propagating through the pattern and hence produce a high signal at the data fetching process. This research will include the blocking process, the blocking material and the block coverage.

The research on the blocking process will investigate the approach to achieve the blockage on a data pit. The block may be applied when the pattern is fabricated. This technique will require least amount of technology and cost, however it will not be capable for writing data onto the disc. It is a technique suitable for manufacturing the movie or music discs. The write once and rewritable discs require different approach to apply the blockage onto the data pit. One possible solution is using the phase change material, similar to the technique that used on CD-RW and DVD-RW. However this approach requires focused laser heating on the particular data pit that requires the phase change and it is difficult to achieve in the design of this thesis. As the spot size is much lager than the data pit, the current design laser source can not focus on such particular pixel without affecting the neighbours.

The blocking material will be investigated respect to different blocking process. The pre-fabricated block could use the same material as the data pattern. The writeable disc will require chemicals or hybrid materials to achieve the phase change effect [13].

There will be two methods for conducting the block coverage research. The first method will be the computational simulation. Experiments will be set to test the blockage performance on its shape and thickness. The XFDTD simulation will be applied to this research once more. The second method will be included in the illumination experiment. The far-zone transmission detection will be test subject to the blockage.

Illumination experiments

Illumination experiments will find the physical evidence to confirm the capability of this research. The basic requirements of the illumination experiment will be the illumination unit, the sample and the transmission detector. A 650nm wavelength red laser will be chosen as the illumination source. The illumination unit will also contain a lens set to adjust the focus and the polarisation module to produce the desired polarised light. The transparent sample will be prepared at the fabrication part of the

research. A sample holder platform will be designed and built to hold and move it. The transmission detector will be placed behind the sample at the opposite side of the illumination unit. This detector will be moveable to suit different requirements.

There will be stationary illumination and dynamic illumination experiments. The stationary illumination will test the single and array samples. The purpose of this experiment will be observing the grating polariser pattern performance and testing the transmission level for different data. The dynamic illumination will simulate the optical data reading phenomena as a laser spot on the data track of the spinning disc. This experiment will also test on the pattern recognising performance and the data error rate.

In summary, the future development of this thesis will include the pattern sample fabrication, blockage research and the source illumination experiment. The titanium wire grating polariser array pattern will be made by using the nano-fabrication technique. The blockage research will investigate the blocking process, blockage material and block effects. The transmission will be test on the stationary illumination experiment and the dynamic illumination will test the overall performance of the designed optical mechanism and the data reading efficiency.

7.4 Summary

The simulations showed that metallic wire grating polariser has good performance for polarising the laser with 650nm wavelength. As the polariser material, low conductivity metal such as titanium has lower transmission and crosstalk coefficients than copper and gold. This results better extinction ratio and polarisation effects to the polariser.

In this thesis, the design of a two by two polarised array pattern for using as the data pit on the optical disc was introduced. The chessboard orientation polariser array potentially stores four bits of data. This digital information could be fetched by illuminating the polarised laser source on the polariser array. The laser spot size was calculated from the simulation results in order to ensure the polariser transmission coefficient is significant and also limit the crosstalk to the neighbouring data pits under a controlled level. The spacing between two data tracks was also calculated and regulated in this thesis based on the simulation results. Data pack header was

introduced in the coding section to optimise the data searching speed and minimise the data error rate.

The technique of using nano-scale metallic wire grating polariser as data pits on optical disc potentially increased the data storage density by four times from the current optical disc storage. This technique achieved the goal without using a shorter wavelength source. It provided a new solution to increase the optical data storage density.

8.0 REFERENCES

[1] A. S. Hoagland, *Digital Magnetic Recording*. New York: John Wiely & Sons, 1963.

[2] L. G. Sebestyen, *Digital Magnetic Tape Recording for Computer Applications*. London: Chapman and Hall, 1973.

[3] A. Ralston, E. D. Reilly, and D. Hemmendinger, *Encyclopedia of Computer Science*. New York: Nature Publishing Group, 2000.

[4] G. L. Davies, *Magnetic Tape Instrumentation*. New York: McGraw-Hill, 1961.

[5] A. S. Hoagland and J. E. Monson, *Digital Magnetic Recording*, Second ed. New York: Hohn Wiley & Sons, 1991.

[6] M. M. Mano and C. R. Kime, *Logic and Computer Design Fundamentals*, Second ed. New Jersey: Prentice-Hall, 2000.

[7] A. K. Sharma, *Semiconductor Memories: Technology, Testing, and Reliablility*. New York: John Wiley & Sons, 1997.

[8] K. D. Moller, *Optics*. Mill Valley, California: University Science Books, 1988.

[9] T. Ohta, "PHASE-CHANGE OPTICAL MEMORY PROMOTES THE DVD OPTICAL DISK," *Journal of Optoelectronics and Advanced Materials*, vol. 3, pp. 609-626, 2001.

[10] D. P. Tsai and W. R. Guo, "Near-Field Optical Rcording On Cyanine Dye Lyaer of a Commercial Compact Disk-Recordable (CD-R)," *Lasers and Electro-Optics Society Annual Meeting*, vol. 1, pp. 245-246, 1996.

[11] H. Iwasaki, "CD-Rewritable and Future Disc Technology," *Optical Data Storage Topical Meeting*, pp. 9-10, 1997.

[12] H. Iwasaki, M. Harigaya, O. Nonoyama, Y. Kageyama, M. Takahashi, K. Yamada, H. Deguchi, and Y. Ide, "Completely Erasable Phase Change Optical Disk II-Application of Ag-In-Sb-Te mixed-phased system for CD-rewritable compatible with CD1X and CD2X," *Joint International Symposium on Optical Memory and Optical Data Storage*, pp. 144-145, 1993.

[13] L. P. Shi, T. C. Chong, H. B. Yao, X. Hu, and X. S. Miao, "Dynamic Crystallization Behavior of Phase Change Optical Recording in Erasing Process," *International Symposium on Optical Memory and Optical Data Storage Topical Meeting*, pp. 317-319, 2002.

[14] J. Hellmig, "DVDs: in the fast lane," in *Physics World*, vol. 17, 2004, pp. 21-24.

[15] K. Manoh, "Small Integrated Optical Head Device Using a Blue-Violet Laser Diode for Blu-Ray Disc System," *International Symposium on Optical Memory and Optical Data Storage Topical Meeting*, pp. 386-388, 2002.

[16] I. Ichimura, "Optical storage with high-numerical-aperture lenses," *The 4th Pacific Rim Conference on Lasers and Electro-Optics*, vol. 2, pp. II-14 - II-15, 2001.

[17] T. Naeve, M. Hohenbild, and P. Seegebrecht, "A Quasi-2-Dimensional Photodiode Model for High-Speed Short-Wavelength Applications," *International Symposium on Electron Devices for Microwave and Optoelectronic Applications*, pp. 66-70, 2004.

[18] L. Ichimura, S. Masuhara, and J. Nakano, "On-Groove Phase-Change Optical Recording for a Capacity of 25GB," *Proceedings of SPIE*, vol. 4342, pp. 168-177, 2002.

[19] B. A. Newmerique, "HD DVD - A Technical Introduction," DVD Forum, 2005.
[20] T. Kubota, "HD DVD - Overview of Next Generation Optical Disc Format," *The IEE 2-Day Seminar on IT to HD: Visions of Broadcasting in the 21st Century*, pp. 213-224, 2004.
[21] Y. Kaneda, "Advanced Optical Disk Mastering and Its Application for Extremely High-Density Magnetic Recording," *IEEE Transactions On Industrial Electronics*, vol. 42, pp. 257, 1995.
[22] R. Katayama and Y. Yamanaka, "Optical Head and Optical Disk Technologies for HD DVD," *International Conference on Consumer Electronics Digest of Technical Papers*, pp. 11-12, 2005.
[23] J. Tominaga, "Near-Field Interactions Appeared Between Recording Marks Beyond the Diffraction Limit," *The 4th Pacific Rim Conference on Lasers and Electro-Optics*, vol. 2, pp. II-18 - II-19, 2001.
[24] J. Tominaga, T. Nakano, and N. Atoda, "An approach for recording and readout beyond the diffraction limit with an Sb thin film," *Applied Physical Letters*, vol. 73, pp. 2078, 1998.
[25] J. K. Inoh Hwang, Hyunki Kim, Insik Park, and Dongho Shin, "Phase Change Materials in Super-RENS Disk," *IEEE TRANSACTIONS ON MAGNETICS*, vol. 41, pp. 1001, 2005.
[26] K. Kataja, J. Oikkonen, J. Aikio, and D. Howe, "Super Resolution Near Field Structure Study," *International Symposium on Optical Memory and Optical Data Storage Topical Meeting*, pp. 135-137, 2002.
[27] M. Katsumura and T. Iida, "High Density Recording Using Electron Beam Recorder," *Optical Data Storage Conference Digest*, pp. 3-5, 2000.
[28] M. Takeda, M. Furuki, M. Yamamoto, Y. Aki, and H. Kawase, "Electron Beam Recording with a Novel Differential Pumping Head Realizing over 50GB/Layer Capacity Disc," *International Symposium on Optical Memory and Optical Data Storage Topical Meeting*, 2002.
[29] T. K. Simpson, *Maxwell on the electromagnetic field : a guided study*. New Brunswick, N.J.: Rutgers University Press, 1997.
[30] S. Ramo, J. R. Whinnery, and T. V. Duzer, *Fields and Waves in Communication Electronics*, Second ed. New York: John Wiley & Sons, 1984.
[31] J. Hendry, *James Clerk Maxwell and the theory of the electromagnetic field*. Bristol: Hilger, 1986.
[32] P. P. Banerjee and T.-C. Poon, *Principles of Applied Optics*: Aksen Associates, 1991.
[33] R. Baierlein, *Newton to Einstein : the trail of light : an excursion to the wave-particle duality and the special theory of relativity*. Cambridge [England] ; New York: Cambridge University Press, 1992.
[34] J. Sladkova, *Interference of light*. London; Prague: Iliffe; Sntl, 1968.
[35] M. Born and E. Wolf, *Principles of optics : electromagnetic theory of propagation, interference and diffraction of light*, 7th expanded ed. Cambridge ; New York: Cambridge University Press, 1999.
[36] P. Rohan, *Introduction to electromagnetic wave propagation*. Boston: Artech House, 1991.
[37] E. Hecht and A. Zajac, *Optics : [By] Eugene Hecht [and] Alfred Zajac*. Reading, Mass.: Addison-Wesley, 1975.
[38] E. Collett, *Polarized Light: Fundamentals and Applications*. New York: Marcel Dekker Inc., 1992.

[39] E. Collett, *Polarized light : fundamentals and applications*. New York: Marcel Dekker, 1993.
[40] D. Clarke and J. F. Grainger, *Polarized light and optical measurement*, [1st]. ed. Oxford ; New York: Pergamon Press, 1971.
[41] W. A. Shurcliff, *Polarized Light*. Cambridge, Massachusetts: Harvard University Press, 1962.
[42] H. Goldstein Dennis, R. A. Chipman, and Society of Photo-optical Instrumentation Engineers., *Polarization analysis and measurement : 19-21 July 1992, San Diego, California*. Bellingham, Wash.: Spie, 1992.
[43] M. H. Hewitt, "Polarization, cross section, and the Stokes parameters," *Proceedings of the IEEE*, vol. 53, pp. 1143-1144, 1965.
[44] R. N. Thurston, J. Cheng, and G. D. Boyd, "Mechanically Bistable Liquid-Crystal Display Structures," *IEEE Transactions on Electron Devices*, vol. 27, pp. 2069-2080, 1980.
[45] K. J. Binns and P. J. Lawrenson, *Analysis and computation of electric and magnetic field problems*. Oxford ; New York: Pergamon Press; [distributed in the Western Hemisphere by Macmillan New York], 1963.
[46] P. J. v. d. Houwen, *Finite difference methods for solving partial differential equations*. Amsterdam: Mathematisch Centrum, 1968.
[47] G. D. Smith, *Numerical solution of partial differential equations : finite difference methods*, 3rd ed. Oxford: Clarendon, 1985.
[48] M. N. O. Sadiku, *Numerical Techniques in Electromagnetics*, second ed. Boca Raton: CRC Press, 2001.
[49] L. Gürel and U. Oguz, "Signal-Processing Techniques to Reduce the Sinusoidal Steady-State Error in the FDTD Method," *IEEE Transactions On Antennas and Propagation*, vol. 48, pp. 585, 2000.
[50] K. S. Kunz and R. J. Luebbers, *The Finite Difference Time Domain Method for Electromagnetics*. Boca Raton: CRC Press, 1993.
[51] K. Chamberlin and D. Vidacic, "Analysis of Finite-Differencing Errors to Determine Cell Size When Modeling Ferrites and Other Lossy Electric and Magnetic Materials Using FDTD," *IEEE TRANSACTIONS ON ELECTROMAGNETIC COMPATIBILITY*, vol. 46, pp. 617, 2004.
[52] R. Nilavalan, I. J. Craddock, and C. J. Railton, "Practical method for the determination of time step in non-orthogonal FDTD," *Electronics Letters*, vol. 37, pp. 679, 2001.
[53] O. M. Ramahi, "Stability of Absorbing Boundary Conditions," *IEEE TRANSACTIONS ON ANTENNAS AND PROPAGATION*, vol. 47, pp. 593, 1999.
[54] X. Yuan, D. Borup, J. W. Wiskin, M. Berggren, R. Eidens, and S. A. Johnson, "Formulation and Validation of Berenger's PML Absorbing Boundary for the FDTD Simulation of Acoustic Scattering," *IEEE TRANSACTIONS ON ULTRASONICS, FERROELECTRICS, AND FREQUENCY CONTROL*, vol. 44, 1997.
[55] D. F. Kelley and R. J. Luebbers, "Piecewise Linear Recursive Convolution for Dispersive Media Using FDTD," *IEEE Transactions On Antennas and Propagation*, vol. 44, pp. 792, 1996.
[56] R. Luebbers, D. Steich, and K. Kunz, "FDTD Calculation of Scattering from Frequency-Dependent Materials," *IEEE TRANSACTIONS ON ANTENNAS AND PROPAGATION*, vol. 41, pp. 1249, 1993.

[57] A. Taflove and S. C. Hagness, *Computational electrodynamices: The Finite-Difference Time-Domain Method*, second ed. Norwood: Artec House, 2000.
[58] P. B. Johnson and R. W. Christy, "Optical Constants of the Nobel Metals," *Physical Review*, vol. 6, pp. 4370, 1972.
[59] Remcom, *XFDTD: Full-wave, 3D, Electromagnetic Analysis Software Reference Manual Version 6.2*: Remcom Inc., 2004.
[60] S. J. McNab and R. J. Blaikie, "Contrast in the evanescent near field of lamda/20
period gratings for photolithography," *APPLIED OPTICS*, vol. 39, pp. 20-25, 2000.
[61] D. R. Lide, *Handbook of Chemistry and Physics*, 78th ed. New York: CRC Press, 1997.

APPENDIX I

goo.m

```
% goo.m
% For analysising the XFDTD simulation data and perform math operations.
% Package includes: LoadFile.m, LoadInFile, LoadOutFile, GetData.m,
% Operation.m, PlotFigure.m, ListFile.m, ngain.m
% Allan T. Chin (BBKNIGHT)
% Created date: 21, 06, 2004
% Last Updated: 12, 10, 2005

clear;

% Initialise the time and mag array address variable.
inLoadCount = 0; outLoadCount = 0;
inFileName = ''; outFileName = '';
inTime = []; outTime = []; inMag = []; outMag = [];
inTimeAvg = 0; inMagAvg = 0; outTimeAvg = 0; outMagAvg = 0;
disp('Switch Testing! ')
disp('XFDTD Simulation Data Processing!')

% Root while loop.
while (1)
	disp('================================================')
	disp('Choose your option from the following functions.')
	disp('    F / f for list the available files.')
	disp('    L / l for load the data file.')
	disp('    O / o for apply the calculation.')
	disp('    P / p for plot the loaded file.')
	disp('    C / c for gain operation.')
	disp('    Q / q for end this program.')
	disp('================================================')

	% Root switch - menu selection
	rootOption = input('Option = ', 's');
	switch rootOption;
		case {'F', 'f'}
			disp('File listing')
			dir *.g0
			io = 2;
			result =
ListFile(io,inLoadCount,outLoadCount,inFileName,outFileName);% List the loaded files.
		case {'L', 'l'}
			disp('Loading')
			io = input('1. for input source file, 0. for output source file, 5. for
predefined files = ');
			switch io;
				case{1}
					[inLoadCount,inFileName,inTime,inMag] =
LoadInFile(inLoadCount,inFileName,inTime,inMag);
				case{0}
					[outLoadCount,outFileName,outTime,outMag] =
LoadOutFile(outLoadCount,outFileName,inTime,inMag);
				case{5}

	[inLoadCount,outLoadCount,inFileName,outFileName,inTime,inMag,outTime,outMag]
= LoadFile(inLoadCount,outLoadCount,inFileName,outFileName);
```

```
                                        otherwise
                                                disp('Wrong entry!');
                                end

                        case {'O', 'o'}
                                disp('Operation')
                                [inTimeAvg,inMagAvg,outTimeAvg,outMagAvg] =
Operation(inLoadCount,outLoadCount,inTime,inMag,outTime,outMag);
                        case {'P', 'p'}
                                disp('Plot')
                                result =
PlotFigure(inLoadCount,outLoadCount,inTime,inMag,outTime,outMag,inTimeAvg,inMagAvg,o
utTimeAvg,outMagAvg,inFileName,outFileName);
                        case {'C', 'c'}
                                disp('Gain operation!')
                                result =
Gain(inMag,outMag,inTimeAvg,inMagAvg,outTimeAvg,outMagAvg);
                        case {'Q', 'q'}
                                disp('Ending')
                                %clear;
                                break;
                        otherwise
                                disp('Wrong choice!')
        end

end
```

LoadFile.m

```
function  [inLoadCount,outLoadCount,inFileName,outFileName,inTime,inMag,outTime,outMag]
= LoadFile(inLoadCount,outLoadCount,inFileName,outFileName)
% LoadFile.m
% Loads the XFDTD simulation input and output data values (.go files)
% Supports the program ngain.m and gain.m
% Allan T. Chin (BBKNIGHT)
% Created date: 21, 06, 2004
% Last Updated: 24, 01, 2005

% Loading while loop for the loading menu. Entering the loading file.
check = false;
while(check ~= true)
        quadrant = input('Witch Quadrant is going to be loaded? q11 or q12? \n', 's');
        direction = input('What direction? x or y? \n', 's');
        switch quadrant;
                case{'q11'}
                        switch direction;
                                case{'x'}
                                        inFileName(1,:) = 'rprojEXT.x00050.y00050.z00010.g0';
                                        inFileName(2,:) = 'rprojEXT.x00050.y00050.z00020.g0';
                                        inFileName(3,:) = 'rprojEXT.x00050.y00050.z00030.g0';
                                        inFileName(4,:) = 'rprojEXT.x00050.y00050.z00040.g0';
                                        inFileName(5,:) = 'rprojEXT.x00050.y00050.z00050.g0';

                                        outFileName(1,:) = 'projEXT.x00050.y00050.z00010.g0';
                                        outFileName(2,:) = 'projEXT.x00050.y00050.z00020.g0';
                                        outFileName(3,:) = 'projEXT.x00050.y00050.z00030.g0';
                                        outFileName(4,:) = 'projEXT.x00050.y00050.z00040.g0';
                                        outFileName(5,:) = 'projEXT.x00050.y00050.z00050.g0';

                                        check = true;
                                case{'y'}
```

```
                                        inFileName(1,:) = 'rprojEXT.x00050.y00050.z00010.g0';
                                        inFileName(2,:) = 'rprojEXT.x00050.y00050.z00020.g0';
                                        inFileName(3,:) = 'rprojEXT.x00050.y00050.z00030.g0';
                                        inFileName(4,:) = 'rprojEXT.x00050.y00050.z00040.g0';
                                        inFileName(5,:) = 'rprojEXT.x00050.y00050.z00050.g0';

                                        outFileName(1,:) = 'projEYT.x00050.y00050.z00010.g0';
                                        outFileName(2,:) = 'projEYT.x00050.y00050.z00020.g0';
                                        outFileName(3,:) = 'projEYT.x00050.y00050.z00030.g0';
                                        outFileName(4,:) = 'projEYT.x00050.y00050.z00040.g0';
                                        outFileName(5,:) = 'projEYT.x00050.y00050.z00050.g0';

                                        check = true;
                                otherwise
                                        disp('Please enter again!');
                        end
                case{'q12'}
                        switch direction;
                                case{'x'}
                                        inFileName(1,:) = 'rprojEXT.x00150.y00050.z00010.g0';
                                        inFileName(2,:) = 'rprojEXT.x00150.y00050.z00020.g0';
                                        inFileName(3,:) = 'rprojEXT.x00150.y00050.z00030.g0';
                                        inFileName(4,:) = 'rprojEXT.x00150.y00050.z00040.g0';
                                        inFileName(5,:) = 'rprojEXT.x00150.y00050.z00050.g0';

                                        outFileName(1,:) = 'projEXT.x00150.y00050.z00010.g0';
                                        outFileName(2,:) = 'projEXT.x00150.y00050.z00020.g0';
                                        outFileName(3,:) = 'projEXT.x00150.y00050.z00030.g0';
                                        outFileName(4,:) = 'projEXT.x00150.y00050.z00040.g0';
                                        outFileName(5,:) = 'projEXT.x00150.y00050.z00050.g0';

                                        check = true;
                                case{'y'}
                                        inFileName(1,:) = 'rprojEXT.x00150.y00050.z00010.g0';
                                        inFileName(2,:) = 'rprojEXT.x00150.y00050.z00020.g0';
                                        inFileName(3,:) = 'rprojEXT.x00150.y00050.z00030.g0';
                                        inFileName(4,:) = 'rprojEXT.x00150.y00050.z00040.g0';
                                        inFileName(5,:) = 'rprojEXT.x00150.y00050.z00050.g0';

                                        outFileName(1,:) = 'projEYT.x00150.y00050.z00010.g0';
                                        outFileName(2,:) = 'projEYT.x00150.y00050.z00020.g0';
                                        outFileName(3,:) = 'projEYT.x00150.y00050.z00030.g0';
                                        outFileName(4,:) = 'projEYT.x00150.y00050.z00040.g0';
                                        outFileName(5,:) = 'projEYT.x00150.y00050.z00050.g0';

                                        check = true;
                                otherwise
                                        disp('Please enter again!');
                        end
                otherwise
                        disp('Please enter again!');
        end
end

max = 5;        % Number of points of recording.
for i = 1:max
        inFID = fopen(inFileName(i,:), 'r');
        inLoadCount = inLoadCount + 1;
        [inTime(inLoadCount,:), inMag(inLoadCount,:)] = GetData(inFID);
        outFID = fopen(outFileName(i,:), 'r');
```

```
        outLoadCount = outLoadCount + 1;
        [outTime(outLoadCount,:), outMag(outLoadCount,:)] = GetData(outFID);
        fclose(inFID);
        fclose(outFID);
end
```

LoadInFile.m

```
function [inLoadCount,inFileName,inTime,inMag] =
LoadInFile(inLoadCount,inFileName,inTime,inMag)
% LoadInFile.m
% Loads the XFDTD simulation input data values (.go files)
% Allan T. Chin (BBKNIGHT)
% Created date: 21, 06, 2004
% Last Updated: 24, 01, 2005

% Loading while loop for the loading menu. Entering the loading file.
flag1 = 0;
while (flag1 ~= 1)
        type = input('Enter the file attribute = ', 's');
        sliceX = input('Enter X slice value = ', 's');
        sliceY = input('Enter Y slice value = ', 's');
        sliceZ = input('Enter Z slice value = ', 's');
        inFileNameTemp = enterFile(type, sliceX, sliceY, sliceZ);

        % Loading sub menu while loop. Confirming the loading file.
        flag2 = 0; ans = 0;
        while(flag2 ~= 1)
                ans = input('Do you want to load this file? = ', 's');
                switch ans;
                        case {'Y', 'y'}
                                FID = fopen(inFileNameTemp, 'r');
                                inLoadCount = inLoadCount + 1
                                [inTime(inLoadCount,:), inMag(inLoadCount,:)] =
GetData(FID);
                                inFileName(inLoadCount,:) = inFileNameTemp;
                                flag2 = 1;
                        case {'N', 'n'}
                                flag2 = 1;
                        otherwise
                                flag2 = 0;
                end
        end

        % 2nd loading sub while loop for more loading files.
        flag2 = 0; ans = 0;
        while(flag2 ~= 1)
                ans = input('Do you want to load another file? = ', 's');
                switch ans;
                        case {'Y', 'y'}
                                flag2 = 1;
                        case {'N', 'n'}
                                flag1 = 1;
                                flag2 = 1;
                        otherwise
                                flag2 = 0;
                end
        end
end
```

LoadOutFile.m

```
function [outLoadCount,outFileName,outTime,outMag] =
LoadOutFile(outLoadCount,outFileName,inTime,inMag)
% LoadOutFile.m
% Loads the XFDTD simulation output data values (.go files)
% Allan T. Chin (BBKNIGHT)
% Created date: 21, 06, 2004
% Last Updated: 24, 01, 2005

% Loading while loop for the loading menu. Entering the loading file.
flag1 = 0;
while (flag1 ~= 1)
	type = input('Enter the file attribute = ', 's');
	sliceX = input('Enter X slice value = ', 's');
	sliceY = input('Enter Y slice value = ', 's');
	sliceZ = input('Enter Z slice value = ', 's');
	outFileNameTemp = enterFile(type, sliceX, sliceY, sliceZ);

	% Loading sub menu while loop. Confirming the loading file.
	flag2 = 0; ans = 0;
	while(flag2 ~= 1)
		ans = input('Do you want to load this file? = ', 's');
		switch ans;
			case {'Y', 'y'}
				FID = fopen(outFileNameTemp, 'r');
				outLoadCount = outLoadCount + 1;
				[outTime(outLoadCount,:), outMag(outLoadCount,:)] = GetData(FID);
				outFileName(outLoadCount,:) = outFileNameTemp;
				flag2 = 1;
			case {'N', 'n'}
				flag2 = 1;
			otherwise
				flag2 = 0;
		end
	end

	% 2nd loading sub while loop for more loading files.
	flag2 = 0; ans = 0;
	while(flag2 ~= 1)
		ans = input('Do you want to load another file? = ', 's');
		switch ans;
			case {'Y', 'y'}
				flag2 = 1;
			case {'N', 'n'}
				flag1 = 1;
				flag2 = 1;
			otherwise
				flag2 = 0;
		end
	end
end
```

Operation.m

```
function [inTimeAvg,inMagAvg,outTimeAvg,outMagAvg] =
Operation(inLoadCount,outLoadCount,inTime,inMag,outTime,outMag)
% Operation.m
% Perform the calculation on input/output magnitude and time.
% Require Package files: Package includes: LoadFile.m, ListFile.m
```

```
% Allan T. Chin (BBKNIGHT)
% Created date: 21, 06, 2004
% Last Updated: 03, 03, 2005

inTimeAvg=0; inMagAvg=0; outTimeAvg=0; outMagAvg=0;
if inLoadCount > 0
        inTimeSum = 0; inMagSum = 0; i = 0;
        for i = 1:inLoadCount
                inTimeSum = inTimeSum + inTime(i,:);
                inMagSum = inMagSum + inMag(i,:);
        end
        inTimeAvg = inTimeSum / inLoadCount;
        inMagAvg = inMagSum / inLoadCount;
end
if outLoadCount > 0
        outTimeSum = 0; outMagSum = 0; i = 0;
        for i = 1:outLoadCount
                outTimeSum = outTimeSum + outTime(i,:);
                outMagSum = outMagSum + outMag(i,:);
        end
        outTimeAvg = outTimeSum / outLoadCount;
        outMagAvg = outMagSum / outLoadCount;
        %else
%       disp('There is no entry!');
End
```

PlotFigure.m

```
function result =
PlotFigure(inLoadCount,outLoadCount,inTime,inMag,outTime,outMag,inTimeAvg,inMagAvg,o
utTimeAvg,outMagAvg,inFileName,outFileName)
% PlotFigure.m
% Choose asingle or the average of all input / output data series to plot.
% Require Package files: Package includes: LoadFile.m, ListFile.m
% Allan T. Chin (BBKNIGHT)
% Created date: 21, 06, 2004
% Last Updated: 03, 03, 2005

figureCount = 1;
while (1)
        disp('1. Plotting the single input data.');
        disp('2. Plotting the single output data.');
        disp('3. Plotting the averaged input data.');
        disp('4. Plotting the averaged output data.');
        disp('5. Plotting the single input and output data.');
        disp('0. Quit the plotting.')
        option = input('What do you want to plot? = ');

        %clf;
        switch option
                case{1}
                        io = 1;
                        result =
ListFile(io,inLoadCount,outLoadCount,inFileName,outFileName)
                        dataNum = input('Which input data file do you want to plot? = ');
                        figure(figureCount); clf;
                        plot(inTime(dataNum,:), inMag(dataNum,:));
                case{2}
                        io = 0;
```

```
                        result =
ListFile(io,inLoadCount,outLoadCount,inFileName,outFileName)
                        dataNum = input('Which output data file do you want to plot? = ');
                        figure(figureCount); clf;
                        plot(outTime(dataNum,:), outMag(dataNum,:));
                case{3}
                        figure(figureCount); clf;
                        plot(inTimeAvg, inMagAvg);
                case{4}
                        figure(figureCount); clf;
                        plot(outTimeAvg, inMagAvg);
                case{5}
                        io = 0;
                        result =
ListFile(io,inLoadCount,outLoadCount,inFileName,outFileName)
                        dataNum = input('Which input and output data file do you want to plot? = ');
                        figure(figureCount); clf;
                        plot(outTime(dataNum,:), outMag(dataNum,:),'r*', inTime(dataNum,:),
inMag(dataNum,:),'b*');
                case{0}
                        result = 1;
                        break;
                otherwise
                        result = -1;
        end
        figureCount = figureCount + 1;
end
```

ngain.m

```
% ngain.m
% calculats the gain of polarization effect in XFDTD Simulation.
% input: 650nm Gaussian Beam without polarizer griding.
% output: Same as input with polarizer.
% XFDTD Simulated Near-Zoom Data files are required.
% Allan T. Chin (BBKNIGHT)
% Created date: 12, 10, 2004
% Last Updated: 12, 10, 2004

inSum = zeros(5,1); outSum = zeros(5,1);
for i = 1:5
        in(i,:) = mean(abs(inMag(i,500:1500)));
        out(i,:) = mean(abs(outMag(i,500:1500)));
end

for i = 1:5
                inSum(i) = sum(abs(inMag(i,500:1500)));
                outSum(i) = sum(abs(outMag(i,500:1500)));
end

gain = out./in
```

APPENDIX II

permittivity.m

```
% permittivity.m
% Caluculate the metal parameters for XFDTD simulations base on first order
% Debye model.
% Allan T. Chin (BBKNIGHT)
% Created date: 12, 01, 2005
% Last Updated: 03, 03, 2005

clear;
FSP = 8.854e-12; %Free_Space_Permittivity

target = -10.512 - 15.4328j;
temp = 0.01 * target;

Wavelength = 650e-9;
Frequency = 3e8 / Wavelength;
Omega = 2 * pi * Frequency;

%IFP = Infinite_Frequencey_Permittivity
%SP = Static_Permittivity
%RT = Relaxation_Time

%Conductivity
%Cond = FSP * (IFP - SP) / RT

%Complex Permittivity
%CP = IFP + ((SP + IFP) / (1+j*Omega*RT)) + (Cond / (j*Omega*FSP))
%CP = 0;
while(abs(real(CP)-real(target)) > real(target)*0.05 | abs(imag(CP)-imag(target)) > imag(target)*0.05)
        for IFP = 1.000:0.01:2.000
                for RT = 1e-15:.5e-17:1e-14
                        for SP = -1:-1:-100
                                Cond = FSP * (IFP - SP) / RT;
                                CP = IFP + ((SP + IFP) / (1+j*Omega*RT)) + (Cond / (j*Omega*FSP));
                                if real(CP) < -10 & real(CP) > -14 & abs(imag(CP)) > 1.0 &
abs(imag(CP)) < 1.5
                                if abs(real(CP)-real(target)) < abs(real(temp)) &
abs(imag(CP)-imag(target)) < abs(imag(temp))
                                        disp('**********************')
                                        CP
                                        IFP
                                        SP
                                        RT
                                        Cond
                                end
                        end
                end
        end
%end
```